UNIVERSITÀ
DEGLI STUDI
DI PADOVA

UNIVERSITÀ DEGLI STUDI DI PADOVA

SEDE AMMINISTRATIVA:

UNIVERSITÀ DEGLI STUDI DI PADOVA

DIPARTIMENTO DI SCIENZE CHIMICHE

SCUOLA DI DOTTORATO DI RICERCA IN SCIENZE MOLECOLARI

INDIRIZZO SCIENZE CHIMICHE

CICLO XXVII

HYBRID NANOSTRUCTURED MATERIALS FOR APPLICATION IN CATALYSIS AND MOLECULAR RECOGNITION

Direttore della Scuola: Ch.mo Prof. Antonino Polimeno

Supervisore: Ch.ma Prof.ssa Giulia Marina Licini

Dottoranda: Rosalia Di Lorenzo

02 Febbraio 2015

Contents

Chapter 1

General introduction

1.1 Introduction

Biological systems are very efficient molecular devices that possess an ordered spatial orientation of suitable functionalities and the ability to undergo dynamic structural rearrangements. Thanks to these properties, they can function as molecular information storage devices, molecular machines and selective catalysts.[1] Their structure comes from self-organizing and self-assembling processes of molecular components that interact in specific ways both chemically and physically. The specificity comes from the mutual recognition displayed by the components of a structure.[2]

A vast number of self-assembled biomolecules is present in Nature, including DNA and ribonuclease, but the first studies on self-assembly originated with the investigation of Tobacco Mosaic Virus (TMV) structure and organization.[3] TMV has a tubular structure, 300 nm in length, with an inner diameter of 4 nm and an outer diameter of 18 nm.[4] This structure stems from the self-assembly of 2130 identical coat proteins (TMVCPs) of 17.5 kDa molecular weight, that form a right-handed helix (with a pitch of 2.3 nm) around a single strand of genomic mRNA.[5]

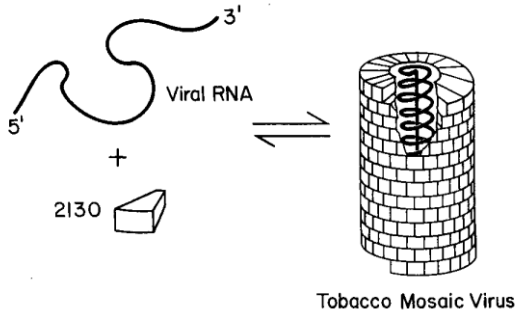

Figure 1. Self-assembly of TMV.[2]

The unique characteristic of TMV lies in the fact that, once dissociated into its component parts, the isolated components are capable of re-assembling the intact virus in concentration, time and pH dependences, similar to a typical chemical reaction. TMV assembly highlights the ability of biological systems to form large, structurally ordered molecular and supramolecular aggregates from small and simple subunits by a self-assembly mechanism. The stability of the final structure is guaranteed by many weak non-covalent interactions between the preformed subunits, so that the ultimate structure represents a thermodynamic minimum for the system.

---

[1] C. A. Schalley, A. Lützen, M. Albrecht *Chem.-Eur. J.* **2004**, *10*, 1072-1080.
[2] D. Philp, J. F. Stoddart *Angew. Chem. Int. Ed.* **1996**, *35*, 1154-1196.
[3] J. S. Lindsey *New J. Chem.* **1991**, *15*, 153-180.
[4] A. Tsugita, D. T. Gish, J. Young, H. Fraenkel-Conrat, C. A. Knight, W. M. Stanley *Proc. Natl. Acad. Sci. U. S. A.* **1960**, *46*, 1463-1469.
[5] K. Namba, R. Pattanayek, G. Stubbs *J. Mol. Biol.* **1989**, *208*, 307-325.

From TMV reconstruction the principles of biological self-assembly have been inferred, which are information (the amount of genetic information is reduced by using a few repeating subunits), control (control on assembly and disassembly can be easily achieved thanks to the association of subunits through multiple bonds of relatively low energy), error checking (defective subunits are automatically excluded as they do not have the required set of binding sites for assembly) and efficiency.[3]

Also enzymes have been widely studied as an interesting example of self-assembling systems and with that the development of enzyme mimics or artificial enzymes has dramatically evolved.[6] Enzymes are nanometer-sized molecules with supramolecular structures that are formed by folding and self-assembly of one or more polymeric chain-like components through non-covalent interactions. They catalyze chemical reactions in a confined microenvironment in a regio- and stereoselective way. Enzymes efficiency is due to the selective substrate recognition and binding through many supramolecular interactions, including hydrogen bonding, electrostatic, Van der Waals, π-π interactions and steric effects. Once bound to the enzyme active site, the induced proximity of two reactants or two functional groups in the same molecule determines a drastic increase in reaction rates. Besides molecular recognition, the stabilization of the transition state postulated by Pauling in 1946 is as well important.[7]

The need for mimicking such natural devices and creating self-assembling materials with certain features has led scientists to develop materials with hierarchical order and a high degree of complexity, trying to control the assembly of components with the same precision as that exhibited by Nature. In this context, the development of nanosized systems has spread largely in the last few years.

"Nanostructured materials" are assemblies of atoms that have dimensions smaller than 100 nm.[8] In the course of history, chemists have developed different procedures for assembling molecules: controlled formation of covalent bonds, covalent polymerization, self-organization and molecular self-assembly.[9] While the first two strategies involve the formation of covalent bonds and lead to the synthesis of large structures and high molecular weight molecules, such as Vitamin B_{12} or polyethylene, self-organization relies on the involvement of weaker and less directional bonds, in order to assemble atoms, ions or molecules into structures: the molecules arrange their positions to reach a thermodynamic minimum. Examples include micelles or self-assembled monolayers. Finally,

[6] (a) Z. Dong, Q. Luo, J. Liu *Chem. Soc. Rev.* **2012**, *41*, 7890- 7908 and references therein. (b) W. B. Motherwell, M. J. Bingham, Y. Six *Tetrahedron* **2001**, *57*, 4663-4686 and references therein.
[7] L. Pauling *Chem. and Eng. News* **1946**, *24*, 1375-1377.
[8] G. M. Whitesides, J. K. Kriebel, B. T. Mayers *et al*. in *Nanoscale Assembly, Chemical Techniques* D. J. Lockwood, Ed., Springer, Cambridge, **2005**, ch. 9, pp. 217-239.
[9] (a) G. M. Whitesides, J. P. Mathias, C. T. Seto *Science* **1991**, *254*, 1312-1319. (b) G. M. Whitesides, B. Grzybowsky Science, **2002**, *295*, 2418-2421.

molecular self-assembly gives rise to structurally well-defined assemblies of atoms, in which the molecules assemble into structured stable and non-covalently linked aggregates. In this process a first sequential covalent synthesis of building blocks is necessary to create the right subunits which, as a consequence of establishment of non-covalent bonds, can aggregate themselves to afford stable and structurally ordered supramolecular assemblies. As non-covalent interactions are orders of magnitude weaker than covalent bonds, large areas of complementary surface must be present in the final structures and the interactions must be favourable and efficient to overcome the entropic penalty paid by the system to assemble in an ordered state.[2]

There are a lot of systems in synthetic chemistry in which the characteristics of biological self-assembly have been adopted. Two distinctive examples include the self-assembly of crystals and host-guest or receptor-substrate chemistry. Both in crystallization and molecular recognition the principles of biological self-assembly listed before are involved: they discriminate molecules by the shape, size, bonding and electronic properties (control); molecules that do not form a specific number of interactions are readily excluded in the process (error-checking) and they give rise to ordered and highly-structured entities under gentle conditions (efficiency).[3]

Another trend in the field of nanostructured materials is the modification of natural proteins in order to use them as templating agents and molecular scaffolds in material sciences. Rod-like viruses, for example, like TMV, have been widely used as high aspect ratio platforms for the assembly of nanoscaled 1D materials in which functional units are precisely organized and spatially resolved. Indeed, such virus particles, also called virions, display surface-exposed reactive groups that facilitate (i) growth/immobilization and deposition of inorganic nanoparticles, (ii) interaction with other 1D nanostructures, surfaces and polymers, (iii) covalent conjugation with organic molecules.[10]

1.2 Self-assembly in metal coordination chemistry

Metal coordination chemistry shows many features that can be applied to self-assembly: the coordination of a metal to a ligand generates a strong bond, transferring stability to the structure, which is kinetically labile, and enabling the reorganization process to take place.[2] One of the first examples of molecular self-assembly involving metal coordination chemistry is presented by Curtis in 1960.[11] In this work, the mechanism of self-assembly seems to involve the coordination of nickel to an ethylendiamine ligand, a repetitive imine formation and the attack of

[10] K. Tao, J. Wang, Y. Li, D. Xia, H. Shan, H, Xu, J. R. Lu *Sci. Rep.* **2013**, *3*, 1-5.
[11] N. F. Curtis *J. Chem. Soc.* **1960**, 4409-4413.

an acetonyl carbanion to the Ni-coordinated imine, as depicted in scheme 1. The Ni^{2+} cation acts as a template for the assembly of the macrocycle.

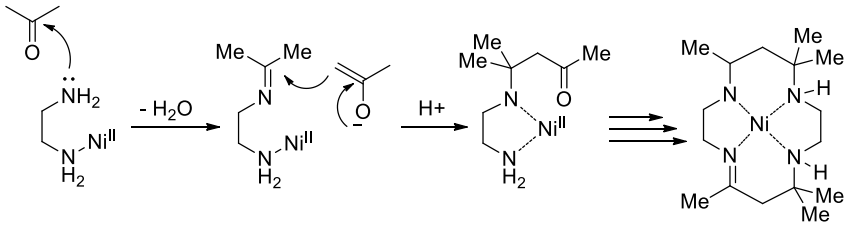

Scheme 1. Self-assembly of a macrocycle around a Ni^{II} ion.

From that moment, a lot of self-assembling clusters with predesigned architectures have been developed, most of which in the form of molecular racks, ladders, squares, molecular boxes, rotaxanes, catenanes and helicates.[12]

The latter ones, the helicates, display many of the characteristics associated with self-assembling biological systems, such as protein α-helix, DNA double helix or α-amilose. Helicates represent a class of metallosupramolecular systems which helped chemists to understand the basic aspects of supramolecular chemistry and self-assembly. Lehn and co-workers reported for the first time helicates formed by a series of oligobipyridine ligands, which spontaneously wrap around Cu^{I} metal centers (Figure 2, a).[2,13] The processes of positive cooperativity and self-recognition coexist: at one hand the binding of the first Cu^{I} ion facilitates the binding of the second and so on; on the other, a given ligand forms a double helix preferentially with an identical strand if a mixture of ligands is used. Inspired by this interesting self-assembling behaviour, they later used artificial oligonucleosides that upon reaction with Cu^{I} ions, give rise to double helical complexes (Figure 2, b). Such these deoxyribonucleohelicates (DNH) evoke natural double-stranded nucleic acids in DNA and represent beautiful examples of the potential of self-assembly to create large unnatural structures in an ordered and highly selective manner.[13]

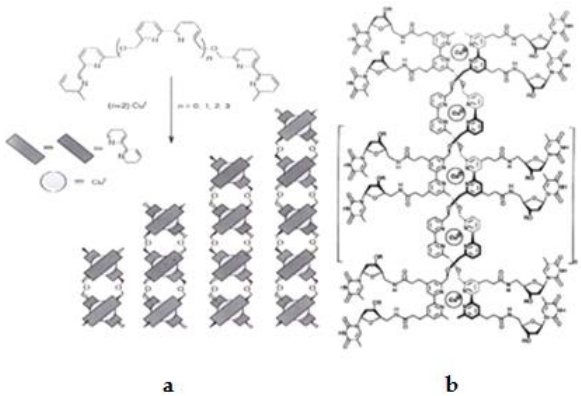

Figure 2. Helicates formed by complexation of Cu^{I} ions with: a) oligopyridines[2] and b) oligonucleosides.[13]

[12] J. P. Sauvage *Transition Metals in Supramolecular Chemistry* Wiley, New York, **1999**.
[13] J.-M. Lehn *Angew. Chem. Int. Ed. Engl.* **1990**, *29*, 1304-1319.

Moreover, most of the principles of supramolecular chemistry have emerged from the study of helicates: a) molecular recognition, in the way of interaction between two or more components in a self-process; b) self-organization, which allows to create a well-defined functional supramolecular architecture from the spontaneous organization of complementary components; c) self-assembly and d) molecular programing, with the incorporation of instructions in the components of self-assembly.[14]

1.2.1 Hierarchical Assembly of Titanium (IV) Complexes

Titanium aryloxides have found wide application mainly as homogeneous[15] and heterogeneous catalysts.[16] However, as soon as the interest in developing structurally ordered supramolecular macromolecules got a foothold, their involvement in host-guest chemistry, coordination chemistry and supramolecular chemistry and their use as precursors of new hybrid organic-inorganic materials has become more and more widespread. Henry and co-workers developed different chelate rings between pyrocathecol (Figure 3), salycilic acid, 2,2′-biphenol and 2,6-bis(hydroxymethyl)-*p*-cresol and Ti(IV) atoms.[17]

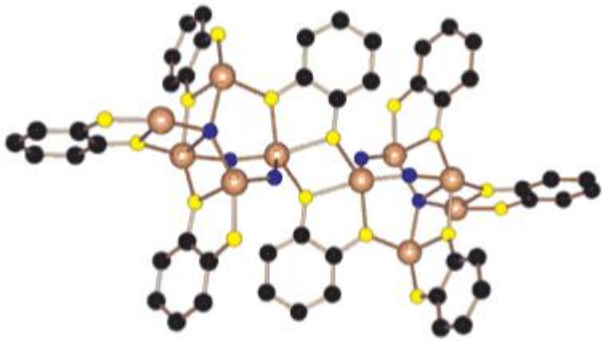

Figure 3. Molecular structure of $[Ti_{10}O_6\text{-}(OBu^n)_{12}(HOBu^n)_2(pc)_8]$, (pc = pyrocatechol). Two coordination modes around the titanium oxo core (blue O atoms) of the eight pyrocatecholato ligands (yellow O atoms).[17a]

In such multinuclear clusters different kinds of non-covalent interaction were detected in the solid state: hydrogen bonds, weak van der Waals, polar and π-π interactions. In the case of Ti(IV) complex obtained from complexation of 2,6-

[14] C. Piguet, G. Bernardinelli, G. Hopfgartner *Chem. Rev.* **1997**, *97*, 2005-2062.
[15] (a) M. Mba, L. J. Prins, G. Licini *Org. Lett.* **2007**, *9*, 21-24. (b) C. Zonta, E. Cazzola, M. Mba, G. Licini *Adv. Synth. Catal.* **2008**, *350*, 2503-2506. (c) M. Mba, L. J. Prins, C. Zonta, M. Cametti, A. Valkonen, K. Rissanen, G. Licini *Dalton Trans.* **2010**, *39*, 7384-7392. (d) A. V. Firth, J. C. Stewart, A. J. Hoskin, D.W. Stephan J. *Organomet. Chem.* **1999**, *591*, 185-193. (e) J. Okuda, S. Fokken, T. Kleinhenn, T. P. Spaniol Eur. J. *Inorg. Chem.* **2000**, 1321-1326. (f) N. W. Eilerts, J. A. Heppert, M. L. Kennedy, F. Takusagawa *Inorg. Chem.* **1994**, *33*, 4813-4814. (g) M. Terada, Y. Matsumoto, Y. Nakamura, K. Mikami *Inorg. Chim. Acta* **1999**, *296*, 267-272.
[16] R. T. Toth, D. W. Stephan *Can. J. Chem.* **1999**, *77*, 2095-2098.
[17] (a) K. Gigant, A. Rammal, M. Henry *J. Am. Chem. Soc.* **2001**, *123*, 11632-11637. (b) A. Rammal, F. Brisach, M. Henry *J. Am. Chem. Soc.* **2001**, *123*, 5612-5613.

bis(hydroxymethyl)-*p*-cresol also a study on the inclusion of solvent molecules in the cavity formed by the complex was conducted.[17b]

Also dinuclear titanium helicate type complexes have been obtained. In these systems two recognition events participate to the assembly of the final architecture: the first is represented by the complexation of catecholate ligand to a Ti(IV) ion; the second is mediated by the templating effect of lithium cations that can be chelated by two salicylic units (Scheme 2). The dimer formed is thermodynamically favoured by both enthalpy and entropy.[14,18] Moreover, the complex represents a nice example of hierarchical self-assembly, in which two non-covalent interactions bring together several individual components in a defined aggregate.

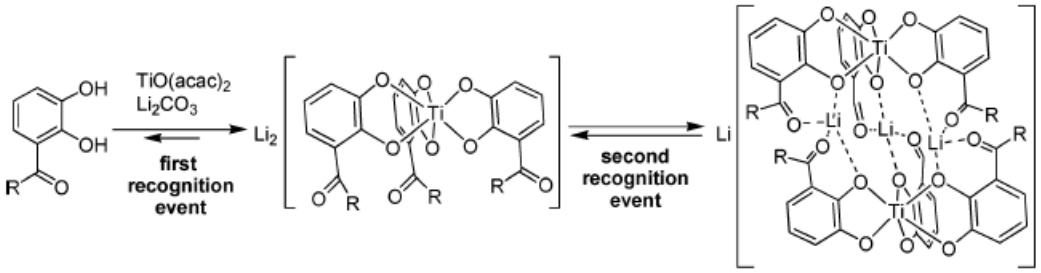

Scheme 2. Hierarchical self-assembly of lithium-bridged Ti(IV) helical type complex.[18a]

If tripodal cathecol imines are used, different geometries are formed upon complexation with Ti(IV) ions (Figure 4).

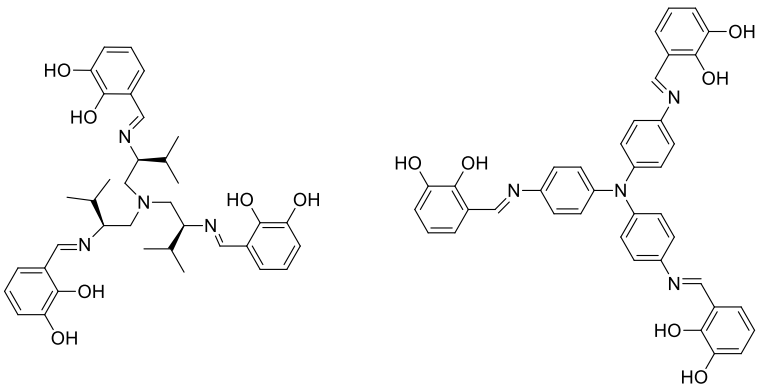

Figure 4. Flexible **1** and rigid **2** tripodal ligands.

In general, flexible ligands would favour the formation of mononuclear complexes, as in the case of ligand **1**, in which the bulky isopropyl groups prevent the ligand from "spreading out" and only a mononuclear species can form; on the

[18] (a) M. Albrecht, S. Mirtschin, M. de Groot, I. Janser, J. Runsink, G. Raabe, M. Kogej, C. A. Schalley, R. Fröhlich *J. Am. Chem. Soc.* **2005**, *127*, 10371-10387. (b) M. Albrecht, R. Fröhlich *Bull. Chem. Soc. Jpn.* **2007**, *80*, 797-808. (c) C. A. Schalley, A. Lützen, M. Albrecht *Chem.-Eur. J.* **2004**, *10*, 1072-1080. (d) M. Albrecht *Chem. Rev.* **2001**, *101*, 3457-3497.

other hand, rigid ligands should lead to the formation of tetrahedra, as demonstrated by complexation of ligand **2** with Ti(IV) ions (Figure 5). In this case a three-dimensional multi-nanometer-sized aggregate can be designed, which present huge internal cavities that can be appropriate to encapsulate organic molecules, such as anilinium cations, as guest species.[18b,19]

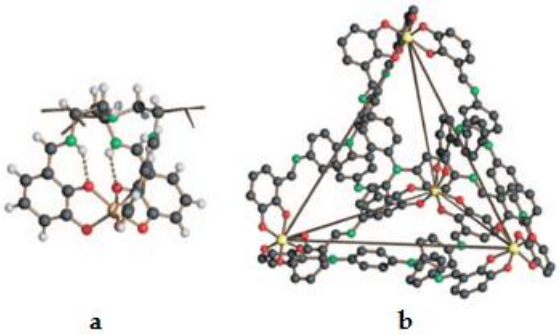

Figure 5. X-ray structures of mononuclear Ti(IV) complex (a) and tetranuclear Ti(IV) complex (b), obtained by complexation of Ti(IV) ions with ligands **1** and **2**, respectively.[18b]

1.3 Coordination chemistry of amine triphenolate ligands

In the context of tripodal ligands and the effects that substituents can have on the development of mono- or dinuclear systems, triphenolamines (TPAs, $\mathbf{LH_3}$) are highly modular tetradentate ligands (Figure 6) that are able to coordinate to a wide variety of early transition metals (d^0, d^5) and main group elements (d^{10}).

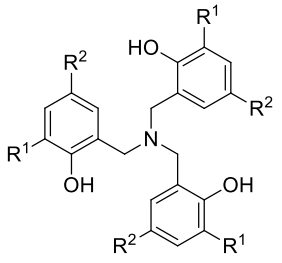

$\mathbf{L_{a\text{-}j}H_3}$

a	R^1=R^2=H
b	R^1=R^2=Me
c	R^1=R^2=*t*-Bu
d	R^1=R^2=Cl
e	R^1=*t*-Bu; R^2=Me
f	R^1=Me; R^2=*t*-Bu
g	R^1=Me; R^2=H
h	R^1=*t*-Bu; R^2=H
i	R^1=Ph; R^2=H
j	R^1=Adm; R^2=*t*-Bu

Figure 6. Structure of triphenolamines $\mathbf{L_{a\text{-}j}H_3}$.

The coordination chemistry of such these ligands is related to the modular nature of the phenol moieties, the three-fold symmetry of the systems and the tetradentate behaviour of the compounds: they provide three anionic binding sites, corresponding to the phenolate residues, and a neutral nitrogen atom, and all coordinate to the metal centre, generating an extremely stable structure, as depicted in scheme 3.

[19] M. Albrecht, I. Janser, S. Burk, P. Weis *Dalton Trans.* **2006**, 2875-2880.

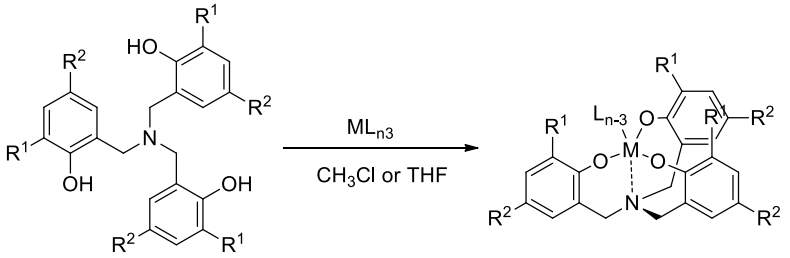

Scheme 3. Complexation reaction of TPA ligands with a metal ion.

In the stability of the resulting metal complexes the steric and electronic features play an important role: the substituents in *ortho* position (R^1) to the phenolate upon complexation are very close to the metal centre, so they affect the steric hindrance and can be used as control elements, while the substituents in *para* position (R^2) influence the electronic properties of the complexes, without affecting the steric demand of the system.[15a,b,20] The latter can be the subject of secondary modifications and can be used as anchoring sites for further functionalization of the complexes.

In the vast majority of cases, mononuclear complexes are obtained with a 1:1 ligand/metal ratio. The most common geometries of the complexes are trigonal bypiramidal (TBP) or octahedral (OCT), while the trigonal monopyramidal (TMP) is less observed (Figure 7).

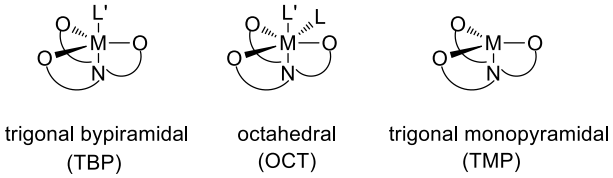

Figure 7. Principal geometries of amine triphenolate complexes.

When the TPA complexes form, the ligands assume a propeller-like arrangement around the metal ion, when viewed along the metal-nitrogen axis. Consequently, the complexes are chiral with configurations Δ/Λ or *P/M*, and they form as a racemic mixture, in which the two enantiomeric complexes rapidly interconvert at room temperature. (Figure 8).

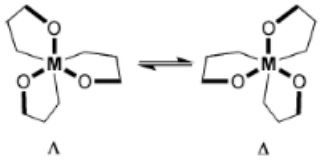

Figure 8. Clockwise and counter-clockwise enantiomeric configurations of TPA complexes.[20]

[20] G. Licini, M. Mba, C. Zonta *Dalton Trans.* **2009**, 5265-5277.

Amine triphenolate complexes have been mainly studied and used as active catalysts for a wide variety of reactions, because of their sharp Lewis acid properties, as a consequence of the ability of tetradentate **LH_3** ligands to stabilize the active sites under turnover conditions. The reactions they catalyse span from polymerizations (ROP and ethylene polymerizations),[21] to Mukayiama aldol additions,[22] Aza-Diel-Alder reactions,[23] sulfoxidations,[15a,b,c,24] oxidations of secondary amines to nitrones,[15b] epoxidations,[24b,25] haloperoxidations,[24b,26] CO_2 fixation[27], methathesis[28] and, very recently, to C-C oxidative cleavage.[29]

1.3.1 Ti(IV) amine triphenolate complexes

The first Ti(IV) amine triphenolate complex was synthesized by Kol and co-workers.[30] The complex possesses a C_3-symmetry, also confirmed by ^{1}H-NMR spectroscopy, and represents the first example of a chiral C_3-symmetrical titanium complex formed from an achiral ligand. The X-ray structure for the complex **3c**, which bears an apical *iso*-propoxy and *t*-butyl substituents in *ortho* and *para* positions to the phenolate, has been obtained (Figure 9). A slightly distorted trigonal bipyramidal geometry was found. The titanium lies 2.04 Å above the plane defined by the three phenolate oxygen atoms. The ligand assumes a propeller-like fashion around the metal. The *iso*-propoxide groups are shielded within the cavity formed by the tripodal ligand, so that the mononuclear complex is highly stable and is protected from aggregation.

---

[21] (a) A. J. Chmura, M. G. Davidson, C. J. Frankis, M. D. Jones, M. D. Lunn *Chem. Commun.*, **2008**, 1293-1295. (b) S. Gendler, S. Segal, I. Goldberg, Z. Goldschmidt, M. Kol *Inorg. Chem.* **2006**, *45*, 4783-4790. (c) L. Michalczyk, S. de Gala, J. W. Bruno *Organometallics* **2001**, *20*, 5547-5556. (d) A. J. Chmura, C. J. Chuck, M. G. Davidson, M. D. Jones, M. D. Lunn, S. D. Bull, M. F. Mahon *Angew. Chem. Int. Ed.* **2007**, *46*, 2280-2283. (e) W. Wang, M. Fujiki, K. Nomura *Macromol. Rapid Commun.* **2004**, *25*, 504-507. (f) C. Redshaw, M. A. Rowan, D. H. Homden, S. H. Dale, M. R. J. Elsegood, S. Matsui, S. Matsuura *Chem. Commun.* **2006**, 3329-3331.

[22] W. Su, Y. Kim, A. Ellern, I. A. Guzei, J. G. Verkade *J. Am. Chem. Soc.* **2006**, *128*, 13727-13735.

[23] S. D. Bull, M. G. Davidson, A. L. Johnson, D. E. J. E. Robinson, M. F. Mahon *Chem. Commun.* **2003**, 1750-1751.

[24] (a) M. Mba, M. Pontini, S. Lovat, C. Zonta, G. Bernardinelli, E. P. Kündig, G. Licini *Inorg. Chem.* **2008**, *47*, 8616-8618. (b) F. Romano, A. Linden, M. Mba, C. Zonta *Adv. Synth. Catal.* **2010**, *352*, 2937-2942.

[25] S. Groysman, I. Goldberg, Z. Goldschmidt, M. Kol *Inorg. Chem.* **2005**, 44, 5073-5080.

[26] M. J. Claque, N. K. Keder, A. Butler *Inorg. Chem.* **1993**, *32*, 4754-4761.

[27] (a) C. J. Whiteoak, B. Gjoka, E. Martin, M. Martinez Belmonte, G. Licini, A. W. Kleij *Inorg. Chem.* **2012**, *51*, 10639-10649. (b) C. J. Whiteoak, E. Martin, M. Martínez Belmonte, J. Benet-Buchholz, A. W. Kleij *Adv. Synth. Catal.* **2012**, *354*, 469-476. (c) C. J. Whiteoak, N. Kielland, V. Laserna, E. C. Escudero-Adán, E. Martin, A. W. Kleij *J. Am. Chem. Soc.* **2013**, *135*, 1228-1231. (d) C. J. Whiteoak, N. Kielland, V. Laserna, F. Castro-Gómez, E. Martin, E. C. Escudero-Adán, C. Bo, A. W. Kleij *Chem.-Eur. J.* **2014**, *20*, 2264-2275.

[28] K.Jyothish, W. Zhang *Angew. Chem. Int. Ed.* **2011**, *50*, 3435 –3438.

[29] E. Amadio, G. Licini *unpublished results*.

[30] M. Kol, M. Shamis, I. Goldberg, Z. Goldschmidt, S. Alfi, E. Hayut-Salant *Inorg.Chem. Commun.* **2001**, *4*, 177-179.

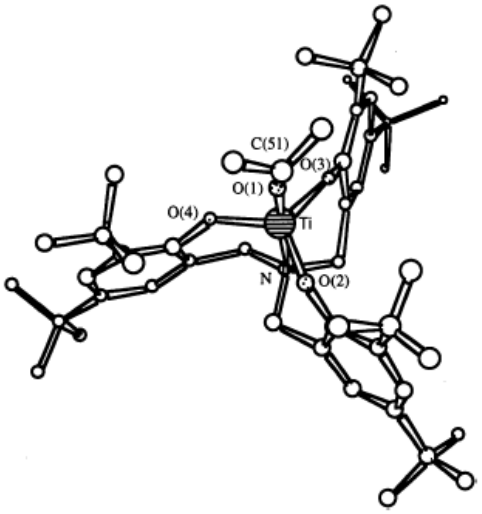

Figure 9. Molecular structure of $\mathbf{L_c}$Ti(O*i*-Pr) **3c**.[30]

However, if less bulky substituents in *ortho* and/or *para* position to the phenolate are present, the *iso*-propoxide group is less shielded and can be hydrolysed off, the mononuclear complex is less stable and aggregates in presence of moisture, giving rise to dinuclear species. [30,31] Indeed, a significant dependence of the thermodynamic stability of Ti(IV) amine triphenolate complexes on the steric size of peripheral substituents in *ortho* position can be inferred.

The most common geometry of Ti(IV) TPA complexes is trigonal bipyramidal. However, Ti(IV) complexes with an octahedral geometry have been reported as well, in which titanium can accommodate an extra ligand or a bidentate monoanionic one, giving rise to a hexacoordinate geometry.[32] In particular, Brown and co-workers reported that $\mathbf{L_c}$Ti(O-^{t}Bu) **4c** rapidly reacts with bidentate enolic ligands troponolate (trop), acetilacetonate (acac) and di-p-toluoylmethanide (dtm) (Scheme 4).

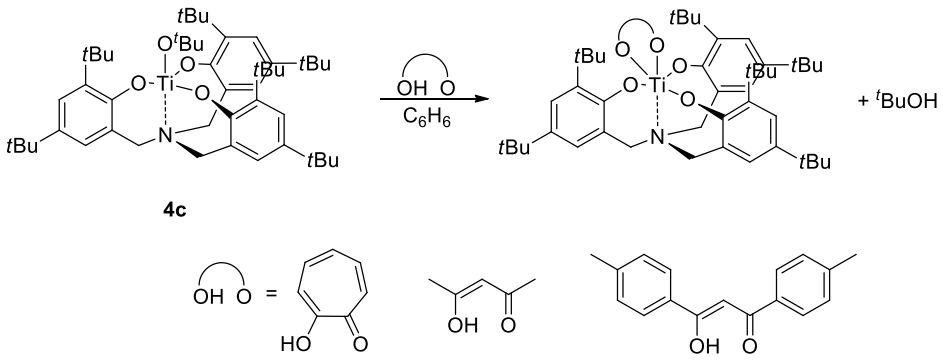

Scheme 4. Coordination of bidentate ligands to Ti(IV) complex **4c**.

[31] A. J. Nielson, C. Shen, J. M. Waters *Polyhedron* **2006**, *25*, 2039-2054.
[32] K. C. Fortner, J. P. Bigi, S. N. Brown *Inorg. Chem.* **2005**, *44*, 2803-2814.

X-ray structures of hexacoordinate complexes show that the complexes are octahedral, with the bidentate ligand occupying both an axial position (*trans* to the nitrogen of the triphenolate ligand) and an equatorial position (*trans* to one of the phenolate of the tripodal ligand). The ligands retains the propeller-like conformation around the metal centre and the complexes possess a C_1-symmetry.

The tendency of titanium to extend its coordination sphere from TBP to OCT in the presence of an external ligand, allows the possibility to use such these complexes as catalysts in oxygen transfer reactions, with activation of alkyl hydroperoxides or hydrogen peroxide upon coordination to the metal centre.[15a,b] A detailed study on the mechanism of Ti(IV) TPA complexes catalysed sulfoxidations and the role that an external ligand, more frequently an alcohol, can have on the catalytic activity has been recently reported by Zonta and Licini.[33] They observed that complex **3h** prepared by *in situ* complexation of $\mathbf{L_hH_3}$ with Ti(O*i*-Pr)$_4$ is much more active in sulfoxidation reactions than the isolated complex, in which the free *iso*-propanol, coming from ligand exchange, was removed under vacuum. In the specific case the free *iso*-propanol has a beneficial effect on the reaction, as a new hexacoordinate species **5h** was identified to be the active one, in which an extra alcohol molecule is coordinated to the metal centre. Indeed, the octahedral geometry of **5h** makes the empty σ* orbital of the oxygen-oxygen bond of the peroxide much more available for the oxygen transfer reaction (Scheme 5).

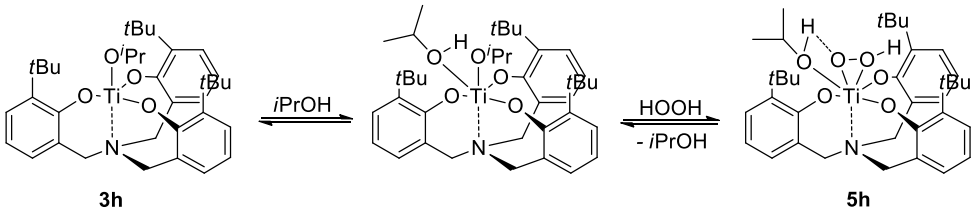

Scheme 5. Hexacoordinate Ti(IV) TPA complex **5h**.

1.3.2 Self-assembly of Ti(IV) TPA *μ*-oxo complexes

As mentioned before, the steric size and the electronic properties of the *ortho* peripheral substituents can influence the steric hindrance of the ligand around the metal, its binding mode and the stability of the corresponding complexes. This behaviour is called "*ortho* effect" and it is very important, as different responses of complexes bearing different *ortho* substituents to moisture can be observed (Figure 10).

[33] C. Zonta, G. Licini *Chem.-Eur. J.* **2013**, *19*, 9438-9441.

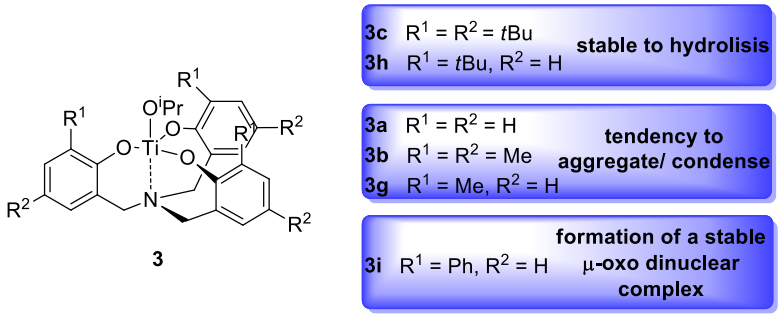

Figure 10. "*Ortho* effect" on the stability of Ti(IV) TPA complexes **3** in solution.

Bulky *ortho* *t*-Bu substituents lead to very stable and moisture tolerant complexes.[15a,b,30,34] Indeed, the apical *tert*-butoxide group in complex **4c** cannot be directly substituted by the hydroxide, but a prior exchange with more acidic trifluoroacetate has to occur, which can then lead to the formation of terminal hydroxide upon reaction with aqueous sodium hydroxide (Scheme 6).[35]

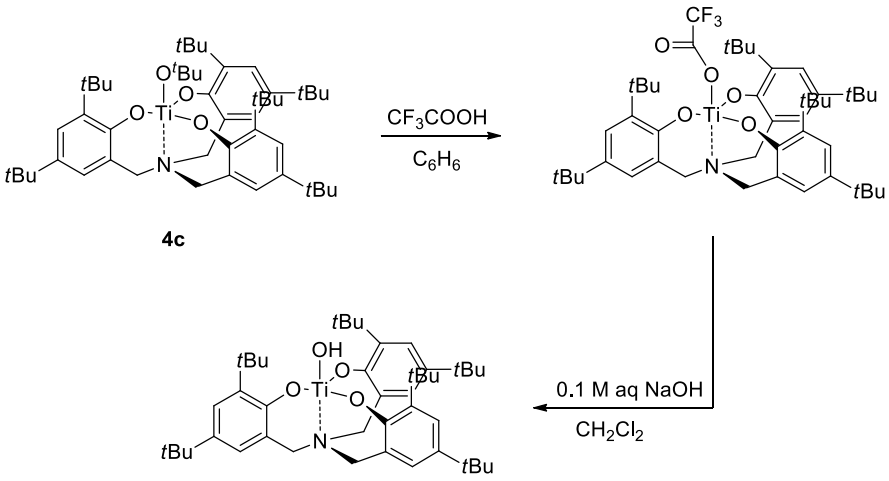

Scheme 6. Apical ligand exchange on Ti(IV) TPA complex **4c**.

The terminal hydroxide then easily condenses to form the μ-oxo species **6c** upon concentration of the solution (Figure 11).

[34] S. D. Bull, M. G. Davidson, A. L. Johnson, D. E. J. E. Robinson, M. F. Mahon *Chem. Commun.* **2003**, 1750-1751.
[35] V. Ugrinova, G. A. Ellis, S. N. Brown *Chem. Commun.* **2004**, 468-469.

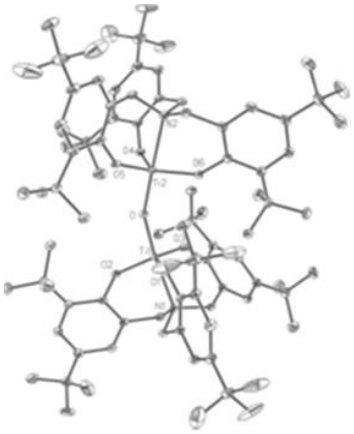

Figure 11. Molecular structure of Ti(IV) μ-oxo complex **6c**.[34]

The crystal structure shows that Ti-O-Ti bridge is bent (155.54°). The complex is stable in anhydrous solutions, but it is cleaved in presence of excess of water. The low hydrolytic stability has to be ascribed to the bulky *t*-Bu substituents that are forced into close contact in the μ-oxo complex **6c**.

When small substituents, like Me or H, are present in the *ortho* and/or *para* positions, the complexes tend to aggregate in solution upon exposure to moisture, forming polynuclear species.[15a,30,31] The first μ-oxo complex, bearing methyl groups both in *ortho* and *para*, was identified by Kol and co-workers.[30] The apical *iso*-propoxide in the complex is now less shielded and more sensitive to hydrolysis and the μ-oxo species can be obtained directly by exposing complex **3b** to air for several days. The X-ray structure shows that the Ti-O-Ti bond angle is smaller (147.48°) than then one in complex **6c**, probably because of the less hindrance of the *ortho* methyl substituents with respect to the *t*-Bu ones.[31]

In the case of complex **3i**, which bears bulky phenyl groups in *ortho* positions, a different behaviour in solution has been observed. Licini and co-workers reported for the first time the spontaneous formation of a highly stable μ-oxo dinuclear complex, upon exposure of **3i** to only traces of water (Scheme 7).[36]

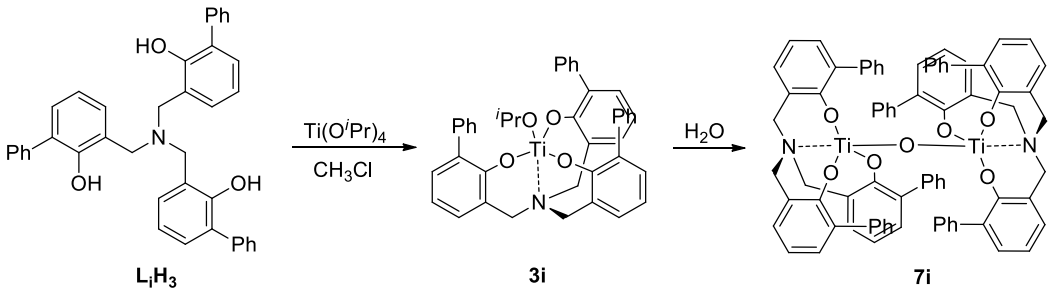

Scheme 7. Spontaneous self-assembly of Ti(IV) TPA μ-oxo complex **7i**.

[36] G. Bernardinelli, T. M. Seidel, E. P. Kündig, L. J. Prins, A. Kolarovic, M. Mba, M. Pontini, G. Licini *Dalton Trans.* **2007**, 1573-1576.

X-ray structure of **7i** shows that the μ-oxo bridge is located on a crystallographic centre of inversion, leading to the formation of a perfectly linear Ti-O-Ti bond angle (180.0°C), in contrast with the values reported before for μ-oxo complexes bearing *t*-Bu or Me groups in *ortho* and *para* positions (Figure 12). The peripheral phenyl rings from the two ligands intercalate around the μ-oxo bridge: each *ortho* proton points towards the π-cloud of the next ring, belonging to the other titanatrane moiety. This structural characteristic is also reflected in solution, as ^{1}H-NMR of **7i** shows a significant upfield shift for the signals of the peripheral aromatic protons (ca. 1 ppm).

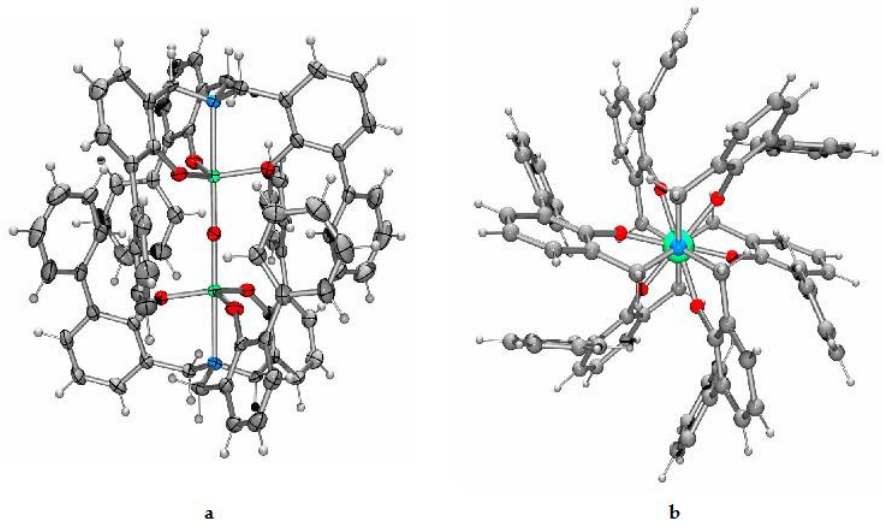

Figure 12. (a) Molecular structure of complex **7i**. (b) View along the N-Ti-O-Ti axis.[35]

Both titanium atoms retain the trigonal bipyramidal geometry and the two titanatrane units maintain the helical conformation around the metal ion, as in the mononuclear complex. However, starting from a racemic mixture of complexes, Λ and Δ, exclusively the heterochiral compound (Δ-Λ) is formed and no traces of homochiral complexes (Λ-Λ and Δ-Δ) are present in ^{1}H-NMR even at high temperature, showing that the formation of the μ-oxo dinuclear complex is a completely stereoselective self-discriminating process.[20]

Whereas in mononuclear complex **3i** the methylene protons appear as a single broad signal in ^{1}H-NMR spectrum, indicating the C_3-symmetry of the complex, in which the two enantiomers racemise at room temperature, in the dinuclear complex **7i** the methylene protons appear as an AB system, indicating that the racemization rate of the titanatrane moiety is slower on the NMR time scale, thus confirming the formation of a diastereomeric species.

The particular characteristic of mononuclear Ti(IV) TPA complex **3i** to spontaneously self-assemble to give the dimeric Ti(IV) μ-oxo complex **7i** makes it possible to build up stable and ordered structures that can be exploited in

supramolecular chemistry[37] for the construction of molecular scaffolds and polyfunctional platforms for further application in material sciences. Ti(IV) μ-oxo complex **7i**, indeed, can be functionalized in its periphery to generate multifunctional platforms with different functions disposed in a controlled way into space (Figure 13).

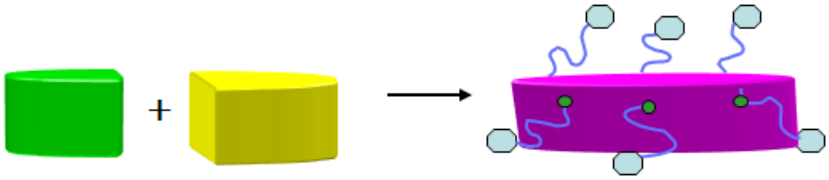

Figure 13. Schematic representation of self-assembly of Ti(IV) μ-oxo complex **7i**.

1.3.3 V(V) amine triphenolate complexes

In the field of enzyme mimics, in recent years, there has been a growing interest in vanadium chemistry. After the discovery of vanadium-dependent haloperoxidase active centre, in which V(V) possesses a trigonal bipyramidal geometry, and it is surrounded by three equatorial oxygen donors and an axial oxygen and nitrogen (hystidine residue) donors,[38] different model compounds have been developed that mimic the metal coordination chemistry of vanadium-dependent enzyme's active centre.[39]

In this context, amine triphenolate ligands (**LH_3**) seem to provide a "natural environment" for vanadium, due to their strong binding to the metal centre and the tunable properties of the complexes they can generate. In particular, Kol and co-workers reported for the first time the formation of V(V) TPA complexes **8d-d**, as a result of complexation reaction between ligands **$L_{b\text{-}d}H_3$** and VO(O*i*-Pr)$_3$ precursor and paved the way for the development of functional and structural models of vanadium-dependent enzymes.[25] Later, Licini and collaborators synthesized complexes **8a,g,h** (Figure 14).[40]

[37] (a) J.-M. Lehn Supramolecular Chemistry, VCH, Weinheim, **1995**. (b) J. W. Steed, J. L. Atwood Supramolecular Chemistry, Wiley, Chichester, **2000**.
[38] (a) A. Messerschmidt, R. Wever *Proc. Natl. Acad. Sci. U. S. A.* **1997**, *93*, 392-396. (b) S. Macedo-Ribeiro, W. Hemrika, R. Renirie, R. Wever, A. Messerschmidt *J. Biol. Inorg. Chem.* **1999**, *4*, 209-219. (c) M. Weyand, H. J. Hecht, M. Kiesz, M. F. Liaud, H. Viter, D. Schomburg *J. Mol. Biol.* **1999**, *293*, 595-611. (d) M. N. Isupov, A. R. Dalby, A. A. Brindley, Y. Izumi, T. Tanabe, G. N. Murshudov, J. A. Littlechild *J. Mol. Biol.* **2000**, *299*, 1035-1049.
[39] (a) D. C. Crans, J. J. Smee, E. Gaidamauskas, L. Yang *Chem. Rev.* **2004**, *104*, 849-902. (b) D. Rehder, G. Santoni, G. M. Licini, C. Schulzke, B. Meier *Coord. Chem. Rev.* **2003**, *357*, 53-63. (c) A. G. J. Ligtenbarg, R. Hage, B. L. Feringa *Coord. Chem. Rev.* **2003**, *237*, 89-101. (d) C. Bolm *Coord. Chem. Rev.* **2003**, *237*, 245-256.
[40] L. J. Prins, M. Mba Blázquez, A. Kolarović, G. Licini Tetrahedron **2006**, *47*, 2735-2738.

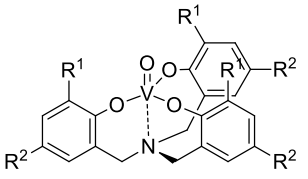

8

a $R^1=R^2=H$
b $R^1=R^2=Me$
c $R^1=R^2=t\text{-}Bu$
d $R^1=R^2=Cl$
g $R^1=Me$; $R^2=H$
h $R^1=t\text{-}Bu$; $R^2=H$

Figure 14. V(V) TPA complexes **8a-d**,**g,h**.

Complexes **8a-c**,**h,h** show a TBP geometry, with the oxo moiety that occupies the axial position *trans* to the nitrogen of the ligand.[21a,24a] In the case of complexes **8g,h**, ^{1}H-NMR spectrum shows the formation of a single C_3-symmetric mononuclear complex, with a single ^{51}V-NMR signal (-381.9 ppm and -389.1 ppm, $CDCl_3$, respectively), while in the case of complex **8a** a mixture of species or aggregates forms, as revealed by a complicate ^{1}H-NMR and the presence of two different signals in ^{51}V-NMR (-396.8 ppm and -428.8 ppm, $CDCl_3$). On the contrary, for the electron deficient complex **8d** an octahedral geometry has been observed, in which the oxo moiety occupies the axial position *trans* to the nitrogen and a molecule of water occupies an equatorial one (Figure 15). The amine triphenolate ligand in this complex does not have a propeller-like arrangement around the metal ion.

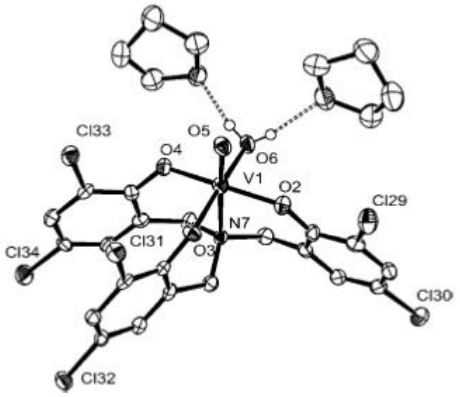

Figure 15. Molecular structure of V(V) TPA complex **8d** (two hydrogen bonds between a water molecule and two molecules of THF are present).[25]

Such these complexes clearly represent functional models of vanadium haloperoxidase. Their catalytic activity in oxidation reactions has been widely investigated. The catalytic activity of V(V) TPA complexes **8b-d** has been tested in the oxidation of styrene to the corresponding epoxide, using *t*-BuOOH as oxidant,[25] while V(V) complexes **8a,g,h** have been used as effective catalysts in oxidation of sulphides and bromide ions, using H_2O_2 as terminal oxidant, with high TONs and TOFs.[24]

1.4 Aim of the thesis

The work developed in this thesis deals with the synthesis of amine triphenolate ligands **LH_3** and their corresponding complexes, for their use in catalysis and material sciences.

Chapter 2 describes the synthesis of new functionalized **LH_3** ligands, *via* Duff reaction, that present highly reactive anchoring formyl groups in *para* position to the phenolate for further functionalization of the amine triphenolate skeleton. In particular, the synthesis of highly decorated **LH_3** ligands is reported, that relies upon a *click*-type reaction, the oxime bond formation, between the aldehyde substituents and different alkoxyamines, allowing the introduction of a wide variety of functional groups on **LH_3** ligands. The synthesis of *ortho*-aryl functionalized amine triphenolate ligands, through a Suzuki coupling reaction, is as well described. The introduction of formyl groups in *meta* position on the *ortho*-aryl moiety makes it possible to address the same functionalization strategy as in the case of the *para* positions.

In *Chapter 3*, the stereoselective self-assembly process of a highly stable, inert S_6-symmetrical Ti(IV) μ-oxo complex is discussed as well as the possibility to obtain highly functionalized Ti(IV) μ-oxo complexes through the complexation of already functionalized **LH_3** ligands or by the direct functionalization of μ-oxo complexes with different alkoxyamines. Some applications in the field of supramolecular chemistry and molecular recognition of pyrene functionalyzed Ti(IV) μ-oxo complexes are also described.

Finally, *Chapter 4* is dedicated to the synthesis of highly functionalized V(V) TPA complexes for the realization of organo metallogels and micellar-like systems. The study of their catalytic activity towards sulfoxidation reactions and C-C oxidative cleavage reactions is reported.

Chapter 2

Synthesis of highly functionalized amine triphenolate ligands

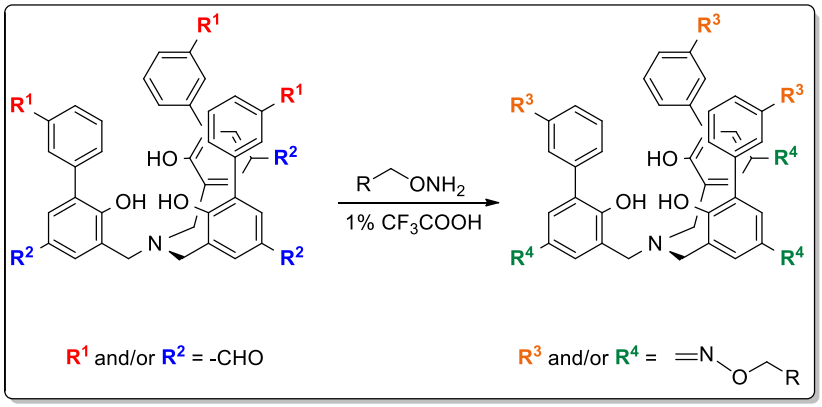

A new synthetic strategy for the functionalization of amine triphenolate ligands has been established. In particular, *ortho* positions to the phenolate have been firstly functionalized by the introduction of three aldehyde groups *via* Duff reaction and a three-fold formyl functionalization of *meta* positions on the peripheral aromatic rings has been obtained through a Suzuki coupling reaction on an iodo- derived triphenolamine by reaction with 3-formyl boronic acid. The formyl groups have been object of further derivatization through a *click*-type reaction, namely oxime bond formation. In this way, both positions have been successfully modified either separately or in some cases on the same amine triphenolate system, giving rise to six-fold decorated ligands.

2.1 Introduction

The realization of nanoscaffolds that possess multiple functionalities disposed in a controlled way into space supposes the design of suitable building blocks, e.g. metal coordination ligands, which can be selectively and efficiently functionalized with appropriate residues. Such these moieties in some cases have physical or chemical properties, which, upon formation of the final scaffold, can be transferred to it, giving rise to functional materials. Protein shells of viruses, for example, provide very promising scaffolds for the construction of new materials,[41] both for their nanoscale dimensions and because of the presence of regularly spaced attachment sites on the viral capsid that can be exploited to add new functionalities to their interior[42] and exterior[43] surfaces.

Tobacco Mosaic Virus (TMV) coat protein has recently become an interesting target for the bottom-up fabrication of nanostructured materials with precise size, structure and organization.[44] Among the modifications it can undergo, covalent functionalization of TMV coat protein is very useful, as it can offer the possibility to decorate the capsid in a selective and ordered way along the protein subunits. Francis and co-workers reported for the first time that some aminoacidic residues on TMV protein surface could be selectively functionalized through covalent bond formation.[45] In particular, they developed two orthogonal synthetic strategies to covalently modify tyrosine 139 residue on the exterior surface and glutamic acids 97 and 106 on the interior surface of TMV coat protein (Figure 1). The procedure enabled them to introduce several functionalities without disrupting the capsid assembly. A double modification of both exterior and interior surfaces was also reported, demonstrating the feasibility of the functionalization strategy and the high stability of the assembled capsid.

[41] (a) T. Douglas, M. Young *Nature* **1998**, *393*, 152-155. (b) T. Douglas, M. Young *Adv. Mater.* **1999**, *11*, 679-681. (c) S.-W. Lee, C. Mao, C. E. Flynn, A. M. Belcher *Science* **2002**, *296*, 892. (d) X. Z. Fan, E. Pomerantseva, M. Gnerlich, A. Brown, K. Gerasopoulos, M. McCarthy, J. Culver, R. Ghodssi *J. Vac. Sci. Technology* **2013**, *31*, 050815-1-24.

[42] (a) J. M. Hooker, E. W. Kovacs, M. B. Francis *J. Am. Chem. Soc.* **2004**, *126*, 3718-3719. (b) S. Meunier, E. Strable, M. G. Finn *Chem. Biol.* **2004**, *11*, 319-326.

[43] (a) Q. Wang, T. Lin, L. Tang, J. E. Johnson, M. G. Finn *Angew. Chem, Int. Ed.* **2002**, *41*, 459-462. (b) Q. Wang, E. Kaltgrad, T. Lin, J. E. Johnson, M. G. Finn *Chem. Biol.* **2002**, *9*, 805-811. (c) Q. Wang, T. R. Chan, R. Hilgraf, V. V. Fokin, K. B. Sharpless, M. G. Finn, *J. Am. Chem. Soc.* **2003**, *125*, 3192-3193.

[44] L. S. Witus, M. B. Francis *Acc. Chem. Res.* **2011**, *44*, 774-783.

[45] T. L. Schlick, Z. Ding, E. W. Kovacs, M. B. Francis *J. Am. Chem. Soc.* **2005**, *127*, 3718-3723.

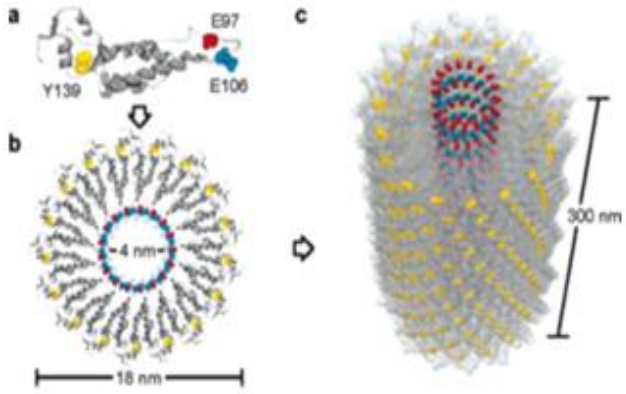

Figure 1. (a) Tyrosine 139 (yellow), glutamate 97 (red), and glutamate 106 (blue) residues in a single TMV capsid monomer. (b) Planar disk aggregate and (c) fully assembled capsid.[5]

Interior glutamates 97 and 106 were object of amide bond formation in the presence of a coupling agent. In this case, different primary or secondary amines could be introduced in the interior surface of TMV capsid, and singly or doubly modified products could be obtained in significant yields. Chromophores or crown ethers could be also attached to the capsid quite efficiently, despite the steric demands they could introduce. However, the most interesting modification regarded the functionalization of tyrosine 139 on TMV coat protein exterior surface. Indeed, after exposure of intact viral capsids to different diazonium salts **2a-d** in pH 9 buffer for 2 h, several TMV azo-adducts could be effectively synthesized (Scheme 1).

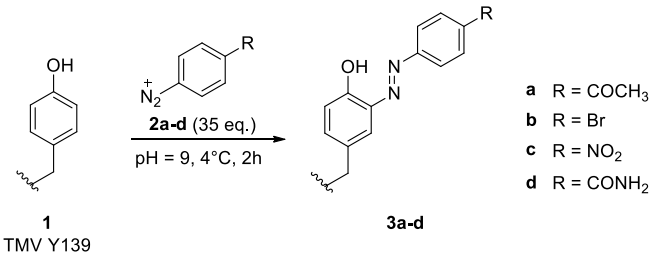

Scheme 1. Exterior modification of tyrosine 139 on TMV capsid.

In particular, coupling with *p*-aminoacetophenone diazonium salt **2a** provided a convenient functionalization site, i.e. carbonyl group, for further conjugation of TMV capsid *via* a "click-type" oxime bond formation with several alkoxyamines (Scheme 2). Adduct **5e-i** were obtained in quantitative yields and the synthetic strategy was carried out without disrupting the viral capsid integrity.

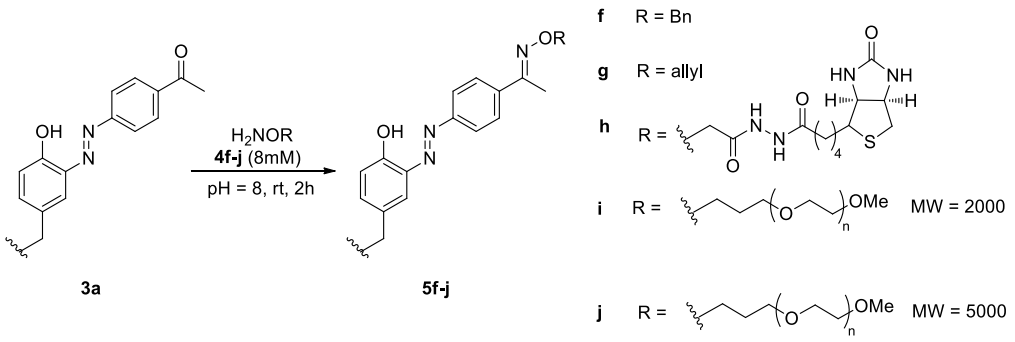

Scheme 2. Oxime bond formation on functionalized tyrosine 139 **3a**.

Moreover, Wang and co-workers reported that tyrosine 139 coupling with diazonium salt **3e** enabled another "click" reaction to take place, more precisely the Cu^{I}-catalyzed azide-alkyne 1,3-dipolar cycloaddition (CuAAC) or Huisgen reaction (Scheme 3).[46]

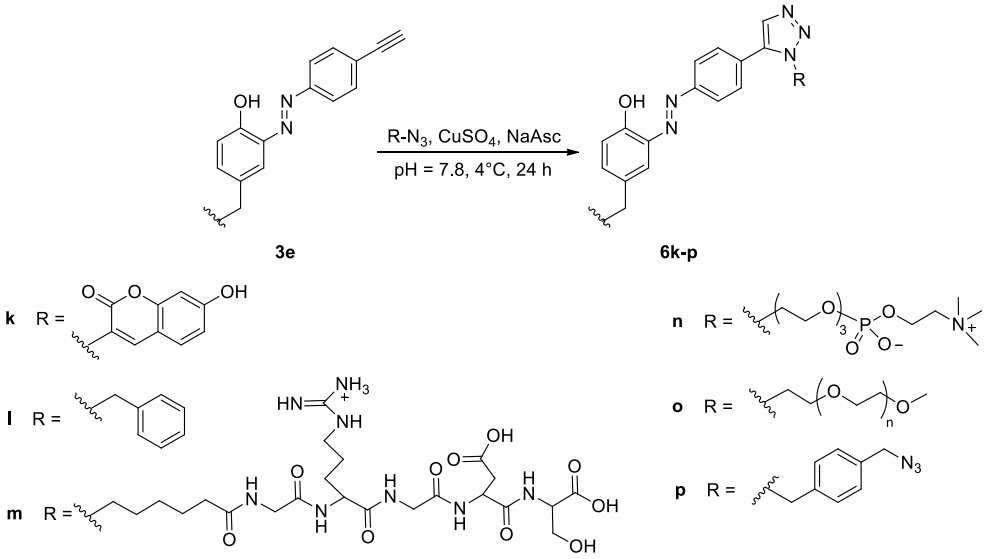

Scheme 3. CuAAC reaction on modified tyrosine 139 **3e**.

Therefore, "click chemistry" in general and CuAAC reactions in particular have been widely used to incorporate diverse functionalities on a wide range of synthetic and biological scaffolds and have given a deep contribute in the development of highly functionalized polymers and polyvalent systems.

2.1.1 "Click chemistry" for molecular scaffolds functionalization

The term "click chemistry" was coined for the first time by Sharpless and co-workers to indicate a synthetic approach for the production of compounds, by joining small units together with heteroatom links (C-X-C), with the final goal of developing a large set of modular and selective building blocks, which can be used in a wide variety of applications.[47]

[46] M. A. Bruckman, G. Kaur, L. A. Lee, F. Xie, J. Sepulveda, R. Breitenkamp, X. Zhang, M. Joralemon, T. P. Russell, T. Emrick, Q. Wang *ChemBioChem* **2008**, *9*, 519-523.
[47] H. C. Kolb, M. G. Finn, K. B. Sharpless *Angew. Chem. Int. Ed.* **2001**, *40*, 2004–2021.

For Sharpless and his collaborators, in order for a process to be named as "click", it has to meet a set of stringent criteria: *the reaction must be modular, wide in scope, give very high yields, generate only inoffensive by-products, that can be removed by non-chromatographic methods and be stereospecific*. Moreover, the process must include *simple reaction conditions, readily available starting materials and reagents*, together with *the use of no solvent or a solvent that is benign (such as water) or easily removed, and simple product isolation*.

In this category, several reactions can be included, such as nucleophilic ring opening reactions (epoxides, aziridines, aziridinium ions), non-aldol carbonyl chemistry (ureas, oximes, hydrazones syntheses), C-C multiple bond additions (oxidative addition, Michael additions of Nu-H reactants) and cycloadditions (1,3-dipolar cycloaddition and Diels-Alder reactions), as depicted in scheme 4.[48]

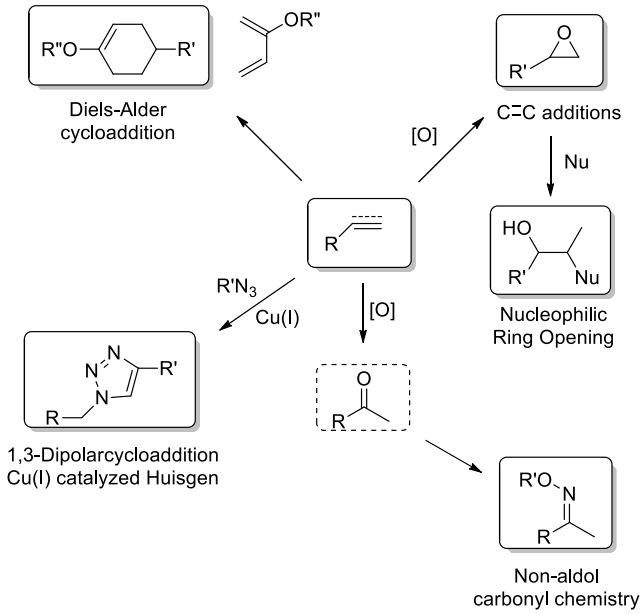

Scheme 4. Examples of reactions that meet "click chemistry" criteria.

Applications of "click chemistry" in material sciences span from dendrimer synthesis,[49] to the design of macrocyclic polymer structures,[50] stabilization of cross-linking in organogel formation,[51] syntheses of high soluble single wall carbon nanotubes (SWCNTs),[52] water soluble calixarenes for molecular

[48] J. E. Moses, A. D. Moorhouse *Chem. Soc. Rev.* **2007**, *36*, 1249-1262.
[49] P. Wu, A. K. Feldman, A. K. Nugent, C. J. Hawker, A. Scheel, B. Voit, J. Pyun, J. M. J. Fréchet, K. B. Sharpless, V. V. Fokin *Angew. Chem. Int. Ed.* **2004**, *43*, 3928-3932.
[50] B. A. Laurent, S. M. Grayson *J. Am. Chem. Soc.* **2006**, *128*, 4238-4239.
[51] D. D. Diaz, K. Rajagopal, E. Strable, J. Schneider, M. G. Finn *J. Am. Chem. Soc.* **2006**, *128*, 6056-6057.
[52] H. Li, F. Cheng, A. M. Duft, A. Adronov *J. Am. Chem. Soc.* **2005**, *127*, 14518-14524.

recognition in water[53] and rotaxanes.[54] In all the examples listed above, Huisgen cycloaddition was involved. However, oxime bond formation is as well an important and recurring "click-type" reaction, especially in bioconjugation, that is the covalent attachment of synthetic residues to biomolecular frameworks, as already seen for TMV modification.[5]

Oxime bond formation has the advantage that no other reagents are required, except for the reacting partners. Therefore, it represents an attractive method to form site-specific bioconjugates. Examples include the synthesis of polysaccharides–b-PEG block copolymers for material sciences and drug delivery applications,[55] large protein-like molecules, as in the case of polyoximes,[56] protein-polymer conjugates,[57] glycopeptide mimetics[58] and oligonucleotide conjugates.[59]

Generally, formation of an oxime bond involves a condensation reaction between a carbonyl group, aldehyde or ketone, with an alkyl- or phenyloxyamine (Scheme 5). The reaction is usually quantitative with no side products formed. Moreover, oxime bond formation is a robust, stable, chemoselective reaction, it is tolerant of a wide range of functional groups and does not require any anhydrous conditions, excessive heat or even any catalyst and it is quite irreversible, having a greater hydrolytic stability than the corresponding hydrazones ($R_{=}NNR^2R^1$).[60]

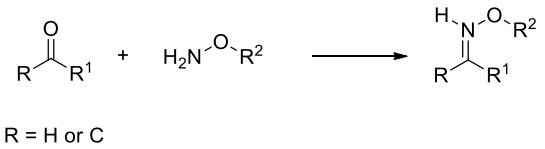

Scheme 5. General oxime bond formation.

Thus, "click-type" oxime bond formation represents a feasible and attractive way to attach different functionalities on specific systems. Its chemoselectivity and stability make this modification very interesting for the easy decoration of synthetic and biological scaffolds. In addition, besides their synthetic importance, oximes are very useful synthones, as they can be successfully transformed into amides, amines, hydroxylamines, hydroxylamine *O*-ethers, nitroalkanes, 1,3-oxazoles, -thiazoles and -diazoles.[61]

---

[53] E.-H. Ryu, Y. Zhao *J. Org. Lett.* **2005**, *7*, 1035-1037.
[54] V. Aucagne, K. D. Hänni, D. A. Leigh, P. J. Lusby, D. B. Walker *J. Am. Chem. Soc.* **2006**, *128*, 2186-2187.
[55] R. Novoa-Carballal, A. H. E. Müller *Chem. Commun.* **2012**, *48*, 3781–3783.
[56] K. Rose, W. Zeng, P.-O. Regamey, I. V. Chernushevich, K. G. Standing, H. F. Gaertner *Bionconjugate Chem.* **1996**, *7*, 552-556.
[57] K. L. Heredia, Z. P. Tolstyka, H. D. Maynard *Macromolecules* **2007,** *40,* 4772-4779.
[58] S. Peluso, B. Imperiali *Tetrahedron Lett.* **2001**, *42*, 2085-2087.
[59] M. Karskela, M. Helkearo, P. Virta, H. Lönnberg *Bionconjugate Chem.* **2010,** *21,* 748–755.
[60] J. Kalia, R. T. Raines *Angew. Chem. Int. Ed.* **2008**, *47*, 7523 –7526.
[61] (a) I. Damljanović, M. Vukićević, R. D. Vukićević *Monatshefte für Chemie* **2006**, *137*, 301–305. (b) R. P. Frutos, D. M. Spero DM *Tetrahedron Lett.* **1998**, *39*, 2475-2478. (c) S. Sasatani, T. Miyazak, K. Maruoka, H. Yamamoto *Tetrahedron Lett.* **1983**, 24, 4711-4712. (d) S. Negi, M. Matsukura, M. Mizuno, K. Miyake *Synthesis*, **1996**, 991-996. (e) H. Miyabe, C. Ushiro, T. Naito *Chem. Commun.* **1997**, 1789-1790. (f) D. S. Bose, G. Vanajatha *Synth. Commun.* **1998**, *28*, 4531-4535. (g) K. Bourgrin, A. Loupy, M. Soufiaoui *Tetrahedron* **1998**, *54*, 8055-8064.

2.2 Synthesis of amine triphenolate ligands

In the view of designing a new class of self-assembled molecular scaffolds based on metal coordination complexes, the development of suitable and functional ligands is essential for the construction of more complex platforms.

Triphenolamines (TPA, **LH_3**) represent a class of highly modular and symmetric ligands, which are able to coordinate to a wide variety of transition metal ions, leading to very robust and stable complexes (Figure 2).

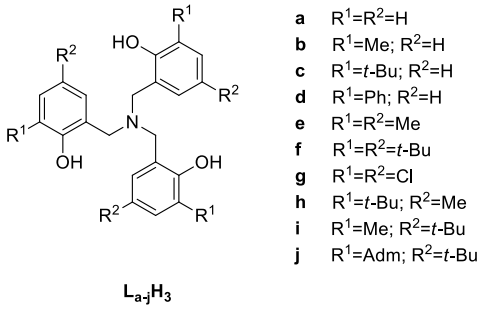

Figure 2. Structure of *tri*-phenolamines **$L_{a\text{-}j}H_3$**.

TPAs were firstly synthesized in 1922 from the natural product salicin (Figure 3), a benzyl alcohol β-glycoside, extracted from willow bark, that was converted to the corresponding benzyl bromide and reacted with ammonia.[62]

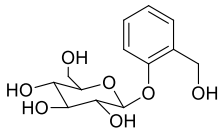

Figure 3. Structure of salicin.

Lately, another strategy was developed, which was based on Mannich reaction of *ortho*, *para*-disubstituted phenols with hexamethylentetramine.[22b,63,64] The reaction can be applied only to *ortho*, *para*-disubstituted phenols (Scheme 6). It consists in a one-step reaction from the phenol to the ligand and it affords the products in quite good yields (40-70%). However, it is not satisfactory in terms of long reaction times, up to two weeks, and harsh reaction conditions.

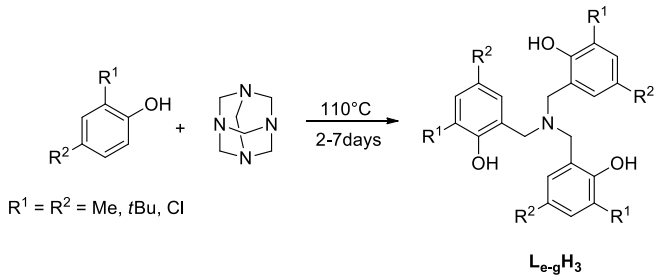

Scheme 6. Synthesis of triphenolamines **$L_{e\text{-}g}H_3$** *via* Mannich reaction.

[62] (a) G. Zemplén, A. Kunz *Chem. Ber.* **1922**, *55*, 979-922. (b) K. Hultzsch *Chem. Ber.* **1949**, *82*, 16-25.
[63] A. Chandrasekaran, R. O. Day, R. R. Holmes *J. Am. Chem. Soc.* **2000**, *122*, 1066-1072.
[64] J. Hwang, K. Govindaswamy, S. A. Koch *Chem. Commun.* **1998**, 1667-1668.

In order to overcome these problems, another synthetic strategy has been set up. It is based on a nucleophilic substitution (S_N2) of a 2-methoxybenzylamine with two equivalents of 2-methoxybenzylbromide.[24] Protection of the phenolic groups is necessary in order to have reasonable yields; the protecting group is then removed by refluxing the product in $AlCl_3$ (Scheme 7). For the synthesis of ligand $\mathbf{L_aH_3}$ a 56% overall yield has been observed.

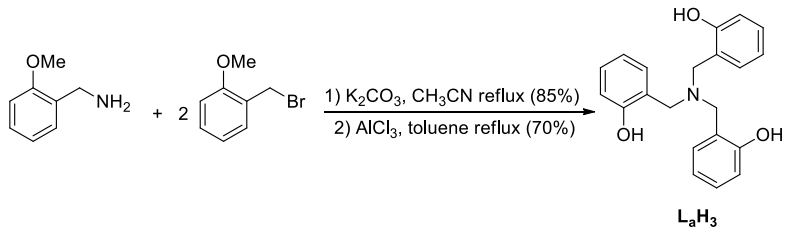

Scheme 7. Synthesis of triphenolamine $\mathbf{L_aH_3}$ *via* S_N2.

This procedure enables the synthesis of triphenolamines starting from two different reaction partners, thus offering the possibility to prepare unsymmetric TPAs, while it can be less practical for the synthesis of symmetric ligands. However, it has been also used for the synthesis of enantiopure amine triphenolate ligands.[65] In this case, a chiral imine is reduced to a secondary amine. Then it is converted to a primary amine by oxidation with $Pd(OAc)_4$, followed by hydrolysis. Finally, the primary amine is reacted with two equivalents of 2-benzyloxy-3-bromomethyl-biphenyl, the benzyl protecting groups are removed by hydrogenolysis and the desired enantiopure triphenolamine is then obtained (Scheme 8).

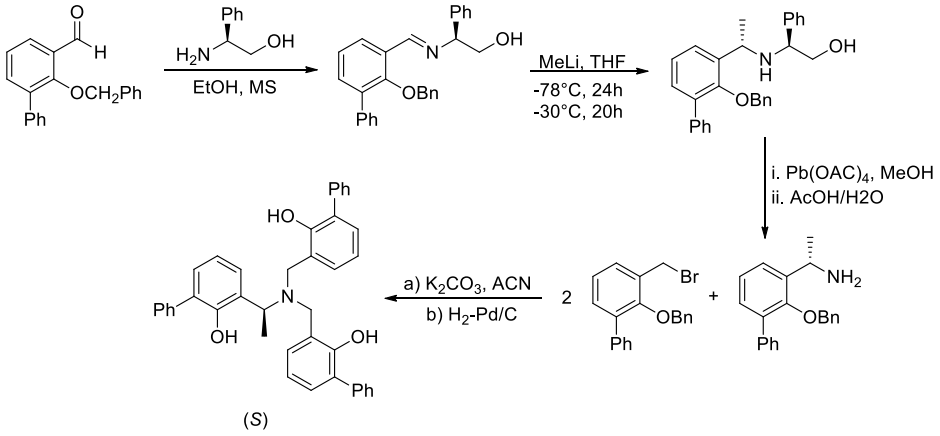

Scheme 8. Synthesis of enantiopure triphenolamine.

More recently, in our group another strategy for the synthesis of C_3-symmetric TPAs was developed.[66] The crucial step is a three-fold reductive amination starting from *ortho*-sustituted salicylic aldehydes using NH_4AcO as nitrogen source and $NaBH(AcO)_3$ as reducing agent. Salicylic aldehydes can be

[65] (a) G. Bernardinelli, D. Fernandez, R. Gosmini, P. Meier, A. Ripa, P. Schüpfer, B. Treptow, E. P. Kündig *Chirality* **2000**, *12*, 529-539. (b) E. P. Kündig, C. Botuha, G. Lemercier, P. Romanens, L. Saudan, S. Thibault *Helv. Chim. Acta* **2004**, *87*, 561-579.

[66] L. J. Prins, M. Mba Blázquez, A. Kolarović, G. Licini *Tetrahedron Lett.* **2006**, *47*, 2735-2738.

either purchased commercially or prepared from the corresponding phenols **7a-d**, protected as benzyl ethers. Benzyl protecting groups facilitate the crystallization of the intermediates and their purification and can be easily removed in the final step *via* hydrogenolysis (Scheme 9).

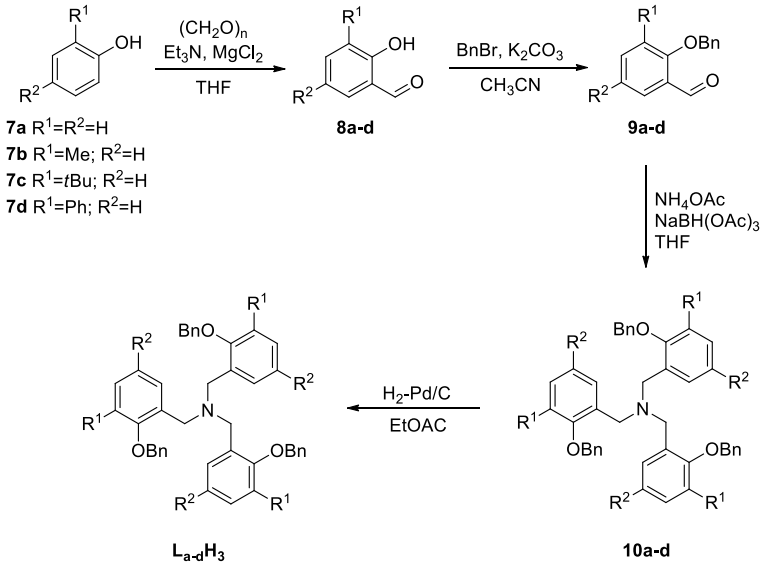

Scheme 9. Synthesis of triphenolamines $\mathbf{L_{a\text{-}d}H_3}$ *via* three-fold reductive amination.

Moreover, in order to expand the scope of TPA synthesis and to study the effect of substituents on the aromatic rings, the well-established three-fold reductive amination was also used in our group to generate a new class of triphenolamines, which bear different substituents in *meta* position on the peripheral aryl rings in *ortho* position to the phenolate. The synthetic strategy we developed uses *ortho*-iodo phenol **11** as starting material, which is firstly formylated in the *ortho* position. The phenolic group on salicylic aldehyde **12** is then protected as methoxymethylether by reaction with MOMCl. The intermediate **13** undergoes a three-fold reductive amination, as described above. The three-iodo protected *tri*-phenolamine **14** is then reacted through a Suzuki coupling reaction with commercially available 3-formyl boronic acid.[67] The MOM group on **15** is then removed by hydrolysis, to give the final triphenolamine **16** (Scheme 10).

[67] (a) N. Miyaura, K. Yamada, A. Suzuki *Tetrahedron Lett.* **1979**, *20*, 3437-3440. (b) N. Miyaura, A. Suzuki *J. Chem. Soc., Chem. Commun.* **1979**, 866-867. (c) K. C. Nicolau, R. M. Evans, A. Roecker, R. Hughes, M. Downes, J. A. Pfefferkorn *Org. Biomol. Chem.* **2003**, *1*, 908-920.

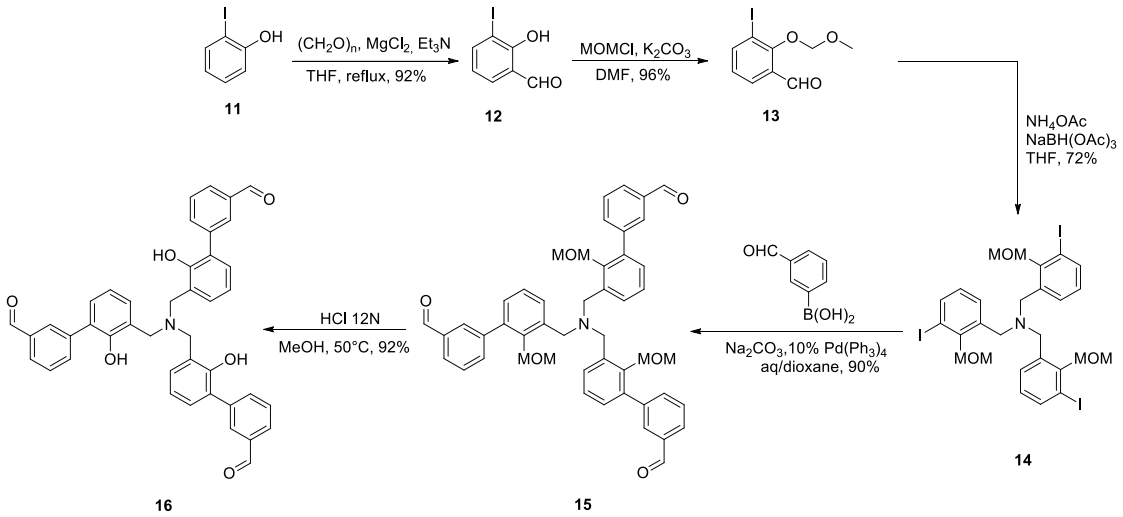

Scheme 10. Synthesis of triphenolamine **16** *via* Suzuki coupling reaction.

2.3 Functionalization of amine triphenolate ligands

The need for developing new active catalysts and multifunctional molecular scaffolds based on metal complexes supposes the design of functionalized ligands that present specific anchoring sites for further derivatization of the systems.

In the field of amine triphenolate ligands functionalization, we wanted to take advantage of the established "click-type" oxime bond formation, that was used for functionalizing exterior surface of TMV coat protein,[5] to decorate our ligands. In order to do so, a previous modification of TPA skeleton was necessary. Thus, we effected an efficient and selective three-fold *para* formylation on triphenolamines $\mathbf{L_{c,d}H_3}$, through the so-called Duff reaction.[68] The method allows the introduction of three aldehyde groups on TPA *para* position to the phenolate upon reaction of $\mathbf{L_{c,d}H_3}$ with hexamethylenetetramine in trifluoroacetic acid (TFA) in very high yields (Scheme 11).

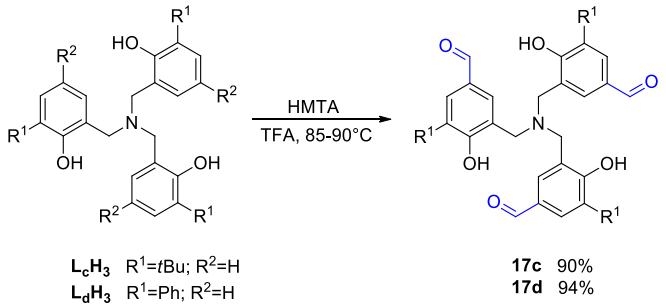

Scheme 11. Duff reaction on TPAs $\mathbf{L_{c,d}H_3}$.

The optimization of formylation reaction has been set up, as depicted in Table 1, by firstly carrying out the reaction using microwave irradiation and then

[68] (a) J. C. Duff, E. J. Bills *J. Chem. Soc.* **1945**, 276-277. (b) A. L. Kurlovich, V. A. Tarasevich, N. G. Kozlov *Russ. J. Org. Chem.* **2009**, *45*, 1503-1508.

by decreasing the amount of TFA, which is both solvent and reagent in the reaction.

Table 1. Optimization of Duff reaction on $\mathbf{L_{c,d}H_3}$.

Entry	R^1	Substrate [M]	T [°C]	Time	Yield [%]
1	Ph	0.05	90	7d	80
2	Ph	0.05	120[a]	4h	70
3	Ph	0.1	90	48h	85
4	Ph	0.33	90	12h	90
5	*t*-Bu	0.05	90	48h	80
6	*t*-Bu	0.33	90	12h	94

[a]Reaction carried out under microwave irradiation at 60 W.

As it can be appreciated from Table 1, a significant acceleration of the reaction has been observed when the amount of TFA is decreased, together with a sensitive increase in yield. Moreover, when microwave irradiation is used, the reaction is much faster, even if not so effective in yield.

The three formyl moieties introduced are very reactive and can be transformed into a wide variety of functional groups, such as alcohols, imines or even into amines, by imines reduction. However, the reaction we were interested in is the formation of an oxime by reaction of the aldehydes with an alkoxyamine, as already seen in scheme 5.

There are several ways to synthesize alkoaxyamines,[69] such as an hydroxyl group amination, in which *N*-protected hydroxylamine derivatives are object of nucleophilic substitution reactions (Scheme 12). However, an electrophilic reagent, such as an appropriately substituted oxaziridine, is required.[29e,f]

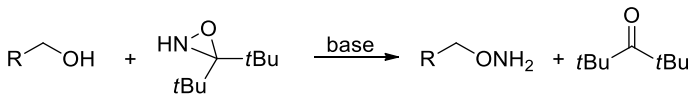

Scheme 12. Synthesis of alkoxyamines based on hydroxyl group amination.

In order to functionalize our systems, we chose another interesting route for alkoxyamine synthesis, which regards an hydroxyl group displacement based on

[69] (a) J. N. Kim, K. M. Kim, E. K. Ryu *Synth. Commun.* **1992**, *22*, 1427–1432. (b) D. S. Jones, J. R. Hammaker, M. E. Tedder *Tetrahedron Lett.* **2000**, *41*, 1531–1533. (c) L. A. Marcaurelle, Y. Shin, S. Goon, C. R. Bertozzi *Org. Lett.* **2001**, *3*, 3691–3694. (d) M. R. Carrasco, R. T. Brown, I. M. Serafimova, O. Silva *J. Org. Chem.* **2003**, *68*, 195–197. (e) I. C. Choong, J. C. Ellman *J. Org. Chem.* **1999**, *64*, 6528–6529; (f) O. F. Foot, D. W. Knight *Chem. Commun.* **2000**, *11*, 975–976. (g) R. Braslau, A. Tsimelzon, J. Gewandter *Org. Lett.* **2004**, *6*, 2233–2235. (h) R. B. Grubbs, J. K. Wegrzyn, Q. Xia *Chem. Commun.* **2005**, 80–82.

a Mitsunobu-like reaction.[70] In this case, *N*-hydroxyphtalimide displaces the hydroxyl group of an alcohol and the phtalimide group is then cleaved in the presence of hydrazine monohydrate (Scheme 13).[71] Also (*t*-alkoxy)-amines can be synthesized through this procedure, starting from a tertiary alcohol.[72]

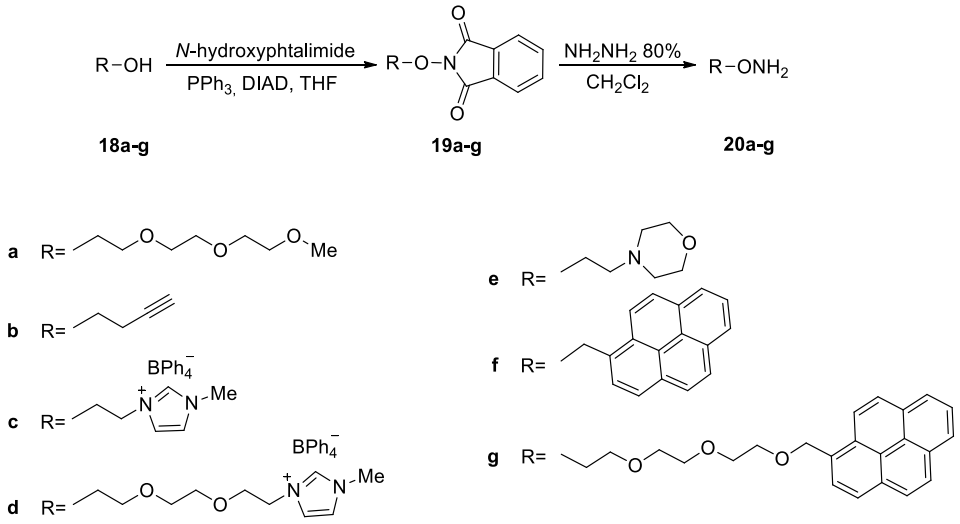

Scheme 13. Synthesis of alkoxyamines *via* Mitsunobu-like reaction.

While alcohols **18a,b** and **18f** were commercially available, the syntheses of **18d-g** were necessary. Alcohol **18c** was obtained by reacting 3-choloro-1-propanol **21** with 1-methyl-1*H*-imidazole **22**.[73] Alcohol **23** in the form of chloride salt underwent an anion exchange reaction with sodium tetraphenylborate, in order to increase its solubility and alcohol **18c** was obtained (Scheme 14).[74]

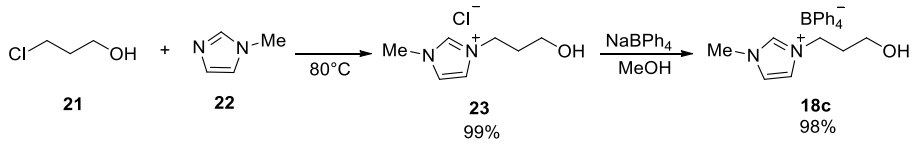

Scheme 14. Synthesis of alcohol **18c**.

Furthermore, 2-(2-(2-Chloroethoxy)ethoxy)ethanol **24** was reacted with 1-methyl-1*H*-imidazole **22** under microwave irradiation.[75] Again, in order to increase

[70] (a) O. Mitsunobu, M. Yamada *Bull. Chem. Soc. Jpn.* **1967**, *40*, 2380-2382. (b) O. Mitsunobu, M. Yamada, M. Teruaki *Bull. Chem. Soc. Jpn*. **1967**, *40*, 935-939. (c) O. Mitsunobu *Synthesis* **1981**, 1-28. (d) M. Karskela, M. Helkearo, P. Virta, H. Lönnberg *Bioconjugate Chem.* **2010**, *21*, 748-755. (e) E. Grochowski, J. Jurczak *Synthesis* **1976**, 682–684. (f) K. C. Nicolaou, R. D. Groneberg *J. Am. Chem. Soc.* **1990**, *112*, 4085–4086. (g) S. Su, J. R. Giguere, S. E., Jr. Schaus, J. A., Jr. Porco *Tetrahedron* **2004**, *60*, 8645–8657.

[71] T. Sasaki, K. Minamoto, H. Itoh *J. Org. Chem.* **1978**, *43*, 2320–2325.

[72] H. Palandoken, C. M. Bocian, M. R. McCombs, M. H. Nantz *Tetrahedron Lett.* **2005**, *46*, 6667-6669.

[73] A. J. Walker, N. C. Bruce *Tetrahedron* **2004**, *60*, 561-568.

[74] S. M. Walter, F. Kniep, L. Rout, F. P. Schmidtchen, E. Herdtweck, S. M. Huber *J. Am. Chem. Soc.* **2012**, *134*, 8507-8512.

[75] J. Fraga-Dubreuil, M.-H. Famelart, J. P. Bazureau *Organic Process Research & Development* **2002**, *6*, 374-378.

alcohol solubility, an anion exchange reaction with sodium tetraphenylborate on chloride salt **25** was performed, giving rise to alcohol **18d** (Scheme 15).[34]

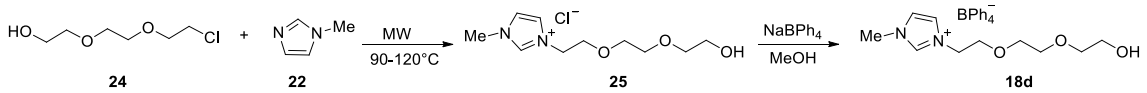

24 **22** **25** **18d**

Scheme 15. Synthesis of alcohol **18d**.

In the case of alcohol **18e**, it was successfully synthesized by reacting 3-chloro-1-propanol **21** with morpholine **26** in dry toluene (Scheme 16).[76]

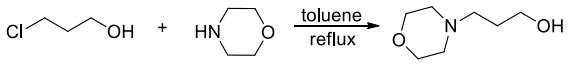

21 **26** **18e**
86%

Scheme 16. Synthesis of alcohol **18e**.

Finally, alcohol **18g** was synthesized starting from 1-hydroxymethylpyrene **27**, which was transformed into the corresponding bromide upon reaction with PBr_3.[77] Successively, (1-bromomethyl)pyrene **28**, *via* nucleophilic substitution with triethylene glycol, gave the desired alcohol **18g** (Scheme 17).[78]

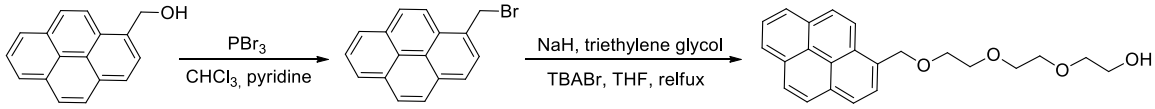

27 **28**
94%
18g
55%

Scheme 17. Synthesis of alcohol **18g**.

Alkoxyamine **20h**, bearing pyrene moieties, was synthesized *via* a different route: a Mitsunobu-like reaction on triethylene glycol **29** was carried out, in which both alcoholic residues were substituted. The phtalimide groups on **30** were then removed, giving rise to the *bis*-alkoxyamine **31**. A first oxime bond on **31** was effected upon reaction with 1-pyrenecarboxaldehyde **32**. In this case, the reaction was not quantitative, as product **33**, which came from double functionalization of **31**, was also formed together with alkoxyamine **20h** (Scheme 18).

[76] P. A. Plé, T. P. Green, L. F. Hennequin, J. Curwen, M. Fennell, J. Allen, C. Lambert-van der Brempt, G. Costello *J. Med. Chem.* **2004**, *47*, 871-887.
[77] S. Akiyama, K. Nakasuji, M. Nakagawa *Bull. Chem. Soc. Jpn.* **1971**, *44*, 2231-2236.
[78] M. A. Pilkington-Miksa, S. Sarkar, M. J. Writer, S. E. Barker, P. Ayazi Shamlou, S. L. Hart, H. C. Hailes, A. B. Tabor *Eur. J. Org. Chem.* **2008**, 2900–2914.

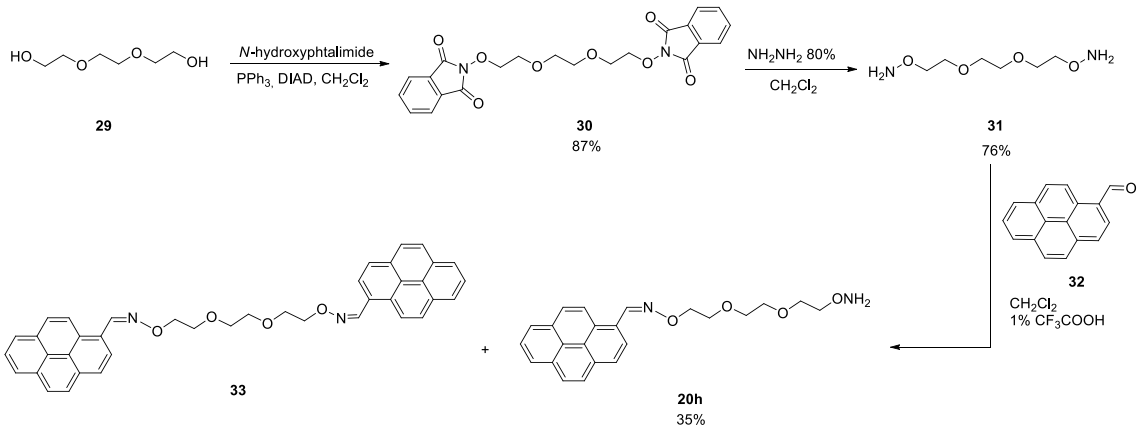

Scheme 18. Synthesis of alkoxyamine **20h**.

Thus, we were able to generate a small library of alkoxyamines, which were used to functionalize formyl-derived triphenolamines. The functionalization reaction through oxime bond formation involved both derivatization of *para* position to the phenolate on TPAs **17c** and **17d**, as well as *meta* positions on the peripheral aromatic rings on TPA **16**. The reactions were carried out by using a catalytic amount of CF_3COOH and yielded the functionalized products quantitatively in most of the cases.

Reaction on ligand **17c** was performed by using alkoxyamine **20f** and in this way functionalized TPA **34f** was obtained (Figure 4).

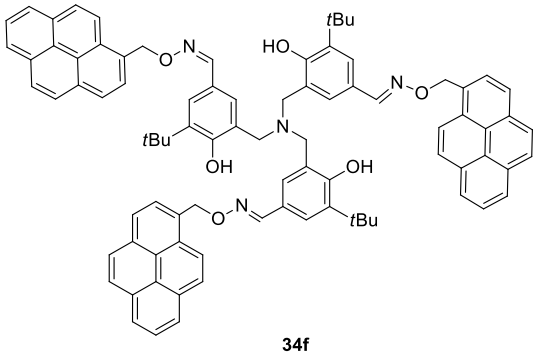

Figure 4. Functionalized TPA **34f**.

In the case of TPAs bearing a phenyl group in *ortho* position to the phenolate, functionalization with alkoxyamines **20a-e** and **20h** lead to the synthesis of highly functionalized TPAs **35a-e** and **35h** (Figure 5).

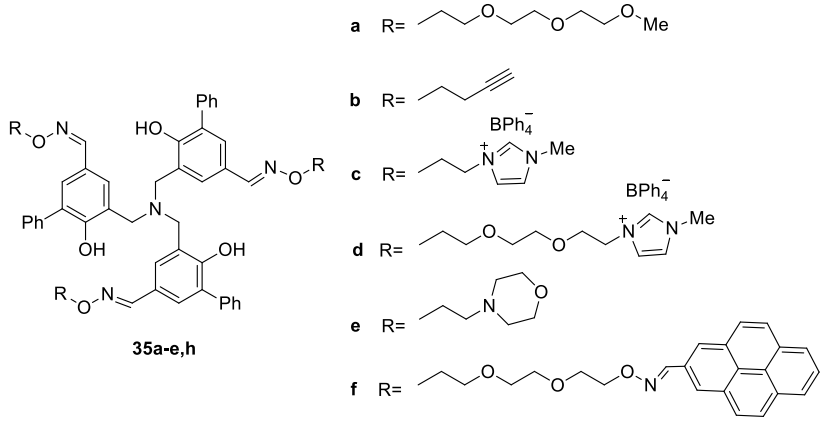

Figure 5. Synthesis of highly functionalized TPAs **35a-e** and **35h**.

The robust and tunable nature of amine triphenolate systems was confirmed also by further modifying the functionalized TPAs, as in the case of TPA **35e**, which was subjected to an *N*-methylation in presence of methyl iodide (Scheme 19).[79]

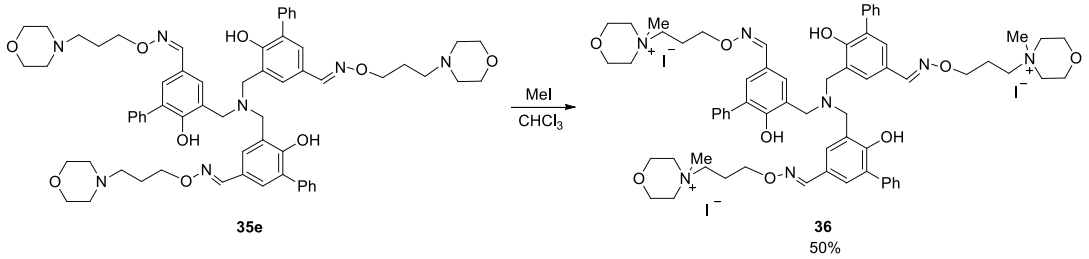

Scheme 19. *N*-Methylation on TPA **35e**.

Finally, the *meta* positions on TPA **16** were functionalized as well and TPAs **37a-c** and **37f** were obtained (Figure 6).

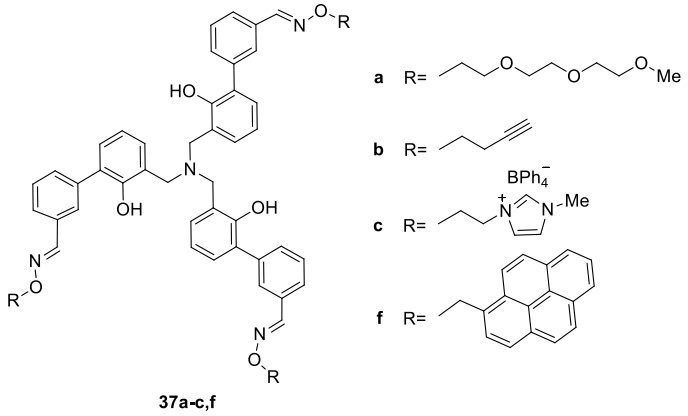

Figure 6. Synthesis of highly functionalized TPAs **37a-c** and **37f**.

The feasibility of functionalization strategy was much more evident when an six-fold modification of TPA systems was performed. Firstly, MOM protected TPA **15** was decorated with three additional formyl groups, through the Duff

[79] C. Hedberg, F. J. Dekker, M. Rusch, S. Renner, S. Wetzel, N. Vartak, C. Gerding-Reimers, R. S. Bon, P. I. H. Bastiaens, H. Waldmann *Angew. Chem Int. Ed.* **2011**, *50*, 9832-9837.

reaction seen above. The acidic reaction conditions made it possible also to remove the protecting groups, so the six-fold formyl TPA **38** could be obtained. Moreover, reaction with six equivalents of alkoxyamine **20a** lead to the formation of the six-fold TEG-functionalized amine triphenolate ligand **39** (Scheme 20).

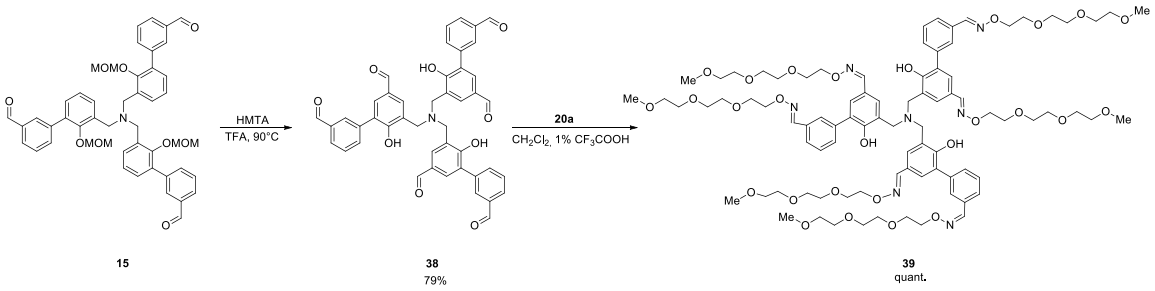

Scheme 20. Orthogonal modification of TPA ligands.

2.4 Conclusions

The development of a new synthetic strategy for the synthesis of highly functionalized amine triphenolate ligands has been set up. The introduction of aldehyde groups in *para* position to the phenolate, *via* Duff reaction, or in *meta* position on the peripheral aryl rings, *via* Suzuki coupling reaction, enabled us to introduce a wide variety of functionalities through a "click-type" oxime bond formation. The robustness of amine triphenolate ligands, together with the high stability of oxime bond, made it possible to generate highly decorated ligands whose coordination ability with titanium and vanadium ions, for the realization of new multifunctional molecular scaffolds and catalysts, will be analysed in the next chapters.

2.5 Experimental

General remarks

Chemicals and dry solvents were purchased from Sigma Aldrich and used without further purification. Where "degassed" solvents or solutions are noted, degassing was carried out by three freeze-pump-thaw cycles. Flash chromatography (FC) was performed as described in literature[80] using Macherey-Nagel silica gel 60 (0.04-0.063 mm, 230-400 mesh). TLC analyses: Macherey-Nagel POLYGRAM® SIL G/UV_{254}; detection by UV/VIS and by treatment with PMA staining reagent made from a solution of phosphomolibdic acid ($H_3PMo_{12}O_{40,}$ 10 g) in 100 mL ethanol. ^1H and $^{13}C\{^1H\}$-NMR spectra were recorded at 301K on Bruker AC-200, 250, 300 MHz instruments. Chemical shifts (δ) have been reported in parts per million (ppm) relative to the residual undeuterated solvent as an internal reference ($CDCl_3$: 7.26 ppm for ^1H-NMR and 77.0 ppm for ^{13}C NMR; CD_3OD: 3.31 ppm for ^1H-NMR and 49.05 ppm for ^{13}C-NMR; CD_3CN: 1.94 ppm for ^1H-NMR and 118.26 ppm for ^{13}C NMR) or tetramethylsilane. The following abbreviations have been used to explain the multiplicities: *s* = singlet, *d* = doublet, *t* = triplet, *dd* = doublet, doublet, *m* = multiplet, *br* = broad. ^{13}C-NMR spectra have been recorded with complete proton decoupling. ESI-MS spectra have been obtained on a LC/MS Agilent series 1100 spectrometer in both positive and negative modes using acetonitrile/formic acid 0.1% as mobile phase, with ESI-ion trap mass detector. In some cases, an ESI-TOF Mariner™ Biospectrometry™ Workstation of Applied Biosystems by flow injection, using acetonitrile or methanol/formic acid 0.1% as mobile phase, was used. Analytical gas chromatography with mass spectrometry detector (GC-MS) has been carried out on a Agilent 6850 spectrometer equipped with a split mode capillary injector and electron impact mass detector. Injector temperature has been set to 250 °C, detector temperature has been set to 280 °C and the carrier gas is He (1 mL/min) with a HP-5MS column. Melting points are uncorrected and have been determined with a Leitz-Laboroux 12. IR spectra have been recorded on a Nicolet 5700 FT-IR, with range 4000-400 cm^{-1} and resolution 4 cm^{-1}, using KBr pellets or NaCl plates. Microwave reactions were performed in 10 mL sealed tubes in a regularly calibrated CEM Discover focused 300 W microwave reactor with IR temperature monitoring and non-invasive pressure transducer.

Ortho substituted 2-hydroxybenzaldehydes (8)

Commercially available *ortho* substituted 2-hydroxybenzenes **7c-d** (294.12 mmol), triethylamine (588.24 mmol) and magnesium chloride (382.35 mmol) were dissolved in dry THF (600 mL) and stirred for 30 min. Paraformaldheyde (150 mg/mmol sub.) was then added and the mixtures were refluxed for 12h. The reaction mixtures were cooled at room temperature, after which HCl_{aq} 1N (900 mL) was added and the producte were extracted with EtOAc (2 x 600 mL). The residues

[80] C. W. Still, M. Khan, A. Mitra *J. Org. Chem.* **1978**, *43*, 2923-2925.

were dried over anhydrous Na_2SO_4 and evaporated to dryness. The crude products were purified by distillation using Kugelrohr apparatus.

8c: yellow oil. Yield: 84%. IR (NaCl) ν (cm^{-1}): 752, 854, 930, 1091, 1197, 1266, 1312, 1386, 1432, 1453, 1483, 1588, 1612, 1653, 2744, 2872, 2912, 2960, 3000. ^{1}H-NMR: (200 MHz, $CDCl_3$) δ 11.78 (1H, *s*), 9.88 (1H, *s*), 7.53 (1H, *d*, *J* = 8 Hz), 7.40 (1H, *d*, *J* = 8 Hz), 6.95 (1H, *t*, *J* = 8 Hz), 1.42 (9H, *s*). ^{13}C{^{1}H}-NMR: (75.5 MHz, $CDCl_3$) δ 198.60 (CHO), 162.70 (C), 139.81 (C), 135.57 (CH), 133.46 (CH), 122.16 (C), 120.71 (CH), 36.32 (C), 30.70 (3xCH_3). MS (GC-MS): *m/z* calc. 178.10; exp. 178 $[M]^+$.

8d: yellow solid. Yield: 84%. IR (KBr) ν (cm^{-1}): 701, 795, 1026, 1097, 1215, 1302, 1452, 1612, 2740, 2830, 3054, 3221. ^{1}H-NMR: (250 MHz, $CDCl_3$) δ 11.53 (1H, *s*), 9.96 (1H, *s*), 7.60 (1H, *d*, *J* = 6.5 Hz), 7.55 (1H, *d*, *J* = 5.75 Hz), 7.49-7.37 (5H, *m*), 7.109 (1H, *t*, *J* = 7.5 Hz). ^{13}C{^{1}H}-NMR: (75.5 MHz, $CDCl_3$) δ 198.30 (CHO), 160.40 (C), 139.29 (CH), 137.80 (C), 134.46 (CH), 130.86 (CH), 130.10 (2xCH), 129.16 (2xCH), 128.64 (C), 121.76 (CH). MS (GC-MS): *m/z* calc. 198.07; exp. 198 $[M]^+$ (100 %), 169 [M - CHO]$^+$ (23.42).

***Ortho* substituted 2-(Benzyloxy) benzaldehydes (9)**

Ortho substituted 2-hydroxybenzaldehydes **8c-d** (31.08 mmol), K_2CO_3 (124.32 mmol), and benzyl bromide (33.87 mmol) were dissolved in dry CH_3CN (62 mL) and refluxed for 18 h. The mixtures were filtered through Celite, washed with ethyl acetate and the filtrates were concentrated under reduced pressure. Product **9c** was used without any further purification, while product **9d** was purified from crystallization in hexane.

9c: yellow oil. Yiled: 99%. IR (NaCl) ν (cm^{-1}): 695, 732, 760, 1215, 1371, 1581, 1686, 2872, 2961. ^{1}H-NMR: (200 MHz, $CDCl_3$) δ 10.35 (1H, *s*), 7.76 (1H, *dd*, *J* = 8.0, *J* = 2.0 Hz), 7.64 (1H, *dd*, J = 8.0, *J* = 2.0 Hz), 7.54-7.37 (5H, *m*), 7.19 (1H, *t*, *J* = 6 Hz), 5.07 (2H, *s*), 1.45 (9H, *s*). ^{13}C{^{1}H}-NMR: (75.5 MHz, $CDCl_3$) δ 190.78 (CHO), 144.27 (C), 133.83 (2xC), 130.51 (CH), 129.45 (CH), 128.94 (CH), 128.47 (CH), 127.84 (C), 127.32 (CH), 126.95 (CH), 124.39 (CH), 123.99 (CH), 80.39 (CH_2), 76.25 (C), 30.57 (3xCH_3). MS (GC-MS): *m/z* calc. 268.15; exp. 268.1 $[M]^+$ (100%), 177.1 [M - Bn]$^+$ (8%), 91.1 [Bn]$^+$ (5%).

9d: white crystals. Yield: 78%. Mp: 99-101 °C. IR (KBr) ν (cm^{-1}): 695, 743, 769, 803, 868, 918, 1026, 1072, 1173, 1205, 1220, 1245, 1274, 1298, 1373, 1433, 1453, 1497, 1573, 1583, 1683, 1804, 1878, 1901, 1953, 2878, 3032, 3061, 3344. ^{1}H-NMR: (250 MHz, $CDCl_3$) δ 10.31 (1H, *s*), 7.82 (1H, *dd*, *J* = 7.5, *J* = 1.75 Hz), 7.64-7.59 (3H, *m*), 7.50-7.40 (3H, *m*), 7.31-7.23 (4H, *m*), 7.05-7.01 (2H, *m*), 4.52 (2H, *s*). ^{13}C{^{1}H}-NMR: (62.9 MHz, $CDCl_3$) δ 190.3 (CHO), 159.2 (C), 137.3 (CH), 137.2 (C), 136.4 (C), 135.5 (C), 130.2 (C), 129.2 (2xCH), 128.7 (2xCH), 128.6 (2xCH), 128.53 (2xCH), 128.49 (CH), 127.9 (CH), 127.4 (CH), 124.7 (CH), 77.1 (CH_2). MS (GC-MS): *m/z* calc. 288.12; exp. 288 $[M]^+$ (9.25%), 259 [M - CHO]$^+$ (16.6%), 91 [Bn]$^+$ (100%).

***Ortho* substituted *tris*-(2-benzyloxy benzyl)amines (10)**

To a solution of *ortho* substituted 2-(benzyloxy) benzaldehydes **9c-d** (261.2 mmol) in dry THF (520 mL) ammonium acetate (73.13 mmol) was added and the mixtures were stirred for 40 min. Then sodium triacetoxy borohydride (334.32 mmol) was added and the mixtures were stirred for 48 h at room temperature and then evaporated to dryness. The residues were dissolved in EtOAc (130 mL) and washed with KOH_{aq} 10% (2 x 30 mL) and brine (2 x 30 mL). The residues were dried over anhydrous Na_2SO_4 and evaporated to dryness. The crude products were purified by precipitation in acetonitrile.

10c: white solid. Yield: 65%. Mp: 101°C. IR (KBr) ν (cm^{-1}): 728, 756, 1020, 1215, 1433, 2957, 3030. ^{1}H-NMR: (200 MHz, $CDCl_3$) δ 7.69 (3H, *dd*, *J* = 8.0, *J* = 2.0 Hz), 7.39-7.27 (15H, *m*), 7.45 (3H, *dd*, *J* = 8.0, *J* = 2.0 Hz), 7.06 (3H, *t*, J = 8 Hz), 4.73 (6H, *s*), 3.62 (6H, *s*), 1.37 (27H, *s*). ^{13}C{^{1}H}-NMR: (75.5 MHz, $CDCl_3$) δ 151.11 (3xC), 142.75 (3xC), 137.71 (3xC), 133.57 (3xCH), 128.79 (3xCH), 128.56 (3xCH), 128.47 (3xCH), 127.59 (3xCH), 126.97 (3xCH), 125.91 (3xCH), 123,94 (3xCH), 75.49 (6xCH_2), 52.61 (6xCH_2), 35.31 (3xC), 31.29 (9xCH_3). MS (ESI): *m/z* calc. 773.48; exp. 774.5 $[M+H]^+$.

10d: yellow solid. Yield: 84%. Mp: 120-122 °C. IR (KBr) ν (cm^{-1}): 697, 764, 1070, 1202, 1429, 1455, 2927, 3030, 3060. ^{1}H-NMR: (250 MHz, $CDCl_3$) δ 7.82 (1H, *d*, *J* = 6.4 Hz), 7.65-7.62 (2H, *m*), 7.46-7.37 (3H, *m*), 7.32-7.18 (5H, *m*), 7.03-7.00 (2H, *m*), 4.36 (6H, *s*), 3.84 (6H, *s*). ^{13}C{^{1}H}-NMR: (62.9 MHz, $CDCl_3$) δ 154.7 (3xC), 139.0 (3xC), 137.1 (3xC), 135.4 (3xC), 133.8 (3xC), 129.6 (6xCH), 129.5 (3xCH), 128.5 (6xCH), 128.4 (6xCH), 128.3 (6xCH), 128.0 (6xCH), 127.3 (3xCH), 124.6 (3xCH), 75.0 (3xCH_2), 52.9 (3xCH_2). MS (ESI): *m/z* calc. 833.39; exp. 834.4 $[M + H]^+$.

***Ortho* substituted t*ris*-(2-hydroxy benzyl)amines $L_{c\text{-}d}H_3$**

Ortho substituted *tris*-(2-benzyloxy benzyl)amines **10c-d** (5.7 mmol) were dissolved in EtOAc (285 mL) and a catalytic amount of 10% Pd/C was added under nitrogen. A H_2-atmosphere (1 atm) was applied and the reactions were stirred for 4 h at room temperature. The reaction mixtures were filtered through Celite, dried over anhydrous Na_2SO_4 and evaporated to dryness. The crude products were purified by crystallization in acetonitrile, affording the final products as white solids (63%).

L_cH_3: yield: 68%. Mp: 164°C. IR (KBr) ν (cm^{-1}): 745, 788, 1076, 1206, 1436, 2958, 3087, 3546. ^{1}H-NMR: (200 MHz, $CDCl_3$) δ 7.23 (3H, *dd*, *J* = 6.0, *J* = 2.0 Hz), 6.98 (3H, *dd*, *J* = 6.0, *J* = 2.0 Hz), 6.79 (3H, *t*, *J* = 6 Hz), 3.64 (6H, *s*), 1.39 (27H, *s*). ^{13}C{^{1}H}-NMR: (50.3 MHz, $CDCl_3$) δ 154.43 (3xC), 138.04 (3xC), 129.27 (3xCH), 127.71 (3xCH), 122.90 (3xC), 120.30 (3xCH), 56.26 (3xCH_2), 34.56 (3xC), 29.38 (9xCH_3). MS (ESI): *m/z* calc. 503.34; exp. 504 $[M+ H]^+$.

L_dH_3: yield: 63%. Mp: 157-158.5 °C. IR (KBr) ν (cm^{-1}): 693, 751, 1063, 1087, 1191, 1230, 1431, 140, 1591, 1611, 2828, 3028, 3058, 3293 (broad OH). ^{1}H-NMR: (250 MHz, $CDCl_3$) δ 7.49-7.35 (15H, *m*), 7.16 (6H, *m*), 6.88 (6H, *m*), 3.89 (6H, *s*). ^{13}C{^{1}H}-NMR: (62.9 MHz, $CDCl_3$) δ 152.5 (3xC), 137.7 (3xC), 130.4 (3xCH), 130.0 (3xCH), 129.5

(6xCH), 128.9 (6xCH), 128.8 (6xC), 127.6 (3xCH), 123.5 (3xC), 120.1 (3xCH), 55.9 (3xCH_2). MS (ESI): *m/z* calc. 563.25; exp. 564.7 $[M + H]^+$.

***Ortho* substituted *tris*-(5-formyl-2-hydroxy benzyl)amines (17)**

A nitrogen purged Schlenk tube was charged with *ortho* substituted t*ris*-(2-hydroxy benzyl)amines $\mathbf{L_{c\text{-}d}H_3}$ (4.03 mmol) and hexamethylenetetramine (24.2 mmol) and diluted with TFA (3 mL/mmol sub.) and the mixtures were stirred at 90°C for 12h. The crude mixtures were evaporated to dryness and HCl_{aq} 4N (36 mL) was added and the mixtures were stirred for 3 h at 90 °C. The precipitates were filtered off, washed with $NaHCO_3$ and extracted with CH_2Cl_2. The organic phases were dried over anhydrous Na_2SO_4 and evaporated to dryness. The final products were obtained by crystallization in acetonitrile.

17c: yellow solid. Yield: 90%. Mp: 130-145°C. IR (KBr) ν (cm^{-1}): 888, 1133, 1299, 1559, 1684, 2722, 2960, 3397. ^{1}H-NMR: (200 MHz, $CDCl_3$) δ 9.86 (3H, *s*), 7.81 (3H, *s*), 7.58 (3H, *s*), 3.84 (6H, *s*), 1.44 (27H, *s*). $^{13}C\{^1H\}$-NMR: (75.5 MHz, $CDCl_3$) δ 191.82 (3xCHO), 160.19 (3xC), 138.27 (3xC), 131.46 (3xC), 130.62 (3xCH), 129.76 (3xCH), 123.66 (3xC), 56.71 (3xCH_2), 34.48 (3xC), 29.31 (9xCH_3). MS (ESI): *m/z* calc. 587.32; exp. 588 $[M+H]^+$.

17d: yellow solid. Yield: 94%. IR (KBr) ν (cm^{-1}): 579, 616, 699, 735, 778, 805, 893, 983, 1030, 1092, 1151, 1317, 1387, 1425, 1475, 1497, 1585, 1694, 1808, 1891, 1957, 2730, 2831, 3055, 3349, 3521, 3643. ^{1}H-NMR: (200 MHz, $CDCl_3$) δ 9.80 (3H, *s*) 7.67 (3H, *d*, *J* = 2 Hz), 7.64 (3H, *d*, *J* = 2 Hz), 7.46-7.36 (15H, *m*), 4.00 (6H, *s*). $^{13}C\{^1H\}$-NMR: (75.5 MHz, $(CD_3)_2CO$) δ 191.1 (3xCHO), 160.45 (3xC), 138.26 (3xC), 132.96 (6xCH), 132.94 (3xC), 130.49 (6xC), 129.97 (6xCH), 129.42 (3xC), 128.48 (3XC), 126.10 (3xC), 57.13 (6xCH_2). MS (ESI): *m/z* calc. 647.23; exp. 648.2 $[M + H]^+$.

2-Hydroxy-3-iodo-benzaldehyde (12)

2-Iodophenol **11** (55.56 mmol, 12.224 g) was dissolved in dry THF (100 mL) and magnesim chloride (72.23 mmol, 6.878 g) and triethylamine (111.12 mmol, 15.55 mL) were added. After 30 min, paraformaldehyde (8.334 g) was added and the reaction mixture was refluxed for 8h. Then HCl 1N (100 mL) was added and the residue was extracted with EtOAc (3 x 50 mL). The organic phases were washed with $NaCl_{aq}$, dried over anhydrous Na_2SO_4 and concentrated under vacuum. The final product was obtained as a brown solid, after recrystallization in hexane (92%).

IR (KBr) ν (cm^{-1}): 711, 773, 892, 1070, 1118, 1215, 1265, 1298, 1385, 1434, 1468, 1560, 1604, 1705, 1886, 2851, 3063, 3422. ^{1}H-NMR: (250 MHz, $CDCl_3$) δ 11.83 (1H, *s*), 9.77 (1H, *s*), 8.02 (1H, *dd*, *J* = 1.55, *J* = 7.75 Hz), 7.58 (1H, *dd*, *J* = 1.53, *J* = 7.74 Hz), 6.85 (1H, *t*, *J* = 7.76 Hz). $^{13}C\{^1H\}$-NMR: (62.9 MHz, $CDCl_3$) δ 195.9 (CHO), 160.3 (CH), 146.0 (CH), 133.9 (CH), 121.6 (CH), 120.4 (C), 85.4 (C). MS (ESI): *m/z* calc. 248.02; exp. 249 $[M+H]^+$.

3-Iodo-2-(methoxymethoxy)benzaldehyde (13)

2-Hydroxy-3-iodo-benzaldehyde **12** (20.16 mmol, 5 g) was dissolved in dry DMF (14 mL) under a N_2 atmosphere. K_2CO_3 (20.16 mmol, 2.79 g) and MOMCl (20.16 mmol, 1.56 mL) were slowly added and the mixture was stirred for 15 hours. The

reaction mixture was diluted with water (50 mL) and extracted with ethyl acetate (3 x 50 mL). The organic phase was washed with a $NaCl_{aq}$ solution (50 mL), dried over anhydrous Na_2SO_4, filtered and concentrated under vacuum. The product was distilled using Kugelrohr apparatus, affording a dark red oil (77%).

IR (NaCl) ν (cm^{-1}): 754, 844, 923, 984, 1108, 1159, 1228, 1244, 1312, 1400, 1429, 1521, 1558, 1616, 1695, 1844, 1897, 1982, 2075, 2340, 2358, 2739, 2829, 2951, 3006, 3060, 3337. ^{1}H-NMR: (250 MHz, CDCl3) δ 10.28 (1H, *s*), 8.05 (1H, *dd*, *J* = 1.55, *J* = 7.8 Hz), 3.62 (3H, *s*), 7.83 (1H, *dd*, *J* = 1.53, *J* = 7.8 Hz), 7.04 (1H, *t*, *J* = 7.8 Hz), 5.16 (2H, *s*). ^{13}C{^{1}H}-NMR: (62.9 MHz, $CDCl_3$) δ 190.1 (CHO), 160.1 (C), 146.3 (C), 145.5(CH), 128.9 (CH), 126.8 (CH), 101.6 (CH_2), 93.5 (C), 58.6 (CH_3). MS (GC-MS): *m/z* calc. 292.07; exp. 292 $[M]^+$.

***Tris*-(2-(methoxymethoxy)-3-iodobenzyl)amine (14)**

To a solution of 3-iodo-2-(methoxymethoxy)benzaldehyde **13** (28.55 mmol, 8.34 g) in dry THF (16 mL) ammonium acetate (9.06 mmol, 698 mg) was added. After 40 min under stirring, sodium triacetoxy borohydride (40.8 mmol, 8.65 g) was added and the mixture was stirred for 24 h at room temperature and then evaporated to dryness. The residue was dissolved in EtOAc (100mL) and washed with $NaHCO_{3aq}$ solution (2 x 50 mL) and brine (2 x 50 mL). The residue was dried over anhydrous Na_2SO_4 and concentrated under reduced pressure. The crude product was purified by crystallization in acetonitrile, affording a transparent solid (72%).

IR (KBr) ν (cm^{-1}): 733, 770, 797, 945, 1079, 1160, 1290, 1363, 1397, 1444, 1466, 1580, 2340, 2359, 2824, 2887, 2928, 2949, 2979, 3065. ^{1}H-NMR: (250 MHz, $CDCl_3$) δ 7.65 (6H, *dt*, *J* = 6 Hz, *J* = 2 Hz), 6.87 (6H, *t*, *J* = 10 Hz), 4.98 (6H, *s*), 3.72 (6H, *s*), 3.58 (9H, *s*). ^{13}C{^{1}H}-NMR: (62.9 MHz, $CDCl_3$) δ 155.9 (3xC), 138.4 (3xCH), 134.7 (3xC), 130.1 (3xCH), 126.7 (3xCH), 100.5 (3xCH_2), 92.7 (3xC), 58.3 (3xCH_3), 53.0 (3xCH_2). MS (ESI): *m/z* calc. 845.24; exp. 846.0 [M + H]+.

***Tris*-(2-(methoxymethoxy)-3-(3′-formyl)-benzyl)amine (15)**

Tris-(2-(methoxymethoxy)-3-iodobenzyl)amine **14** (2.8 mmol, 2.5 g) and 3-formylphenylboronic acid (16.9 mmol, 2.53 g) were added in a Schlenk tube under nitrogen. Degassed dioxane (31 mL), degassed Na_2CO_{3aq} 2M (40 mL) and $Pd(PPh_3)_4$ (0.28 mmol, 323 mg) were added and the reaction was stirred at 100°C for 15 h. The reaction mixture was cooled down to room temperature, filtered over Celite and then concentrated under vacuum. The residue was diluted with CH_2Cl_2 (50 mL), washed with $NaOH_{aq}$ 1M (2 x 50 mL) and $NaCl_{aq}$ sat. (2 x 50 mL). The organic phase was dried over anhydrous Na_2SO_4, concentrated under reduced pressure and the residue was purified by column chromatography on silica gel (petroleum ether/ethyl acetate 6:4), affording a white powder (62%).

IR (KBr) ν (cm^{-1}): 732, 787, 960, 1067, 1180, 1304, 1401, 1449, 1576, 1600, 1699, 1734, 2724, 2825, 2934, 3058. ^{1}H-NMR: (250 MHz, $CDCl_3$) δ 10.06 (3H, *s*), 8.05 (3H, *s*), 7.87-7.53 (9H, *m*), 7.39 (3H, *t*, *J* = 8 Hz), 7.06 (6H, *m*), 4.55 (6H, *s*), 3.90 (6H, *s*), 3.10 (9H, *s*). ^{13}C{^{1}H}-NMR: (62.9 MHz, $CDCl_3$) δ 184.6 (3xCHO), 153.1 (3xC), 140.0 (3xC),

136.4 (3xC), 135.4 (3xCH), 133.9 (3xC), 133.5 (3xC), 130.8 (3xCH), 129.8 (3xCH), 129.4 (3xCH), 128.9 (3xCH), 128.0 (3xCH), 124.7 (3xCH), 99.6 (3xCH_2), 57.9 (3xCH_2), 52.6 (3xCH_3). MS (ESI): *m/z* calc. 779.31; exp. 780.6 $[M + H]^+$.

***Tris*-(2-hydroxy-3-(3′-formyl)-benzyl)amine (16)**

Tris-(2-(methoxymethoxy)-3-(3′-formyl)-benzyl)amine **15** (2.8 mmol, 2.5 g) was dissolved in THF (84 mL) and then HCl 1.25 M in methanol (16.8 mL) was added. The reaction mixture was heated at 50 °C for 18 h. A solution of HCl_{aq} 1M was added and the reaction was vigorously stirred for 3 h. Then $NaHCO_{3aq}$ sat. was added till pH = 8 was reached. The residue was extracted with EtOAc. The organic phases were dried over anhydrous Na_2SO_4 and concentrated under vacuum. The product, a brownish foam, was used without any further purification (70%).

IR (KBr) ν (cm^{-1}): 743, 772, 868, 907, 1071, 1185, 1262, 1303, 1383, 1425, 1462, 1576, 1595, 1696, 2730, 2828, 2962, 3372. ^{1}H-NMR: (250 MHz, $CDCl_3$) δ 9.77 (3H, *s*) 7.78 (3H, *s*), 7.63 (6H, *m*), 7.39 (3H, *t, J* = 8 Hz), 7.06 (6H, *m*), 6.82 (3H, *t*, *J* = 6 Hz), 3.83 (6H, *s*). ^{13}C{^{1}H}-NMR: (62.9 MHz, $CDCl_3$) δ 192.10 (3xCHO), 152.06 (3xC), 138.43 (3xC), 136.23 (3x*C*), 135.3 (3x*C*H), 130.8 (3x*C*H), 130.5 (3x*C*H), 130.1 (3x*C*H), 128.8 (3x*C*H), 128.1 (3x*C*H), 127.6 (3x*C*), 123.9 (3x*C*), 120.3 (3x*C*H), 57.9 (3xCH_2). MS (ESI): *m/z* calc. 647.23; exp. 648.5 $[M + H]^+$.

***Tris*-(2-hydroxy-3-(3′-formyl)-5-formylbenzyl)amine (38)**

A nitrogen purged Schlenk tube was charged with *tris*-(2-(methoxymethoxy)-3-(3′-formyl)-benzyl)amine **15** (0.67 mmol, 0.522 g) and hexamethylenetetramine (4.02 mmol, 0.563 g) and diluted with TFA (6 mL/mmol sub., 4.02 mL) and the mixture was stirred at 90 °C for 18h. The crude was evaporated to dryness and HCl_{aq} 4N (36 mL) was added and the mixture was stirred for 3 h at 90°C. The precipitate was filtered off, washed with $NaHCO_3$ and extracted with CH_2Cl_2. The organic phase was dried over anhydrous Na_2SO_4 and evaporated to dryness. A dark yellow solid was obtained, which was used without any further purification (79%).

IR (KBr) ν (cm^{-1}): 694, 802, 891, 1078, 1099, 1150, 1378, 1456, 1554, 1623, 1635, 1646, 1684, 1699, 1717, 2336, 2361, 2989, 3420. ^{1}H-NMR: (250 MHz, CD_2Cl_2) δ 9.96 (3H, *s*), 9.84 (3H, *s*), 7.88 (3H, *d*, *J* = 2 Hz), 7.85 (3H, *t*, *J* = 2 Hz), 7.70-7.56 (12H, *m*), 5.39 (3H, *br*), 4.10 (6H, *s*). ^{13}C{^{1}H}-NMR: (50.03 MHz, CD_2Cl_2) δ 191.97, 190.32, 158.48, 137.25, 137.07, 135.25, 131.96, 130.30, 129.79 129.42, 128.45, 124.90, 57.73. MS (ESI): *m/z* calc. 731.22; exp. 732.3 $[M + H]^+$.

3-(3-Hydroxypropyl)-1-methyl-1*H*-imidazol-3-ium chloride (23)

3-Chloro-1-propanol **21** (121.8 mmol, 11.50 g) and 1-methyl-1*H*-imidazole **22** (121.8 mmol, 10 g) were placed in a round-bottom flash and the mixture was heated at 80 °C for 48 h under N_2 with continuous stirring. The reaction mixture was cooled to room temperature and washed three times with diethyl ether. A dense yellow oil formed, which was used without any further purification (99%).

IR (KBr) ν (cm^{-1}): 756, 837, 1062, 1166, 1339, 1456, 1635, 1652, 2880, 2953, 3148, 3386. ^{1}H-NMR: (200 MHz, CD_3CN) δ 9.52 (1H, *s*), 7.58 (1H, *s*), 7.40 (1H, *s*), 4.38 (2H, *t*, *J* =

6 Hz), 3.87 (3H, *s*), 3.47 (2H, *t*, *J* = 6 Hz), 2.04-1.94 (2H, *m*). $^{13}C\{^1H\}$-NMR: (50.03 MHz, $CDCl_3$) δ 136.69, 123.86, 122.85, 56.68, 47.40, 41.92, 32.32. MS (ESI): *m/z* calc. 176.07; exp. 140.8 $[M - Cl]^+$.

3-(3-Hydroxypropyl)-1-methyl-1*H*-imidazol-3-ium tetraphenylborate (18c)

To a solution of 3-(3-hydroxypropyl)-1-methyl-1*H*-imidazol-3-ium chloride **23** (1.025 mmol, 0.16 g) in methanol (10 mL), $NaBPh_4$ (1.025 mmol, 0.35 g) was added and the mixture was stirred for 2.5 h at room temperature. The precipitate was filtered off, washed with 14 mL of methanol and 14 mL of diethyl ether and dried under vacuum, obtaining a white solid (98%).

IR (KBr) ν (cm^{-1}): 736, 997, 1067, 1166, 1261, 1423, 1455, 1566, 2882, 2982, 3015, 3140, 3512. ^1H-NMR: (200 MHz, $CDCl_3$) δ 7.53-7.49 (8H, *m*), 7.01 (8H, *t*, *J* = 6 Hz), 6.83 (4H, *t*, *J* = 6 Hz), 6.48 (1H, *s*), 6.30 (1H, *s*), 4.90 (1H, *s*), 3.51 (2H, *t*, *J* = 6 Hz), 2.95 (3H, *s*), 1.63-1.55 (2H, *m*). $^{13}C\{^1H\}$-NMR: (75.5 MHz, $CDCl_3$) δ 136.18, 132.53, 131.09, 130.22, 129.81, 129.41, 128.7, 58.26, 48.69, 38.19, 33.44. MS (ESI): *m/z* calc. 460.27; exp. 140.8 $[M - BPh_4]^+$.

3-(2-(2-(2-Hydroxyethoxy)ethoxy)ethyl)-1-methyl-1*H*-imidazol-3-ium chloride (25)

A mixture of 2-(2-(2-chloroethoxy)ethoxy)ethanol **24** (21.92 mmol, 3.7 g, 3.18 mL) and 1-methyl-1*H*-imidazole **22** (21.92 mmol, 18 g, 1.74 mL) was placed in a 10 mL sealed tube, which was introduced into a regularly calibrated CEM Discover microwave reactor. The stirred liquid mixture was irradiated at 20% power level for 2 min at 90 °C, then at 5% power level for 4 min at 120 °C and finally at 15% power level for 24 min at 120 °C. Then the mixture was allowed to cool and a brown oil formed rapidly. The oil was washed with diethyl ether (3 x 4 mL) and acetonitrile (2 x 2.5 mL) and dried under vacuum (90%).

IR (KBr) ν (cm^{-1}): 758, 831, 930, 1120, 1249, 1352, 1456, 1575, 1669, 1695, 1734, 2872, 3148, 3386. ^1H-NMR: (200 MHz, $CDCl_3$) δ 9.96 (1H, *s*), 7.65 (1H, *s*), 7.43 (1H, *s*), 4.61-4.52 (2H, *m*), 4.06 (3H,*s*), 3.94-3.87 (2H, *m*), 3.75-3.63 (8H, *m*). $^{13}C\{^1H\}$-NMR: (50.03 MHz, $CDCl_3$) δ 137.08, 123.21, 122.87, 70.56, 70.41, 70.21, 61.85, 61.29, 49.91, 36.82. MS (ESI): *m/z* calc. 250.11; exp. 214.7 $[M - Cl]^+$.

3-(2-(2-(2-Hydroxyethoxy)ethoxy)ethyl)-1-methyl-1*H*-imidazol-3-ium tetraphenylborate (18d)

To a solution of 3-(2-(2-(2-hydroxyethoxy)ethoxy)ethyl)-1-methyl-1*H*-imidazol-3-ium chloride **25** (4.65 mmol, 1 g) in methanol (18 mL), $NaBPh_4$ (4.65 mmol, 1.6 g) was added and the mixture was stirred for 2.5 h at room temperature. The precipitate was filtered off, washed with 30 mL of methanol and 30 mL of diethyl ether and dried under vacuum, obtaining a white solid (99%).

IR (KBr) ν (cm^{-1}): 849, 1032, 1110, 1169, 1268, 1352, 1426, 1479, 1579, 2998, 3140, 3446,. ^1H-NMR: (300 MHz, CD_3CN) δ 8.54 (1H, *s*), 7.42 (1H, *s*), 7.29 (1H, *s*), 7.28-7.23 (8H, *m*), 6.99 (8H, *t*, *J* = 6 Hz), 6.84 (4H, *t*, *J* = 6 Hz), 4.28-4.25 (2H, *m*), 3.83 (3H, *s*), 3-80-3.77 (4H, *m*), 3.60-3.53 (6H, *m*). $^{13}C\{^1H\}$-NMR: (75.5 MHz, $CDCl_3$) δ 137.32,

130.22, 129.83, 129.39, 128.64, 127.47, 123.59, 73.86, 71.73, 71.49, 70.10, 62.87, 50.67, 37.35. MS (ESI): *m/z* calc. 534.30; exp. 215.2 $[M - BPh_4]^+$.

3-Morpholinopropan-1-ol (18e)
To a solution of 3-chloro-1-propanol **21** (52.88 mmol, 5 g) in dry toluene, morpholine **26** (105.77 mmol, 9.21 g) was added and the mixture was refluxed for 4 h. The solid formed was removed by filtration and the filtrate was evaporated to dryness. The crude product was purified by distillation using Kugelrohr apparatus to give the final product as a pale yellow liquid (86%).

IR (NaCl) ν (cm^{-1}): 802, 880, 1049, 1089, 1264, 1383, 1453, 1642, 2895, 2927, 2974, 3386. ^{1}H-NMR: (250 MHz, $CDCl_3$) δ 4.98 (1H, *br*), 3.78 (2H, *t*, *J* = 4 Hz), 3.69 (4H, *t*, *J* = 2 Hz), 2.59 (2H, *t*, *J* = 4 Hz), 2.50 (4H, *t*, *J* = 2 Hz), 1.75-1.66 (2H, *m*). ^{13}C{^{1}H}-NMR: (50.03 MHz, $CDCl_3$) δ 66.76, 63.89, 58.93, 53.81, 27.08. MS (ESI): *m/z* calc. 145.11; exp. 146 $[M + H]^+$.

1-(bromomethyl)pyrene (28)
To an ice-cooled suspension of 1-hydroxymethylpyrene **27** (8.61 mmol, 2 g) in chloroform (34 mL) containing pyridine (0.35 mL), a solution of phosphorous tribromide (4.30 mmol, 1.16 g) in chloroform (10 mL) was added over a period of 20 min. The temperature was gradually raised to room temperature and stirring was continued for 30 min. The reaction mixture was again chilled with an ice-bath, and cracked ice and chloroform (5 mL) were added. The organic layer was successively washed with water, $NaHCO_{3aq}$ and water and then dried. A pale yellow solid formed, which was used without any further purification (94%).

IR (KBr) ν (cm^{-1}): 681, 700, 756, 816, 840, 844, 1181, 1602, 1635, 1652, 1684, 1695, 1700, 3395. ^{1}H-NMR: (200 MHz, $CDCl_3$) δ 8.41 (1H, *d*, *J* = 10 Hz), 8.38-8.24 (3H, *m*), 8.24-8.01 (5H, *m*), 5.27 (2H, *m*). ^{13}C{^{1}H}-NMR: (50.03 MHz, $CDCl_3$) δ 145.21, 128.48, 128.27, 127.94, 127.58, 126.51, 125.86, 125.09, 123.07. MS (GC-MS): *m/z* calc. 294.00; exp. 216 $[M - Br]^+$.

2-(2-(2-(pyren-1-ylmethoxy)ethoxy)ethoxy)ethanol (18g)
Sodium hydride 60% w/w in mineral oil (7.65 mmol, 0.3 g) was added cautiously to triethylene glycol (51.02 mmol, 7.66 g) and tetrabutylammonium bromide (0.4 mmol, 0.128 g) in dry THF (4 mL). After stirring for 20 min, 1-(bromomethyl)pyrene **28** (5.10 mmol, 1.5 g) was added and the reaction was refluxed for 24 h. The reaction was then cooled to room temperature and concentrated in vacuum to give a yellow oil. The oil was dissolved in dichloromethane (20 mL) and partitioned with sat. $NaCl_{aq}$ (2 x 5 mL). The organic phase was dried with anhydrous Na_2SO_4 and concentrated in vacuum to give a yellow oil, that was purified by column chromatography on silica gel (chloroform/methanol 95:5), affording the final product as a yellow oil (55%).

IR (NaCl) ν (cm^{-1}): 711, 759, 818, 846, 935, 1087, 1183, 1245, 1417, 1456, 1487, 1603, 1717, 2867, 3039, 3415. ^{1}H-NMR: (200 MHz, $CDCl_3$) δ 8.35 (1H, *d*, *J* = 10 Hz), 8.20-7.96 (8H, *m*), 5.26 (2H, *s*), 3.77-3.66 (4H, *m*), 3.64 (4H, *s*), 3.61-3.54 (2H, *m*). ^{13}C{^{1}H}-

NMR: (50.03 MHz, $CDCl_3$) δ 131.45, 131.33, 130.93, 129.53, 127.82, 127.54, 127.22, 126.08, 125.35, 124.59, 123.61, 72.69, 71.94, 70.61, 70.42, 69.55, 61.83. MS (ESI): calc. 364.17; exp. 364.2 $[M]^+$, 382 $[M + H_2O]^+$, 387 $[M + Na]^+$, 403 $[M + K]^+$.

General procedure for the synthesis of *N*-phtalimide derivatives (19a-g)
To a solution of alcohols **18a-g** (27.74 mmol) in dry THF (180 mL) *N*-hydroxyphthalimide (55.48 mmol), and triphenylphosphine (55.48 mmol) were added. The mixtures were cooled to 0 °C and di-*iso*propyl azodicarboxylate (DIAD, 55.48 mmol) in dry THF (20 mL) was added dropwise. The reaction mixtures were stirred for 20 h at room temperature and evaporated to dryness. Crude products were purified by precipitation in diethyl ether: Purification by chromatography (chloroform/methanol 99:1) was necessary for product **19g**.
19a: yellow liquid. Yield: 85%. IR (NaCl) ν (cm^{-1}): 699, 748, 878, 953, 999, 1027, 1119, 1245, 1375, 1467, 1521, 1624, 1652, 1733, 1789, 2877, 3056. ^{1}H-NMR (250 MHz, $CDCl_3$): δ 7.86-7.80 (2H, *m*), 7.74-7.67 (2H, *m*), 4.36 (2H, *t*, *J* = 8.75 Hz), 3.86 (2H, *t*, *J* = 8.75 Hz), 3.68-3.64 (2H, *m*), 3.58-3.53 (4H, *m*), 3.50-3.47 (2H, *m*), 3.34 (3H, *s*). ^{13}C{^{1}H}-NMR: (50.03 MHz, $CDCl_3$) δ 163.71, 135.03, 134.60, 134.11, 133.73, 128.94, 123.65, 72.06, 70.98, 70.69, 69.49, 59.17. MS (ESI): *m/z* calc. 309.12; exp. 332.2 $[M+Na]^+$.

19b: white solid. Yield: 89%. IR (KBr) ν (cm^{-1}): 790, 884, 965, 1016, 1127, 1184, 1377, 1465, 1582, 1730, 1863, 2119, 2865, 2981, 3253, 3503. ^{1}H-NMR (200 MHz, $CDCl_3$): δ 7.90-7.75 (4H, *m*), 4.86 (2H, *d*, *J* = 2.4 Hz), 2.58 (1H, *t*, *J* = 4.8 Hz). ^{13}C{^{1}H}-NMR: (75.5 MHz, $CDCl_3$) δ 163.54, 134.82, 132.15, 129.02, 123.91, 78.33, 66.05, 65.19. MS (GC-MS): *m/z* calc. 200.04; exp. 200 $[M]^+$.

19c: white solid. Yield: 85%. IR (KBr) ν (cm^{-1}): 735, 877, 1031, 1186, 1373, 1426, 1506, 1559, 1652, 1669, 1684, 1734, 2336, 2361, 2982, 3052, 3075, 3111, 3141, 3447, 3744, 3854,. ^{1}H-NMR (200 MHz, $CDCl_3$): δ 7.85-7.81 (2H, *m*), 7.77-7.73 (2H, *m*), 7.50 (8H, *m*), 6.98 (8H, *t*, *J* = 8 Hz), 6.79 (4H, *t*, *J* = 8 Hz), 6.63 (1H, *s*), 6.00 (1H, *s*), 5.14 (1H, *s*), 3.92 (2H, *t*, *J* = 6 Hz), 3.61 (2H, *t*, *J* = 6 Hz), 2.83 (3H, *s*), 1.75-1.63 (2H, *m*). ^{13}C{^{1}H}-NMR: (62.9 MHz, $CDCl_3$) δ 163.83, 136.13, 135.11, 134.92, 131.26, 128.94, 128.1, 127.54, 127.38, 126.18, 124.01, 123.07, 122.54, 122.28, 74.25, 46.62, 36.52, 29.24. MS (ESI): *m/z* calc. 605.28; exp. 285 $[M - BPh_4]^+$.

19d: yellow oil. Yield 70%. IR (NaCl) ν (cm^{-1}): 702, 754, 1028, 1121, 1187, 1262, 1373, 1419, 1456, 1506, 1569, 1602, 1635, 1695, 1700, 1733, 1792, 2336, 2361, 3383. ^{1}H-NMR (300 MHz, $CDCl_3$): δ 7.82-7.80 (2H, *m*), 7.77-7.73 (2H, *m*), 7.50 (10H, *m*), 7.36 (1H, *s*), 7.25 (1H, *s*), 6.98 (10H, *t*, *J* = 6 Hz), 6.79 (5H, *t*, *J* = 6 Hz), 6.48 (1H, *s*), 4.33-4.30 (2H, *m*), 3.78-371 (2H, *m*), 3.56-3.46 (8H, *m*), 3.10 (3H, *s*). ^{13}C{^{1}H}-NMR: (75.5 MHz, $CDCl_3$) δ 164.96, 137.35, 136.28, 136.21, 132.50, 130.95, 130.22, 129.92, 129.39, 128.64, 127.46, 128.72, 128.12, 123.56, 71.90, 71.68, 71.58, 70.24, 50.92, 37.48. MS (ESI): *m/z* calc. 679.32; exp. 285.4 $[M - BPh_4]^+$.

19e: white crystals. Yield: 80%. IR (KBr) ν (cm^{-1}): 793, 899, 977, 1060, 1171, 1225, 1380, 1436, 1506, 1539, 1576, 1684, 1700, 2338, 2361, 2423, 2527, 2876, 2960. ^{1}H-NMR

(200 MHz, $CDCl_3$): δ 7.84-7.80 (2H, *m*), 7.75-7.69 (2H, *m*), 4.27 (2H, *t*, *J* = 7.5 Hz), 3.72-3.69 (4H, *t*, *J* = 5 Hz), 2.62-2.56 (2H, *t*, *J* = 7.5 Hz), 2.50-2.46 (4H, *t*, *J* = 5Hz), 2.02-1.91 (2H, *m*). $^{13}C\{^1H\}$-NMR: (50.03 MHz, $CDCl_3$) δ 165.02, 136.28, 133.61, 133.48, 130.19, 130.05, 129.89, 77.08, 65.45, 56.69, 53.84, 2.42. MS (ESI): *m/z* calc. 290.13; exp. 290.3 $[M]^+$.

19f: white solid. Yield: 87%. IR (KBr) ν (cm^{-1}): 711, 732, 839, 1012, 1082, 1172, 1243, 1353, 1385, 1472, 1558, 1616, 1737, 2336, 2361, 2900, 3044. ^1H-NMR (200 MHz, $CDCl_3$): δ 8.87 (1H, *d*, *J* = 9.4 Hz), 8.32-8.01 (8H, *m*), 7.79-7.72 (2H, *m*), 7.85-7.80 (2H, *m*), 5.95 (2H, *s*). $^{13}C\{^1H\}$-NMR: (75.5 MHz, $CDCl_3$) δ 163.83, 134.64, 132.81, 131.35, 131.21, 131.04, 129.50, 129.19, 128.81, 128.50, 127.52, 126.72, 126.30, 125.93, 125.78, 125.07, 124.67, 123.87, 123.73, 78.30. MS (ESI): *m/z* calc. 377.11; exp. 378.11 $[M + H]^+$.

19g: yellow oil. Yield: 50%. IR (NaCl) ν (cm^{-1}): 846, 978, 1037, 1185, 1229, 1318, 1374, 1419, 1490, 1506, 1539, 1569, 1646, 1662, 1675, 1751, 1772, 1792, 2361, 2921, 2979, 3392. ^1H-NMR (200 MHz, $CDCl_3$): δ 8.36 (1H, *d*, *J* = 10 Hz), 8.21-8.00 (8H, *m*), 7.77-7.73 (2H, *m*), 7.65-7.61 (2H, *m*), 5.26 (2H, *s*), 4.34-4.30 (2H, *m*), 3.85-3.81 (2H, *m*), 3.70-3.61 (8H, *m*). $^{13}C\{^1H\}$-NMR: (50.03 MHz, $CDCl_3$) δ 163.53, 134.49, 131.67, 131.46, 131.04, 129.57, 129.13, 127.85, 127.62, 127.22, 126.13, 125.39, 124.68, 123.76, 123.58, 77.40, 72.00, 71.04, 70.92, 70.82, 69.72, 69.51. MS (ESI): *m/z* calc. 209.18; exp. 527 $[M + H_2O]^+$, 532 $[M + Na]^+$.

General procedure for the synthesis of alkoxyamines (20a-g)

To a solution of *N*-phtalimide derivatives **19a-g** (2.26 mmol) in CH_2Cl_2 (226 mL), hydrazine monohydrate 80% (5.24 mmol) was added and the mixtures were stirred for 1 h. The solids formed were removed by filtration and the filtrates were evaporated to dryness. The products were used without any further purification.

20a: yellow oil. Yield: 79%. IR (KBr) ν (cm^{-1}): 851, 945, 1106, 1200, 1247, 1288, 1349, 1456, 1594, 1652, 2876, 3312, 3444. ^1H-NMR (250 MHz, $CDCl_3$)*:* δ 5.2 (2H, *br*), 3.83-3.79 (2H, *m*), 3.67-3.60 (8H, *m*), 3.55-3.50 (2H, *m*), 3.35 (3H, *s*). $^{13}C\{^1H\}$-NMR: (62.9 MHz, $CDCl_3$) δ 74.1, 71.4, 70.1, 70, 69.9, 69, 58.4. MS (ESI): *m/z* calc. 179.12; exp. 180 $[M + H]^+$.

20b: colourless oil. Yield: 86%. IR (KBr) ν (cm^{-1}): 694, 756, 920, 1027, 1071, 1179, 1261, 1387, 1472, 1490, 1558, 1646, 1695, 1733, 2336, 2361, 2936, 2980, 3056, 3239. ^1H-NMR (200 MHz, $CDCl_3$)*:* δ 5.58 (2H, *br*), 4.25 (2H, *d*, *J* = 2.4 Hz), 2.43 (1H, *t*, J = 4.8 Hz). $^{13}C\{^1H\}$-NMR: (50.03 MHz, $CDCl_3$) δ 74.61, 70.88, 69.34. MS (GC-MS): *m/z* calc. 71.08; exp. 72 $[M +H]^+$.

20c: white solid. Yield: 80%. IR (KBr) ν (cm^{-1}): 709, 714, 744, 832, 868, 943, 1041, 1214, 1261, 1426, 1456, 1564, 1580, 1652, 2336, 2361, 2941, 2983, 3034, 3050, 3083, 3116, 3130, 3158, 3315. ^1H-NMR (200 MHz, CD_2Cl_2): δ 7.54-7.45 (8H, *m*), 7.05 (8H, *t*, *J* = 8 Hz), 6.85 (4H, *t*, *J* = 8 Hz), 6.81 (1H, *s*), 6.78 (1H, *s*), 5.60 (1H, *s*), 3.71 (2H, *t*, *J* = 6 Hz), 3.57 (2H, *t*, *J* = 6 Hz), 3.27 (3H, *s*), 1.84-1.93 (2H, *m*). $^{13}C\{^1H\}$-NMR: (50.03 MHz, $CDCl_3$) δ 136.06, 128.50, 126.19, 125.76, 122.54, 122.27, 121.16, 71.11, 46.83, 35.96, 29.91. MS (ESI): *m/z* calc. 475.28; exp. 155.8 $[M - BPh_4]^+$.

20d: white solid. Yield: 90%. IR (KBr) ν (cm^{-1}): 707, 843, 911, 1032, 1166, 1349, 1427, 1436, 1506, 1559, 1616, 1675, 1695, 1700, 2336, 2361, 2871, 2998, 3081, 3112, 3142, 3314. ^{1}H-NMR (200 MHz, CD_3CN): δ 8.44 (1H, *s*), 7.40 (1H, *s*), 7.31-7.23 (8H, *m*), 7.20 (1H, *s*), 7.00 (8H, *t*, *J* = 8 Hz), 6.84 (4H, *t*, *J* = 8 Hz), 4.25-4.21 (2H, *m*), 3.79 (3H, *s*), 3.77-3.73 (2H, *m*), 3.71-3.66 (2H, *m*), 3.60-3.53 (6H, *m*). ^{13}C{^{1}H}-NMR: (62.9 MHz, $CDCl_3$) δ 136.00, 135.50, 132.94, 127.18, 126.18, 122.43, 122.28, 74.99, 74.64, 69.57, 69.41, 68.61, 49.12, 35.63. MS (ESI): *m/z* calc. 549.32; exp. 230.6 $[M - BPh_4]^+$.

20e: pale yellow oil. Yield: 80%. IR (NaCl) ν (cm^{-1}): 799, 918, 993, 1034, 1117, 1272, 1306, 1401, 1373, 1447, 1458, 1539, 1594, 1652, 1695, 1700, 1733, 2689, 2811, 2856, 2954, 3157, 3310. ^{1}H-NMR (200 MHz, $CDCl_3$): δ 3.72 (6H, *dt*, *J* = 2 Hz, *J* = 6 Hz), 2.47-2.37 (6H, *m*), 1.92-1.71 (2H, *m*). ^{13}C{^{1}H}-NMR: (50.03 MHz, $CDCl_3$) δ 74.28, 67.05, 55.85, 55.82, 25.66. MS (ESI): *m/z* calc. 160.12; exp. 160.6 $[M]^+$, 199.5 $[M+ K]^+$.

20f: pale yellow solid. Yield: 84%. IR (KBr) ν (cm^{-1}): 708, 777, 839, 957, 978, 1064, 1105, 1204, 1366, 1418, 1539, 1588, 1695, 1700, 1909, 2336, 2361, 2879, 2932, 3038, 3237, 3300. ^{1}H-NMR (200 MHz, $CDCl_3$): δ 8.42 (1H, *d*, *J*= 9.2 Hz), 8.25-7.99 (8H, *m*), 5.52 (2H, *br*), 5.43 (2H, *s*). ^{13}C{^{1}H}-NMR: (75.5 MHz, $CDCl_3$) δ 131.78, 131.45, 131.02, 130.65, 129.96, 128.11, 128.05, 127.80, 127.60, 126.18, 125.49, 125.17, 124.94, 124.71, 123.75, 76.82. MS (ESI): *m/z* calc. 247.10; exp. 247.23 $[M]^+$.

20g: colourless oil. Yield: 99%. IR (NaCl) ν (cm^{-1}): 711, 818, 939, 1108, 1243, 1348, 1419, 1456, 1506, 1558, 1616, 1652, 1700, 1717, 2336, 2361, 2867, 3041, 3309. ^{1}H-NMR (200 MHz, $CDCl_3$): δ 8.38 (1H, *d*, *J* = 10 Hz), 8.22-7.97 (8H, *m*), 5.30 (2H, *s*), 3.88-3.75 (2H, *m*), 3.72-3.59 (10H, *m*). ^{13}C{^{1}H}-NMR: (50.03 MHz, $CDCl_3$) δ 132.58, 131.46, 131.04, 130.84, 127.94, 127.64, 127.36, 126.69, 126.16, 125.44, 124.70, 123.75, 74.67, 72.04, 70.88, 70.67, 69.96, 69.65. MS (ESI): *m/z* calc. 379.18; exp. 380 $[M + H]^+$.

2,2′-(((ethane-1,2-diylbis(oxy)bis(ethane-2,1-diyl))bis(oxy))bis(isoindoline-1,3-dione) (30)

N-hydroxyphthalimide (79.92 mmol, 13.10 g), triphenylphosphine (79.92 mmol, 21 g) and tri(ethylene glycol) **29** (33.3 mmol, 5 g) were dissolved in dry dichloromethane (100 mL). The mixture was cooled to 0 °C and a solution of di-*iso*propyl azodicarboxylate (DIAD, 79.92 mmol, 16.16 g) in dry THF (10 mL) was added dropwise. The mixture was stirred for 20 h at room temperature and evaporated to dryness. The product was purified by recrystallization from diethyl ether and a pale brown solid was obtained (87%).

IR (KBr) ν (cm^{-1}): 697, 798, 859, 880, 977, 1012, 1035, 1117, 1242, 1344, 1356, 1416, 1539, 1559, 1608, 1739, 1837, 1891, 2336, 2361, 2869, 2889, 2913, 2955, 3101, 3496. ^{1}H-NMR (200 MHz, $CDCl_3$): δ 7.85-7.80 (4H, *m*), 7.75-7.71 (4H, *m*), 4.33 (4H, *t*, *J* = 8.75 Hz), 3.8 (4H, *t*, *J* = 8.75 Hz), 3.61 (4H, *s*). ^{13}C{^{1}H}-NMR: (75.5 MHz, $CDCl_3$) δ 160.1, 134.61, 132.44, 123.68, 70.96, 69.45. MS (ESI): *m/z* calc. 440.12; exp. 441.2 $[M + H]^+$.

***O,O′*-((ethane-1,2-diylbis(oxy))bis(ethane-2,1-diyl))bis(hydroxylamine) (31)**

To a solution of 2,2′-(((ethane-1,2-diylbis(oxy)bis(ethane-2,1-diyl))bis(oxy))bis(isoindoline-1,3-dione) **30** (31.52 mmol, 13.87 g) in

dichloromethane (100 mL) hydrazine monohydrate 80% (151.31 mmol, 9.46 g) was slowly added and the mixture was stirred for 1h at room temperature. A white solid formed, which was removed by filtration. The solvent was concentrated in vacuum, to give a pale yellow oil (76%).

IR (KBr) v (cm^{-1}): 850, 945, 1062, 1106, 1210, 1297, 1348, 1464, 1593, 1652, 1717, 2869, 3155, 3307, 3426. ^{1}H-NMR (250 MHz, $CDCl_3$): δ 5.35 (2H, *br*), 3.88-3.84 (4H, *m*), 3.71-3.69 (4H, *m*), 3.67 (4H, *s*). $^{13}C\{^{1}H\}$-NMR: (62.9 MHz, CDCl3)δ 74.82, 70.44, 69.53. MS (ESI): *m/z* calc. 180.11; exp. 181.1 $[M + H]^+$.

Pyrene-1-carbaldehyde *O*-(2-(2-(2-(aminooxy)ethoxy)ethoxy)ethyl) oxime (20h)
To a solution of *O,O'*-((ethane-1,2-diylbis(oxy))bis(ethane-2,1-diyl))bis(hydroxylamine) (20.55 mmol, 3.7 g) in chloroform (70 mL), 1-pyrenecarboxaldehyde (24.66 mmol, 5.67 g) and trifluoroacetic acid (TFA, 1%) were added and the mixture was stirred at room temperature for 12 h. The mixture was basified with sat. $NaHCO_{3aq}$ and the product was extracted three times with dichloromethane. The organic phase was dried over anhydrous Na_2SO_4 and evaporated to dryness. The product was purified by column chromatography on silica gel (hexane/ethyl acetate 1:1), affording the final product (35%), together with by-product **33**.

20h: yellow oil. IR (NaCl) v (cm^{-1}): 682, 718, 849, 950, 1137, 1212, 1297, 1348, 1461, 1595, 1659, 1936, 2244, 3000, 3310, 3500. ^{1}H-NMR: (250 MHz, $CDCl_3$) δ 9.10 (1H, *s*), 8.57 (1H, *d*, *J* = 8.25 Hz), 8.36 (1H, *d*, *J* 8.25 Hz), 8.38-7.95 (7H, *m*), 5.50 (2H, *br*), 4.47 (2H, *t*, *J* = 9.25 Hz), 3.88 (2H, *t*, *J* = 9.25), 3.85-3.66 (8H, *m*). $^{13}C\{^{1}H\}$-NMR: (62.9 MHz, $CDCl_3$) δ 148, 132.3, 131.2, 130.6, 128.9, 128.5, 128.2, 127.3, 126.1, 125.7, 125.5, 125.2, 125, 124.9, 124.5, 122.7, 74.7, 73.7, 70.6, 69.8, 69.6. MS (ESI): *m/z* calc. 393.45; exp. 394.2 $[M +H]^+$.

33: pale yellow solid. IR (KBr) v (cm^{-1}): 678, 711, 704, 838, 879, 933, 1035, 1068, 1134, 1241, 1233, 1456, 1487, 1595, 1652, 1700, 2866, 2879, 2924, 2971, 3038, 3397. ^{1}H-NMR: (200 MHz, $CDCl_3$) δ 9.08 (2H, *s*), 8.49 (2H, *d*, *J* = 8 Hz), 8.30 (2H, *d*, *J* = 8 Hz), 8.17-7.93 (14H, *m*), 4.52-4.48 (4H, *m*), 3.97-3.93 (4H, *m*), 3.82 (4H, *s*). $^{13}C\{^{1}H\}$-NMR: (50.03 MHz, $CDCl_3$) δ 148.35, 128.76, 71.05, 70.09. MS (ESI): *m/z* calc. 604.24; exp. 604.1 $[M]^+$, 627 $[M + Na]^+$.

General procedure for the synthesis of oxime functionalized TPA ligands (34f, 35a-e and **35h, 36a-c** and **36f** and **39)**
To a solution of TPAs **16**, **17c-d** and **38** (0.052 mmol) in chloroform (10 mL/mmol) alkoxyamines **20a-h** (0.156 mmol; 0.312 mmol for ligand **37**) were added and the mixtures were stirred for 15 min. Then trifluoroacetic acid (TFA, 1%) was added and the mixtures were stirred for 12 h at room temperature. The reaction mixtures were washed with sat. $NaHCO_{3aq}$ and the organic phases were extracted three times with dichloromethane, dried over anhydrous Na_2SO_4 and evaporated to dryness. The products were purified by precipitation from diethyl ether.

34f: pale yellow solid. Yield: 85%. IR (KBr) ν (cm^{-1}): 710, 756, 842, 945, 993, 1041, 1063, 1172, 1227, 1362, 1394, 1419, 1447, 1456, 1521, 1539, 1616, 1635, 1646, 1652, 1695, 1700, 1717, 1734, 2336, 2361, 2951, 3447. ^{1}H-NMR: (200 MHz, $CDCl_3$) δ 8.41 (3H, *d*, *J* = 8 Hz), 8.20-7.94 (27H, *m*), 7.43 (3H, *s*), 7.24 (3H, *s*), 5.90 (6H, *s*), 3.61 (6H, *s*), 1.36 (27H, *s*). ^{13}C{^{1}H}-NMR: (50.03 MHz, $CDCl_3$) δ 155.63 (3xC), 149.37 (3xCH), 137.92 (3xC), 131.75 (6xC), 131.44 (3xC), 131.01 (3xC), 130.83 (3xC), 129.91 (3xC), 128.00 (3xCH), 127.76 (3xCH), 127.63 (3xCH), 127.08 (3xCH), 126.14 (3xCH), 125.47 (3xCH), 124.83 (3xCH), 124.22 (3xC), 123.86 (3xC), 123.15 (3xCH), 74.82 (3xCH_2), 56.51 3x(CH_2), 34.85 (3xC), 29.64 (9xCH_3). MS (ESI): *m/z* calc. 1274.59; exp. 1273.7 $[M - H]^-$.

35a: yellow solid. Yield: 95%. IR (KBr) ν (cm^{-1}): 700, 750, 784, 851, 965, 1068, 1105, 1198, 1237, 1348, 1458, 1590, 2875, 2925, 3058, 3417. ^{1}H-NMR: (250 MHz, $CDCl_3$) δ 8.00 (3H, *s*), 7.43-7.33 (21H, *m*), 4.26 (6H, *t*, *J* = 9.5 Hz), 3.88 (6H, *s*), 3.75 (6H, *t*, *J* = 9.5 Hz), 3.66-3.50 (24H, *m*), 3.35 (9H, *s*). ^{13}C{^{1}H}-NMR: (62.9 MHz, $CDCl_3$) δ 152.4, 148.8, 138.2, 132.7, 130.8, 130.5, 130, 129, 128.1, 128, 126, 123.6, 120.1, 73.6, 71.9, 70.7, 70.6, 70.5, 69.7, 59.1, 56.1. MS (ESI): *m/z* calc. 1130.55; exp. 1132.2 $[M + H]^+$.

35b: yellow solid. 80%. IR (KBr) ν (cm^{-1}): 702, 885, 949, 1007, 1096, 1170, 1214, 1347, 1412, 1440, 1473, 1558, 1603, 1646, 1695, 1717, 1784, 2120, 2336, 2361, 2919, 3030, 3282, 3340, 3509. ^{1}H-NMR: (250 MHz, $CDCl_3$) δ 7.92 (3H, s), 7.34-7.25 (21H, *m*), 4.62 (6H, *d*, *J* = 2.25 Hz), 3.81 (6H, *s*), 2.39 (3H, *t*, *J* = 4.75 Hz). ^{13}C{^{1}H}-NMR: (50.03 MHz, $CDCl_3$) δ 154.52, 149.74, 136.83, 134.48, 129.51, 129.09, 128.02, 124.09, 123.72, 79.87, 74.83, 61.76, 56.53. MS (ESI): *m/z* calc. 806.91; exp. 807.7 $[M + H]^+$.

35c: pale yellow solid. Yield: 70%. IR (KBr) ν (cm^{-1}): 844, 949, 1031, 1064, 1249, 1352, 1426, 1456, 1476, 1539, 1569, 1600, 1616, 1652, 2336, 2361, 2983, 2998, 3053, 3109, 3509. ^{1}H-NMR: (200 MHz, CD_3CN) δ 8.10 (3H, *s*), 7.98 (3H, *s*), 7.42-7.34 (21H, *m*), 7.31-7.25 (24H, *m*), 6.99 (24H, *t*, *J* = 8 Hz), 6.83 (12H, *t*, *J* = 8 Hz), 4.18-4.05 (12H, *m*), 4.00 (3H, *s*), 3.64 (9H, *s*), 2.17-2.12 (6H, *m*). ^{13}C{^{1}H}-NMR: (50.03 MHz, $CDCl_3$) δ 148.41, 146.94, 138.30, 137.89, 135.70, 129.78, 129.36, 128.66, 128.31, 128.16, 127.15, 125.60, 121.75, 69.92, 54.16, 51.59, 50.33, 29.21, 23.89. MS (ESI): *m/z* calc. 2019.24; exp. 690.7 $[M - 2BPh_4]^{2+}$, 1699.7 $[M - BPh_4]^+$, 2020.5 $[M]^+$.

35d: pale yellow solid. 65%. ^{1}H-NMR: (300 MHz, CD_3CN) δ 8.57 (3H, *s*), 8.50 (3H, *s*), 8.32 (3H, *s*), 7.96 (3H, s), 7.39-7.35 (15H, *m*), 7.28-7.25 (24H, *m*), 7.21-7.17 (6H, *m*), 6.99 (24H, *t*, *J* = 9 Hz), 6.83 (12H, *t*, *J* = 9 Hz), 4.25-4.21 (12H, *m*), 4.18-4.10 (12H, *m*), 3.82-3.76 (12H, *m*), 3.57 (6H, *s*), 3.54 (9H, *s*). ^{13}C{^{1}H}-NMR: (75.5 MHz, $CDCl_3$) δ 165.78 (3xC), 165.06 (3xC), 164.53 (3xC), 163.82 (3xC), 155.89 (3xC), 149.19 (3xCH), 139.15 (3xCH), 137.43 (6xCH), 136.70 (24xCH), 130.38 (9xCH), 129.19 (6xCH), 128.22 (3xC), 126.56 (24xCH), 124.18 (3xC), 123.89 (12xCH), 74.15 (3xCH_2), 70.96 (6xCH_2), 70.19 (3xCH_2), 69.21 (6xCH_2), 50.37 (3xCH_2), 36.81 (3xCH_3). MS (ESI): *m/z* calc. 2241.15; exp. 1921.0 $[M – BPh_4]^+$.

35e: pale yellow solid. Yield: 75%. IR (KBr) ν (cm^{-1}): 700, 914, 1057, 1066, 1116, 1169, 1249, 1305, 1363, 1394, 1436, 1456, 1465, 1472, 1652, 1700, 1734, 2336, 2361, 2809,

2955, 3420. ^{1}H-NMR: (200 MHz, $CDCl_3$) δ 7.95 (3H, *s*), 7.41-7.33 (21H, *m*), 4.14 (6H, *t*, *J* = 6 Hz), 3.89 (6H, *s*), 3.71-3.59 (12H, *m*), 2.46-2.35 (18H, *m*), 1.96-1.84 (6H, *m*). ^{13}C{^{1}H}-NMR: (50.03 MHz, $CDCl_3$) δ 154.23, 148.23, 137.05, 133.30, 129.53, 129.03, 128.11, 127.95, 124.37, 124.25, 124.13, 73.09, 71.40, 67.05, 56.50, 55.80, 53.84, 26.39. MS (ESI): *m/z* calc. 1073.56; exp. 1073.0 $[M]^+$.

35h: yellow solid. Yield: 99%. IR (KBr) ν (cm^{-1}): 623, 732, 774, 847, 911, 958, 1070, 1109, 1242, 1348, 1474, 1603, 2245, 2873, 2928, 3044, 3409, 3500. ^{1}H-NMR: (250 MHz, $CDCl_3$) δ 9.07 (3H, *s*), 8.52 (3H, *d*, *J* = 10 Hz), 8.31 (3H, *d*, *J* = 10 Hz), 8.17-7.94 (21H, *m*), 7.24-7.34 (21H, *m*), 4.45 (6H, *t*, *J* = 9.25 Hz), 4.26 (6H, *t*, *J* = 9.25 Hz), 3.88 (6H, *t*, *J* = 9.25 Hz), 3.60-3.81 (24H, *m*). ^{13}C{^{1}H}-NMR: (62.9 MHz, $CDCl_3$) δ 56.7, 70.3, 70.4, 71.3, 73.9, 74.3, 123.3, 124.3, 124.5, 125.4, 125.7, 125.9, 126.1, 126.3, 126.7, 127.9, 128.4, 128.8, 129.1, 129.2, 129.3, 129.4, 129.5, 129.6, 129.8, 131.1, 131.8, 132.8, 137.3, 148.6, 149, 154.7. MS (ESI): *m/z* expt. 1769.72; exp. 1770.7 $[M + H]^+$.

36a: yellow solid. Yield: 92%. IR (KBr) ν (cm^{-1}): 622, 702, 774, 849, 950, 1103, 1200, 1244, 1349, 1475, 1604, 1678, 2876, 2925, 3257, 3500. ^{1}H-NMR: (250 MHz, $CDCl_3$) δ 8.09 (3H, *s*), 7.61-7.37 (12H, *m*), 7.15 (6H, *d*, *J* = 7.75 Hz), 6.87 (3H, *t*, *J* = 15 Hz), 4.31 (6H, *t*, *J* = 9.75 Hz), 3.87 (6H, s), 3.78 (6H, *t*, *J* = 9.75 Hz), 3.69-3.61 (18H, *m*), 3.53-3.50 (6H, *m*), 3.34 (9H, *s*). ^{13}C{^{1}H}-NMR: (62.9 MHz, $CDCl_3$) δ 154.23, 148.51, 136.74, 132.29, 132.09, 129.51, 129.38, 128.94, 127.91, 134.30, 123.20, 73.47, 72.02, 70.73, 70.63, 69.78, 59.23, 56.41. MS (ESI): *m/z* calc. 1130.5; exp. 1131.6 $[M + H]^+$.

36b: yellow solid. Yield: 97%. IR (KBr) ν (cm^{-1}): 693, 747, 927, 1006, 1074, 1164, 1237, 1313, 1386, 1472, 1539, 1603, 1653, 1711, 1739, 2336, 2361, 2938, 2979, 3054, 3253. ^{1}H-NMR: (200 MHz, $CDCl_3$) δ 8.09 (3H, *s*), 7.63-7.38 (12H, *m*), 7.15 (6H, *d*, *J* = 7.2 Hz), 6.88 (3H, *t*, *J* = 15 Hz), 4.75 (6H, *d*, *J* = 2.4 Hz), 3.89 (6H, *s*), 2.50 (3H, *t*, *J* = 4.8 Hz). ^{13}C{^{1}H}-NMR: (50.03 MHz, $CDCl_3$) δ 153.9, 143.25, 136.5, 133.9, 130.14, 129.79, 129.49, 128.1, 127.0, 126.8, 126.2, 123.5, 121.8, 78.5, 74.70, 61.89, 55.9. MS (ESI): *m/z* calc. 806.31; exp. 807.7 $[M + H]^+$.

36c: pale yellow solid. Yield: 80%. IR (KBr) ν (cm^{-1}): 705, 783, 844, 949, 997, 1031, 1162, 1267, 1340, 1426, 1456, 1559, 1616, 2336, 2361, 2983, 2998, 3053, 3109, 3139, 3528. ^{1}H-NMR: (200 MHz, CD_3CN) δ 8.15 (3H, *s*), 8.04 (3H, *s*), 7.65 (3H, *s*), 7.52-7.40 (12H, *m*), 7.31-7.24 (24H, *m*), 7.20-7.13 (12H, *m*), 6.99 (24H, *t*, *J* = 12 Hz), 6.83 (12H, *t*, *J* = 12 Hz), 4.19-4.10 (12 H, *m*), 3.90 (6H, *s*), 3.62 (9H, *s*), 2.24-2.14 (6H, *m*). ^{13}C{^{1}H}-NMR: (50.03 MHz, CD_3CN) δ 158.93, 149.20, 135.92, 132.24, 131.40, 130.79, 130.70, 129.98, 12906, 128.95, 128.78, 128.57, 128.23, 125.77, 124.73, 123.73, 122.61, 121.98, 70.49, 55.57, 55.24, 47.11, 35.87, 29.45. MS (ESI): *m/z* calc. 2019.04; exp. 690.9 $[M - 2BPh_4]^{2+}$, 850.7 $[M + H - BPh_4]^{2+}$, 1699.5 $[M - BPh_4]^+$.

36f: pale brown solid. Yield: 97%. IR (KBr) ν (cm^{-1}): 704, 777, 845, 968, 990, 1103, 1195, 1228, 1339, 1436, 1456, 1472, 1506, 1539, 1558, 1589, 1616, 1652, 1684, 1695, 1700, 2336, 2361, 2876, 3040, 3385. ^{1}H-NMR: (200 MHz, $CDCl_3$) δ 8.40 (3H, *d*, *J* = 9.2 Hz), 8.18-7.94 (24H, *m*), 7.56 (3H, *s*), 7.41-7.31 (6H, *m*), 7.05 (6H, *d*, *J* = 8.6 Hz), 6.81 (3H, *t*, *J* = 15 Hz), 5.84 (6H, *s*), 3.76 (6H, *s*). ^{13}C{^{1}H}-NMR: (62.9 MHz, $CDCl_3$) δ 152.62, 149.41, 132.80, 131.86, 131.57, 131.12, 130.85, 130.02, 129.40, 128.40, 128.21,

127.88, 127.76, 126.25, 125.64, 125.07, 124.96, 123.96, 75.10, 56.99. MS (ESI): *m/z* calc. 1334.50; exp. 1335.3 $[M + H]^+$.

39: yellow solid. Yield: 87%. IR (KBr) ν (cm^{-1}): 700, 749, 851, 949, 1068, 1107, 1198, 1236, 1348, 1419, 1456, 1558, 1591, 1616, 1635, 1684, 1695, 1700, 1734, 2336, 2361, 2874, 3056, 3420. ^{1}H-NMR: (250 MHz, $CDCl_3$) δ 8.08 (3H, *s*), 8.00 (3H, *s*), 7.56.7.32 (18H, *m*), 4.30-4.26 (12H, *m*), 3.88-3.48 (66H, m), 3.35 (9H, *s*), 3.33 (9H, *s*). ^{13}C{^{1}H}-NMR: (50.03 MHz, $CDCl_3$) δ 152.56, 148.98, 138.30, 132.97, 130.98, 130.70, 130.26, 129.28, 128.40, 128.19, 126.24, 123.76, 123.64, 120.32, 73.76, 72.13, 70.85, 70.75, 69.86, 59.21, 56.27. MS (ESI): *m/z* calc. 1697.85; exp. 1699.4 $[M + H]^+$.

_N_-methylated oxime functionalized TPA 36

To a solution of **35e** (0.037 mmol, 0.04 g) in dry chloroform (0.5 mL), methyl iodide (0.44 mmol, 0.062 g) was added and the mixture was stirred at room temperature for 3 h. The reaction mixture was then concentrated under reduced pressure and washed with diethyl ether, to give the final product as a dark yellow solid (50%).

IR (KBr) ν (cm-1): 776, 910, 952, 1061, 1106, 1167, 1233, 1307, 1354, 1419, 1436, 1456, 1473, 1496, 1576, 1603, 1616, 1635, 1652, 2336, 2361, 2874, 2932, 3420. ^{1}H-NMR: (250 MHz, $CDCl_3$) δ 8.02 (3H, *s*), 7.42-7.30 (7H, *m*), 4.13 (6H, *t*, *J* = 5 Hz), 3.89-3.85 (12H, *m*), 3.37-3.33 (18H, *m*), 3.08 (9H, *s*), 2.15-2.07 (6H, *m*). ^{13}C{^{1}H}-NMR: (62.9 MHz, $CDCl_3$) δ 154.70, 149.33, 146.24, 139.94, 129.64, 129.10, 128.80, 127.84, 124.17, 70.81, 70.05, 62.38, 62.05, 60.42, 60.01, 56.38, 55.96, 47.35, 22.75, 21.89. ESI (MS): *m/z* calc. 1499.25; exp. 621.1 $[M - 2I]^{2+}$.

Chapter 3

Self-assembly of highly functionalized Ti(IV)

TPA *μ*-oxo complexes

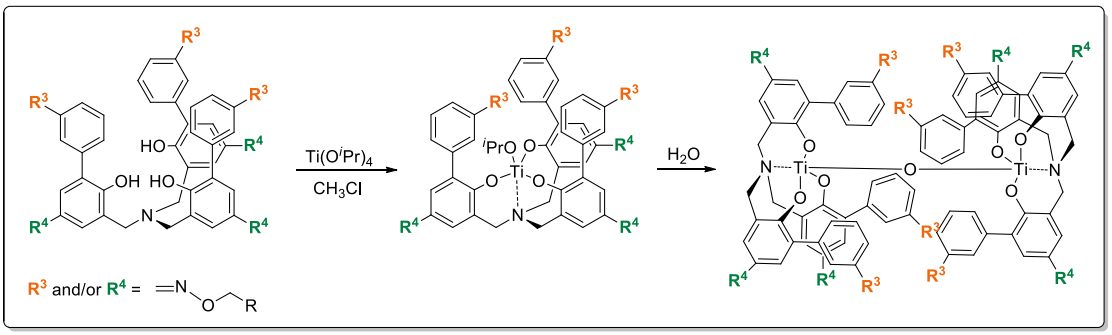

Amine triphenolate ligands react with Ti(O*i*-Pr)$_4$ to give stable mononuclear complexes. When phenyl substituents in *ortho* position to the phenolate are present, the mononuclear complexes spontaneously and quantitatively self-assemble into the corresponding *μ*-oxo dinuclear complexes as the only heterochiral S_6-symmetric diasteroisomers, upon reaction with water. The possibility to functionalise the systems by insertion of the right anchoring sites in *para* position to the phenolate and/or in *meta* position on the peripheral aryl rings can lead to the construction of stable and spatially ordered structures with multiple functionalities disposed in a controlled way into space.

3.1 Introduction

The development of smart functional materials supposes the precise and ordered organization of the building blocks they are made of. Within the field of nanotechnology and material sciences, most of the time the correct arrangement of building blocks into defined systems comes from self-assembly.

Self-assembly is driven by the formation of many weak but specific interaction forces that enable the systems to reach their thermodynamic minimum. In Nature, many functional systems are created by the self-assembly of a set of complementary components, and molecular recognition and self-organization are involved in order to generate a well-defined functional supramolecular architecture with a high degree of complexity. Examples of hierarchical self-assembly include TMV coat protein folding, DNA double helix, multienzyme complexes, formation of cell membranes with receptors, ion channels and transmembrane proteins and finally molecular motors, such as ATP synthase.[81]

In the effort of mimicking and reproducing the ability of biological systems to self-assemble in high ordered structures, recently, a huge number of nanoscale molecular assemblies has been developed, with molecular-recognition and directed self-assembly being the principal processes and non-covalent interactions, such as hydrogen bonding, π-π interactions and metal coordination, as the main forces involved.[82] For example, pyrene-containing derivatives have found many applications in host-guest chemistry, with cyclodextrins[83], calixarenes[84] and cucurbit[n]urils,[85] or as molecular receptors for metal analytes[86] or nitroaromatics.[87] In such these systems, non-covalent π-π interactions or ions

[81] J. S. Lindsey *New J. Chem.* **1991**, *15*, 153-180.

[82] (a) J.–M. Lehn *Angew. Chem. Int. Ed.* **1988**, *27*, 89-112. (b) G. M. Whitesides, E. E. Simanek, J. P. Mathias, C. T. Seto, D. Chin, M. Mammen, D. M. Gordon *Acc. Chem. Res.* **1995**, *28*, 37-44. (c) F. Garcia-Tellado, S. J. Geib, S. Goswami, A. D. Hamilton *J. Am. Chem. Soc.* **1991**, *113*, 9265-9269. (d) U. Hahn, J. J. González, E. Huerta, M. Segura, J.-F. Eckert, F. Cardinali, J. de Mendoza, J.-F. Neirengarten *Chem.-Eur. J.* **2005**, *11*, 6666-6672. (e) J. Xiao, Y. Liu, Y. Li, J.-P. Le, Y. Li, X. Xu, X. Li, H. Liu, C. Huang, S. Cui, D. Zhu *Carbon* **2006**, *44*, 2785-2792.

[83] (a) A. Le Goff, K. Gorgy, M. Holzinger, R. Haddad, M. Zimmerman, S. Cosnier *Chem.-Eur. J.* **2011**, *17*, 10216-10221. (b) M. Yu, S.–Z. Zu, Y.–P. Liu, B.-H. Han, Y. Liu *Chem.-Eur. J.* **2010**, *16*, 1168-1174. (c) M. Toda, N. Ogawa, H. Itoh, F. Hamada *Anal. Chim. Acta* **2005**, *548*, 1-10. (d) B. Chen, K. L. Liu, Z. Zhang, X. Ni, S. H. Goh, J. Li *Chem. Commun.* **2012**, *48*, 5638-5640.

[84] (a) M. Inouye, K. Hashimoto, K. Isagawa *J. Am. Chem. Soc.* **1994**, *116*, 5517-5518. (b) K. N. Koh, K. Araki, A. Ikeda, H. Otsuka, S. Shinkai, *J. Am. Chem. Soc.* **1996**, *118*, 755-758. (c) S.-D.Tan, W.-H. Chen, A. Satake, B. Wang, Z.-L. Xu, Y. Kobuke *Org. Biomol. Chem.* **2004**, *2*, 2719-2721.

[85] (a) D. Jiao, J. Geng, X. J. Loh, D. Das, T.-C. Lee, O. A. Scherman *Angew. Chem. Int. Ed.* **2012**, *51*, 9633-9637. (b) V. N. Sueldo Occello, A. V. Veglia *Anal. Chim. Acta* **2011**, *689*, 97-102.

[86] (a) E. Manandhar, K. J. Wallace *Inorg. Chim. Acta* **2012**, *381*, 15-43 and references therein. (b) E. Manandhar, J. H. Broome, J. Myrick, W. Lagrone, P. J. Cragg, K. J. Wallace *Chem. Commun.* **2011**, *47*, 8796-8798. (c) J. Y. Choi, D. Kim, J. Yoon *Dyes and Pigments* **2013**, *96*, 176-179. (d) F. Wang, R. Nandhakumar, J. H. Moon, K. M. Kim, J. Y. Lee, J. Yoon *Inorg. Chem.* **2011**, *50*, 2240–2245.

[87] (a) R. Vaiyapuri, B. W. Greenland, J. M. Elliott, W. Hayes, R. A. Bennett, C. J. Cardin, H. M. Colquhoun, H. Etman, C. A. Murray *Anal. Chem.* **2011**, *83*, 6208-6214. (b) Y. H. Lee, H. Liu, J. Y. Lee, S. H. Kim, S. K. Kim, J. L. Sessler, Y. Kim, J. S. Kim *Chem.-Eur. J.* **2010**, *16*, 5895-5901.

coordination are involved and quenching of pyrene fluorescence is used to detect and proof the actual interaction between the two entities.

More interestingly, in recent years, pyrene functionalized systems have been widely used to modify nanosized graphene-like carbon surfaces, such as fullerene (C_{60}) or carbon nanotubes (CNTs) *via* π-π interactions,[88] with the aim of realizing supramolecular nanodevices, with novel electronic, optical or catalytic properties.[89]

Thus, the interest in the design of systems that are able to self-assemble into ordered and functional scaffolds is rapidly increasing nowadays. Moreover, in this context, the ability of Ti (IV) TPA complexes to self-assemble under certain conditions, together with the possibility to functionalize the systems with specific residues, can lead to the preparation of functional molecular scaffolds, with potential applications in material sciences and supramolecular chemistry.

3.2 Self-asssembly of Ti(IV) amine triphenolate complexes

The robustness of amine triphenolate ligands is reflected in their ability to give rise to very stable complexes upon reaction with metal ions. However, in the case of Ti(IV) TPA complexes **2**, their stability in solution deeply depends on the steric size of the peripheral *ortho* substituents (Figure 1).

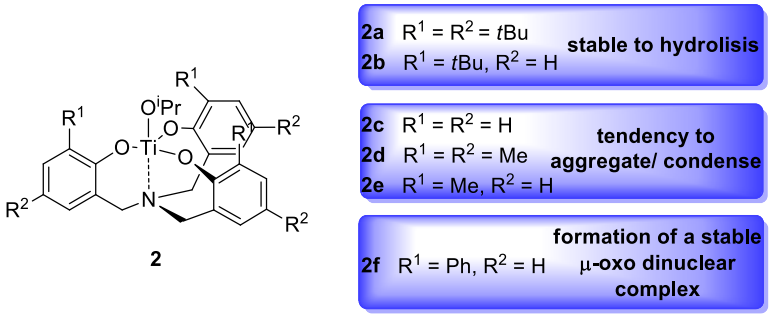

Figure 1. Influence of peripheral *ortho* substituents on stability of Ti(IV) TPA complexes in solution.

Complexes bearing *tert*-butyl *ortho* groups are very stable and resistant to hydrolysis, as the *t*-butyl substituents efficiently shield the *iso*-propoxide groups. As X-ray structure demonstrates, indeed, the C(*i*-Pr)-O-Ti bond on complex **2a** is shorter (1.788 Å) than the other Ti-O bonds on the phenolate oxygens (1.825-1.866 Å), indicating a strong π-interaction. Moreover, the complex possesses a slightly

[88] (a) R. J. Chen, Y. Zhang, D. Wang, H. Dai *J. Am. Chem. Soc.* **2001**, *123*, 3838-3839. (b) E. D. McQueen, J. I. Goldsmith *J. Am. Chem. Soc.* **2009**, *131*, 17554–17556. (c) N. Nakashima, Y. Tomonari, H. Murakami *Chem. Lett.* **2002**, 638-639. (d) J. Jeong, S. H. Lee, N. W. Song, C. S. Lee, B. H. Chung *Carbon* **2009**, *47*, 2112-2142. (e) F. Tournus, S. Latil, M. I. Heggie, J.-C. Charlier *Phys. Rev. B* **2005**, *72*, 075431-1-5. (f) G. Modugno, Z. Syrgiannis, A. Bonasera, M. Carraro, G. Giancane, L. Valli, M. Bonchio, M. Prato *Chem. Commun.* **2014**, *50*, 4881-4883.

[89] (a) S. Fujii. T. Morita, S. Kimura *Langmuir* **2008**, *24*, 5608-5614. (b) D. Eder *Chem. Rev.* **2010**, *110*, 1348-1385.

distorted trigonal bipyramidal geometry, with the metal lying above the plane defined by the three oxygen atoms of the phenolate rings.[90] Furthermore, in solution and in solid phase, the C_3-symmetric complex is present as a racemic mixture of Δ and Λ mononuclear complexes, as a result of a helical wrapping of the ligand around the metal ion.[10,91]

When small substituents (Me or H) are present in *ortho* positions to the phenolate, the complexes tend to aggregate even in presence of traces of water, to give μ-oxo[92] and bis μ-oxo complexes.[93] Thus, the complexes are more sensitive to hydrolysis and in the case of complex **2d**, it was possible to detect the μ-oxo species after exposure of the complex to air for a few days.[10,12b]

Finally, in the case of complex **1f**, that presents a phenyl group in *ortho* to the phenolate, it rapidly and spontaneously self-assembles into the dinuclear μ-oxo complex **3** in presence of very few traces of water (Scheme 1).[94]

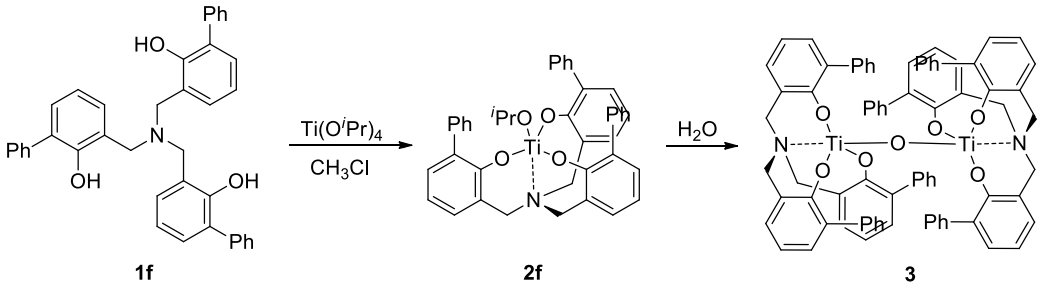

Scheme 1. Self-assembly of complex **2f** in solution.

Complex **3** shows unique characteristics, as it can be appreciated from X-ray structure (Figure 2). The Ti-O-Ti bond is linear (180.0°C), the peripheral aryl rings intercalate and are disposed in a propeller like fashion, while the two chiral titanatrane moieties have opposite configurations (Λ and Δ).

[90] M. Kol, M. Shamis, I. Goldberg, Z. Goldschmidt, S. Alfi, E. Hayut-Salant *Inorg. Chem. Commun.* **2001**, *4*, 177-179.
[91] C. Moberg *Angew. Chem. Int. Ed. Engl.* **1998**, *37*, 248-268.
[92] (a) A. J. Nielson, C. Shen, J. M. Waters *Polyhedron* **2006**, *25*, 2039-2054. (b) K. C. Fortner, J. P. Bigi, S. N. Brown *Inorg. Chem.* **2005**, *44*, 2803-2814.
[93] A. Senouci, M. Yaakoub, C. Hugeunard, M. Henry *J. Mater. Chem.* **2004**, *14*, 3215-3230.
[94] G. Bernardinelli, T. M. Seidel, E. P. Kündig, L. J. Prins, A. Kolarovic, M. Mba, M. Pontini, G. Licini *Dalton Trans.* **2007**, 1573-1576.

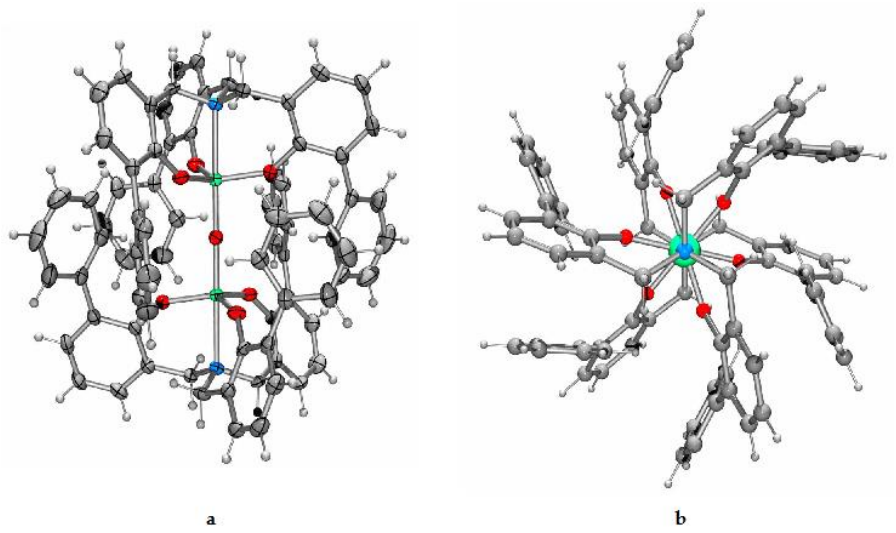

Figure 2. (a) Molecular structure of complex **3**. (b) View along the N-Ti-O-Ti axis.[14]

The interesting behaviour of complex **3** in solution can be followed by NMR spectroscopy (300 MHz, $CDCl_3$): ^{1}H-NMR spectrum of complex **2f** shows a single set of signals at 3.62 ppm for the methylene protons in α to the nitrogen, due to the fast interconversion of the two enantiomeric complexes on the NMR time scale (Figure 3a). However, upon standing in solution, complex **2f** rapidly evolves into a new, highly symmetric species, which precipitates over time form solution, giving rise to the dinuclear μ-oxo complex **3**. In this case, ^{1}H-NMR spectrum of **3** shows the formation of an AB system at 4.36 and 3.28 ppm, respectively. The signals, that correspond to the methylene protons, indicate that the racemization rate is much slower and the system formed is very stable, rigid and air and moisture tolerant. Moreover, the five protons of the peripheral aryl rings are shifted up field (ca. 1 ppm), as a consequence of the intercalation of the rings around the μ-oxo bridge (Figure 3b).

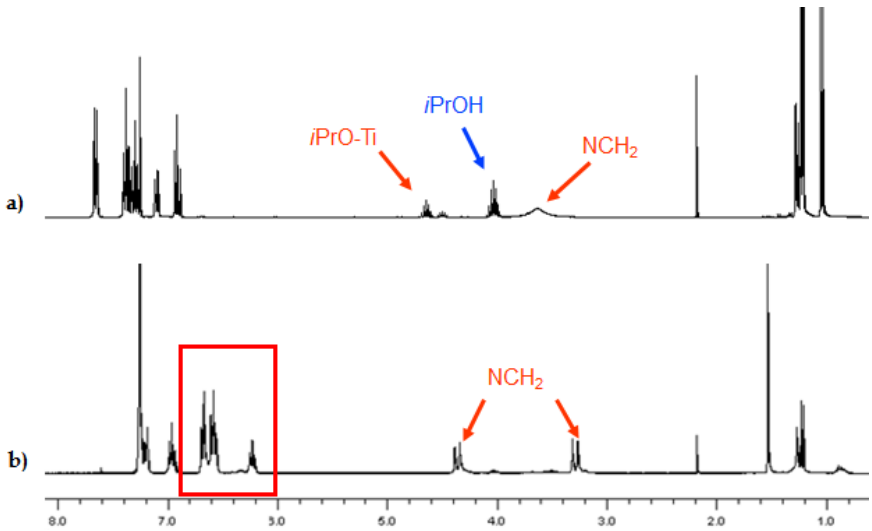

Figure 3. a) ^{1}H-NMR spectrum of complex **2f**; b) ^{1}H-NMR spectrum of complex **3**.

Interestingly, the two titanatrane moieties in **3** maintain the helical conformation around the metal ion, as in the case of monomeric complex **2f**, but, remarkably, starting from a racemic mixture of Λ and Δ complexes, exclusively the heterochiral compound (Λ-Δ) is formed. No traces of the diastereomeric homochiral complexes (Λ-Λ or Δ-Δ) are present in ^{1}H-NMR spectrum. Therefore, the exclusive presence of an S_6-symmetric heterochiral diastereoisomer in solution clearly indicates that complex **3** formation is a completely stereoselective self-discrimination process. This selective self-discrimination between enantiomeric units can make complex **3** suitable for interesting applications in supramolecular chemistry[95] and material sciences.

3.3 Ti(IV) TPA *μ*-oxo complexes as multifunctional molecular scaffolds

The ability of complex **2f**, bearing phenyl substituents, to self-assemble spontaneously in solution, giving rise to ordered and stable structures can be exploited to build up supramolecular systems[15] and molecular scaffolds for further applications in material sciences.

Dinuclear Ti(IV) TPA *μ*-oxo complex can be selectively functionalized in its periphery in order to be used as platform with multiple functions disposed in a controlled way into space (Figure 4). In this way, by introducing regularly distributed anchoring sites, the system can be decorated with other molecules, paving the way for the development of more complex structures.

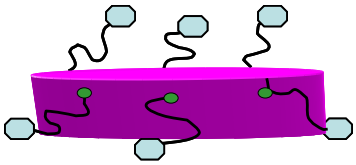

Figure 4. Schematic representation of a multifunctional platform.

The exceptional characteristics of Ti(IV) TPA *μ*-oxo complex **3**, i.e. its stability to further hydrolysis and its self-organization, make it an ideal candidate for the design of novel functionalized molecular scaffolds. In particular, the construction of proper functionalized *tri*-phenolamines should be the key element for the self-organized construction of more complex platforms. However, a suitable modification strategy has to be set up for the introduction of specific functionalities in *μ*-oxo complex **3** periphery, as its integrity and self-assembling process have to be preserved.

More in detail, the dinuclear complex **3** has twelve potential anchoring sites. Six sites correspond to the *para* positions of the phenolate group of the ligand (Figure 5). These residues can be functionalized through the introduction of three

[95] (a) Lehn, J.-M. *Supramolecular Chemistry*, VCH, Weinheim, **1995**. (b) Steed, J. W.; Atwood, J. L. *Supramolecular Chemistry*, Wiley, Chichester, **2000**.

formyl groups *via* Duff reaction.[96] The choice of introducing aldehyde moieties lies in the fact that they are highly reactive and can be further transformed into a wide variety of functional groups.

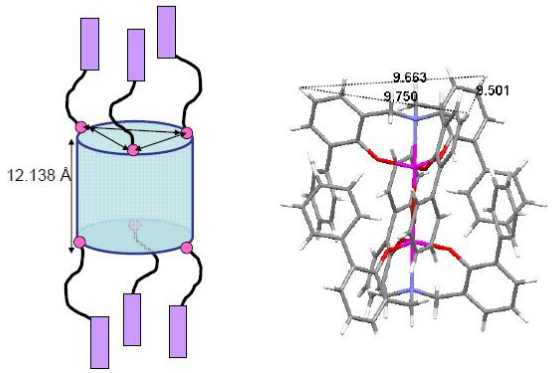

Figure 5. Anchoring sites for the formation of linear structures.

The other six potential anchoring sites are found in the *meta* positions of the peripheral *ortho* phenyl moieties, affording a six-tip star structure (Figure 6). In order to perform this functionalization a specific synthesis of the ligands *via* Suzuki-Miyaura coupling reaction has to be carried out, as depicted in chapter 2.[97] Even in this case, the introduction of three formyl groups is the best choice for further derivatizing the systems.

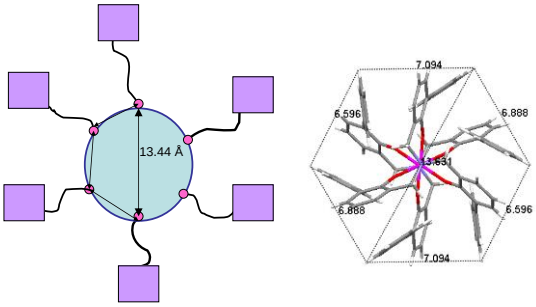

Figure 6. Anchoring sites in the periphery for the construction of star structures.

3.3.1 Ti(IV) TPA μ-oxo complexes functionalization

From a synthetic viewpoint, complex **3** is obtained by reaction of ligand **1f** with one equivalent of Ti(O*i*-Pr)$_4$ in chloroform. Firstly, complex **2f** forms, which, upon standing in solution, readily transforms into dinuclear complex **3**. In order to address the functionalization strategy on **3**, complexation reaction on ligand **4**, which is obtained by insertion of three aldehyde groups on **1f** *via* Duff reaction,[16]

[96] (a) J. C. Duff, E. J. Bills *J. Chem. Soc.* **1945**, 276-277. (b) A. L. Kurlovich, V. A. Tarasevich, N. G. Kozlov *Russ. J. Org. Chem.* **2009**, *45*, 1503-1508.
[97] (a) N. Miyaura, K. Yamada, A. Suzuki *Tetrahedron Lett.* **1979**, *20*, 3437-3440. (b) N. Miyaura, A. Suzuki *J. Chem. Soc., Chem. Commun.* **1979**, 866-867. (c) K. C. Nicolau, R. M. Evans, A. Roecker, R. Hughes, M. Downes, J. A. Pfefferkorn *Org. Biomol. Chem.* **2003**, *1*, 908-920.

has to be performed. In this way, the six-fold formylated Ti(IV) TPA μ-oxo complex **6** is generated (Scheme 2).

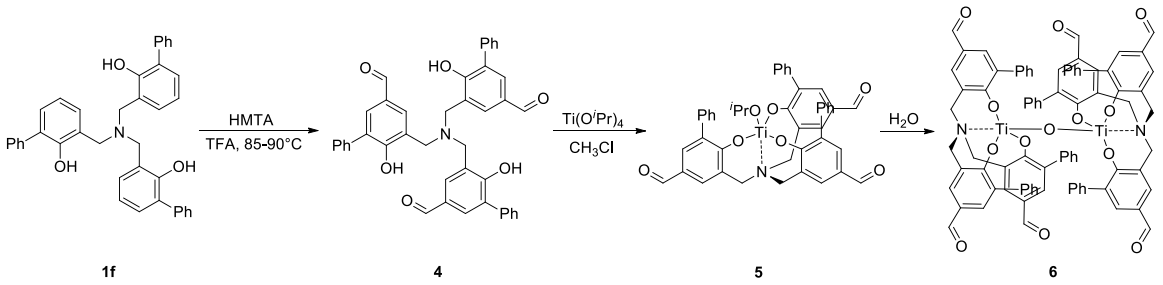

Scheme 2. Synthesis of Ti(IV) TPA μ-oxo complex **6**.

As we can see, also in this case, when complex **5** forms, it rapidly reacts with water to give dinuclear μ-oxo complex **6**. By comparing ^{1}H-NMR spectra of complexes **5** and **6** (Figure 7a and 7b, respectively), we can notice again that the self-assembling process is stereoselective and complex **6** is present in solution as a single diastereoisomer, as demonstrated by the AB system relative to the methylene protons, with peaks at 3.52 and 4.30 ppm, respectively.

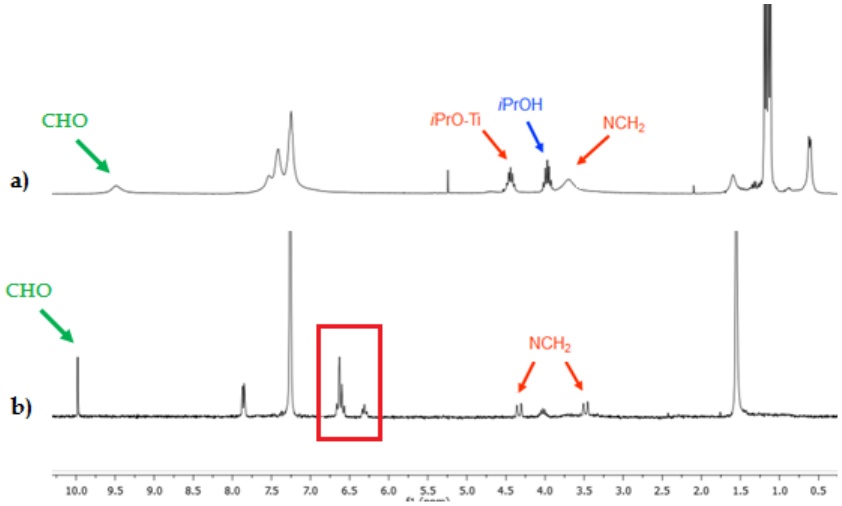

Figure 7. ^{1}H-NMR spectra (300 MHz, $CDCl_3$) of: a) mononuclear complex **5**; b) dinuclear μ-oxo complex **6**.

ESI-MS spectra of complex **6** both in positive and negative modes clearly show the formation of the complex and all the experimental isotopic distributions are in agreement with the calculated ones (Figure 8).

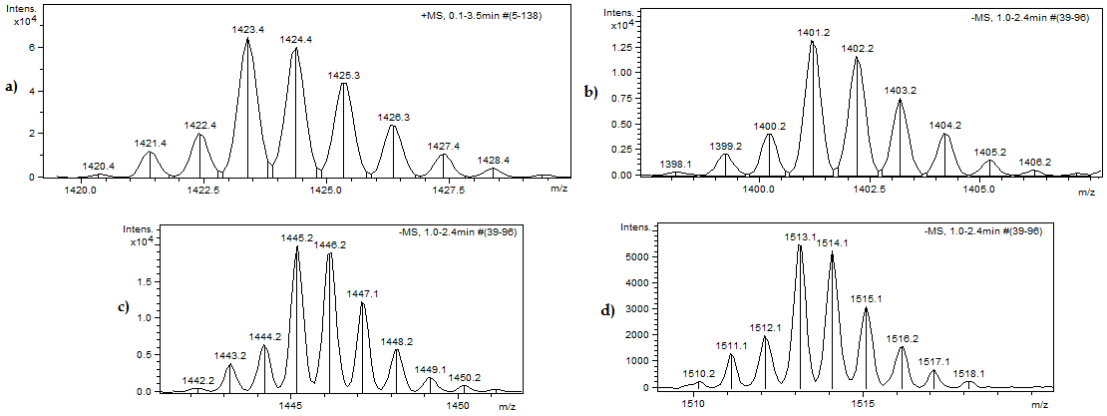

Figure 8. ESI-MS spectra of complex **6**, with its isotopic distributions: a) $[M + Na]^+$; b) $[M]^-$; c) $[M + HCOO]^-$; d) $[M + CF3COO]^-$.

Even the stability of the μ-oxo complex **6** has been examined, in particular in presence of an excess competitive ligand, such as deuterated methanol. After only 5 min, the dinuclear complex is completely transformed into the mononuclear complex **7**, bearing very likely a molecule of methanol as apical ligand. However, upon evaporation of the methanolic solution and addition of water, it is possible to restore the dinuclear complex **6** (Figure 9).

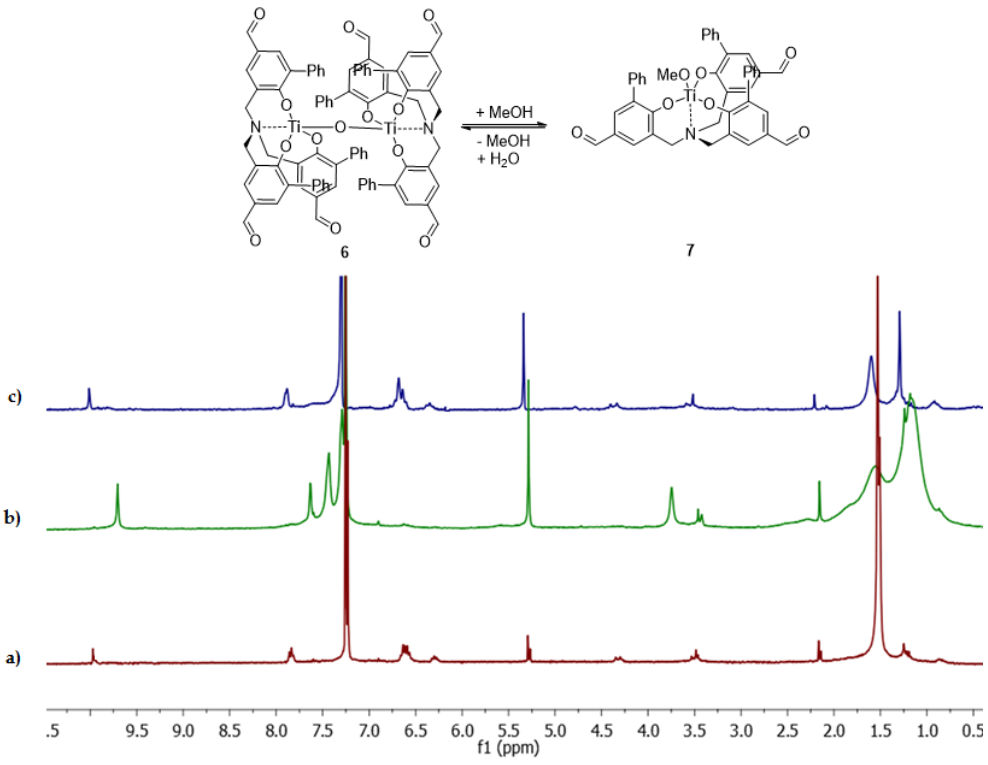

Figure 9. ^{1}H-NMR spectra (300 MHz, $CDCl_3$) of complex **6**: a) before MeOH addition; b) after MeOH addition; c) after MeOH evaporation and H_2O addition.

Similarly, when TPA **8**, bearing three aldehyde groups in *meta* position on the peripheral aromatic rings, is reacted with Ti(O*i*-Pr)$_4$, mononuclear complex **9** gives dinuclear μ-oxo complex **10** upon reaction with water (Scheme 3).

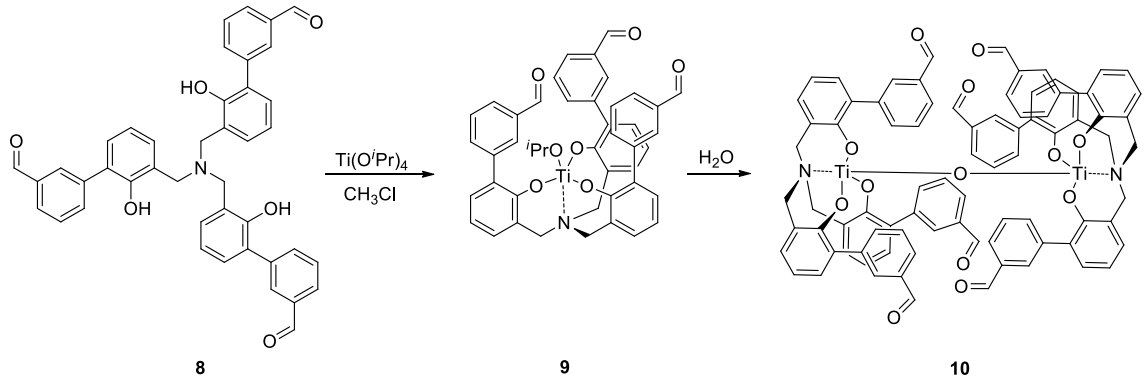

Scheme 3. Synthesis of Ti(IV) TPA μ-oxo complex **10**.

Again, the same behaviour in solution is observed for Ti(IV) TPA μ-oxo complex **10**, as ^{1}H-NMR spectrum in figure 10 shows.

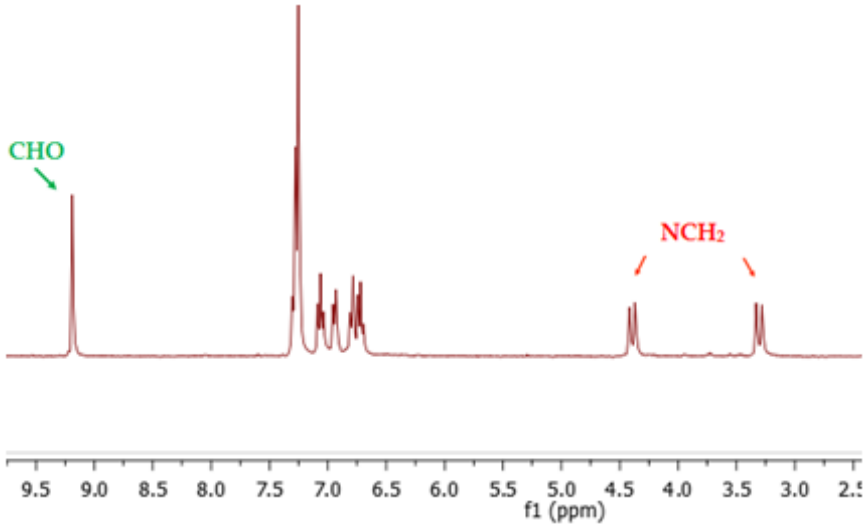

Figure 10. ^{1}H-NMR spectrum (300 MHz, $CDCl_3$) of dinuclear Ti(IV) TPA μ-oxo complex **10**.

The insertion of anchoring formyl sites in *para* or *meta* positions offers the possibility to further functionalize the μ-oxo complexes through a "click-type" oxime bond formation by reaction of the aldehyde groups with different alkoxyamines, as already mentioned in chapter 2.

Ideally, a double functionalization pathway for the modification of μ-oxo complexes can be applied: we can functionalize the TPA ligand **4** with an appropriate alkoxyamine **11a-f** and then effect the complexation reaction to obtain functionalized μ-oxo complexes **14a-f**, upon reaction of the mononuclear complexes **13a-f** with water. Alternatively, we can carry out the functionalization reaction directly on six-fold formylated complex **6** (Scheme 4). In both cases, the reactions are almost quantitative and the products are obtained by precipitation in diethyl ether in the form of yellow-orange solids.

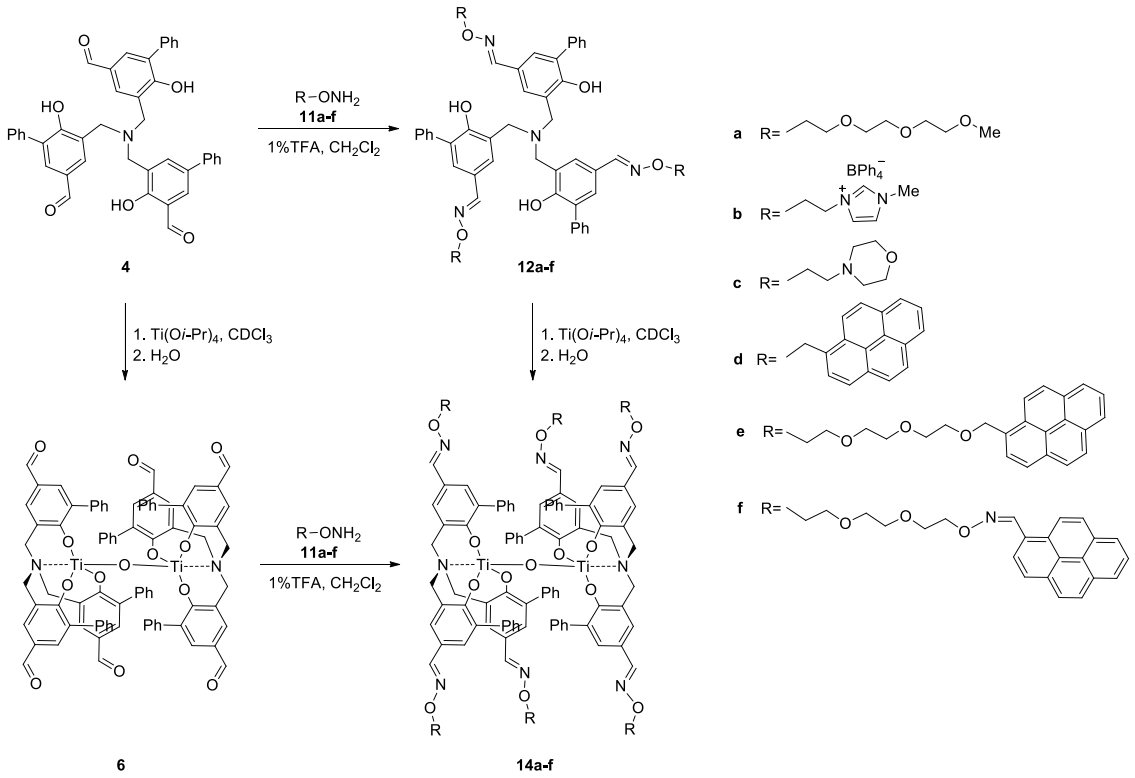

Scheme 4. Synthesis of *para* functionalized of Ti(IV) TPA μ-oxo complexes through oxime bond formation (mononuclear complexes **13a-f** are omitted for clarity).

The speciation of Ti(IV) TPA μ-oxo complexes **14a-f** was confirmed both via ^{1}H-NMR spectroscopy and ESI-MS spectrometry (ESI_TOF or ESI-Ion Trap). As an example, in figure 11 ^{1}H-NMR spectrum of complex **12a** is reported. The methylene protons are not clearly detectable, as they fall in the same region as protons coming from TEG chain. A significant shift of the aromatic protons of the ortho-phenyl groups (red square in figure 11) can be observed, due to the shielding of the aromatic groups in the μ-oxo complex, proving the formation of the dinuclear complex.

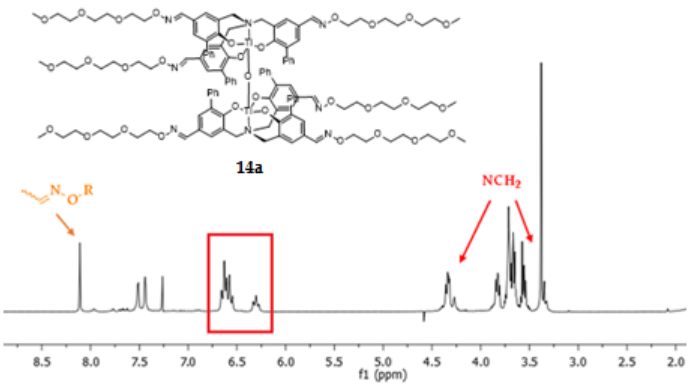

Figure 11. ^{1}H-NMR spectrum (300 MHz, $CDCl_3$) of complex **14a**.

In the case of positively charged complex **14b**, ^{1}H-NMR spectrum was too complex for an unequivocal interpretation, very likely because of aggregate

formation in solution. However, ESI-TOF spectrum of the complex (methanol as mobile phase) clearly shows the formation of the complexes. Beside the dinuclear complex also the mononuclear hydroxyl or methoxy complexes could be detected. The mononuclear form under the experimental conditions required for the ESI-MS analysis. Furthermore, as different counterions can be present due the electron spray conditions, several clusters were detected as double-, triple- or even quadruple-charged species (Figure 12). All the peaks detected in the spectra showed the characteristic isotopic distribution of mono and dinuclear titanium complexes and are in complete agreement with the theoretical ones.

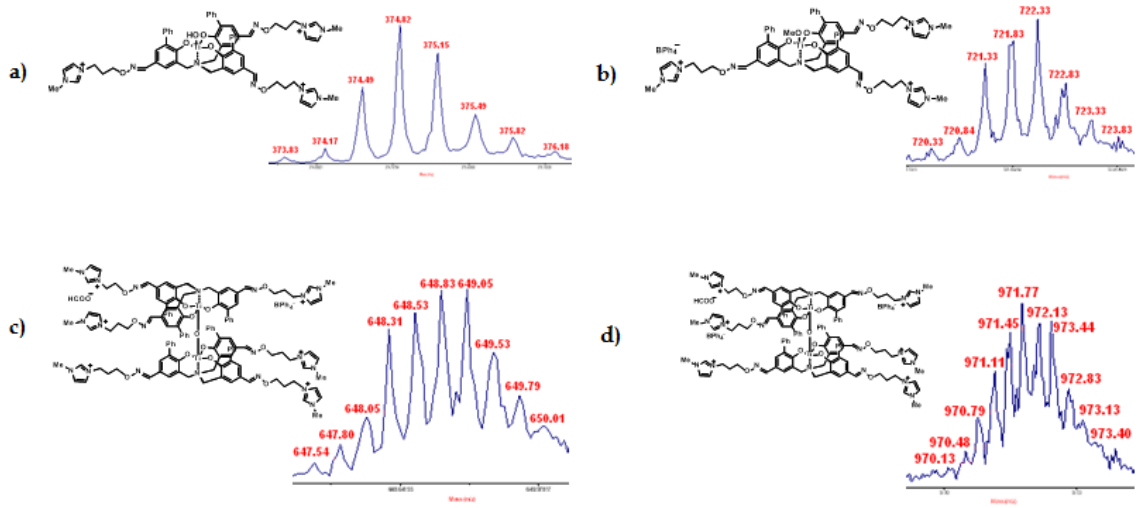

Figure 12. ESI-TOF of complex **14b**, with isotopic distributions for: a) $[M/2(Ti\text{-}OH) - 3BPh_4]^{3+}$; b) $[M/2(Ti\text{-}OMe) - 2BPh_4]^{2+}$; c) $[M - 5BPh_4 + HCOO]^{4+}$; d) $[M - 4BPh_4 + HCOO]^{3+}$.

Interestingly, μ-oxo complex **14c** could be *N*-methylated upon reaction for 72 h with methyl trifluoromethansulfonate (MeOTf). Complex **15** separates from solution in the form of an orange oil (Scheme 5).[98]

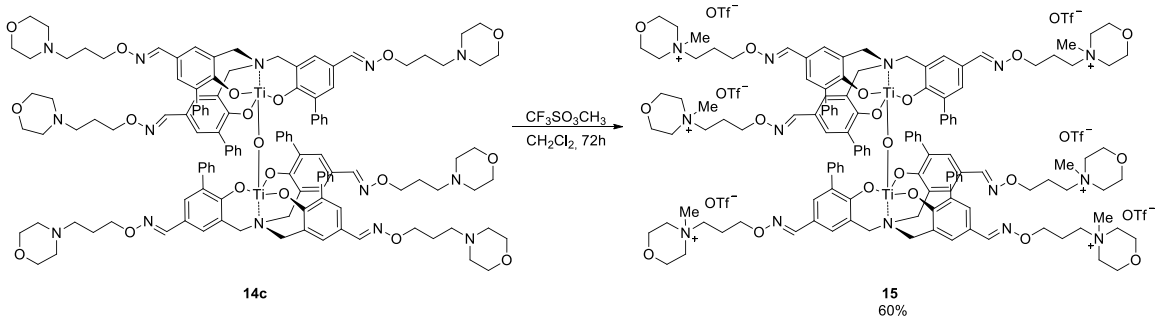

Scheme 5. *N*-methylated Ti(IV) TPA μ-oxo complex **15**.

[98] A. J. Walker, N. C. Bruce *Tetrahedron* **2004**, *60*, 561-568.

In figure 13, ESI-MS spectra of complexes **14c** and **15** are reported. In this case only the mononuclear derivatives could be detected.

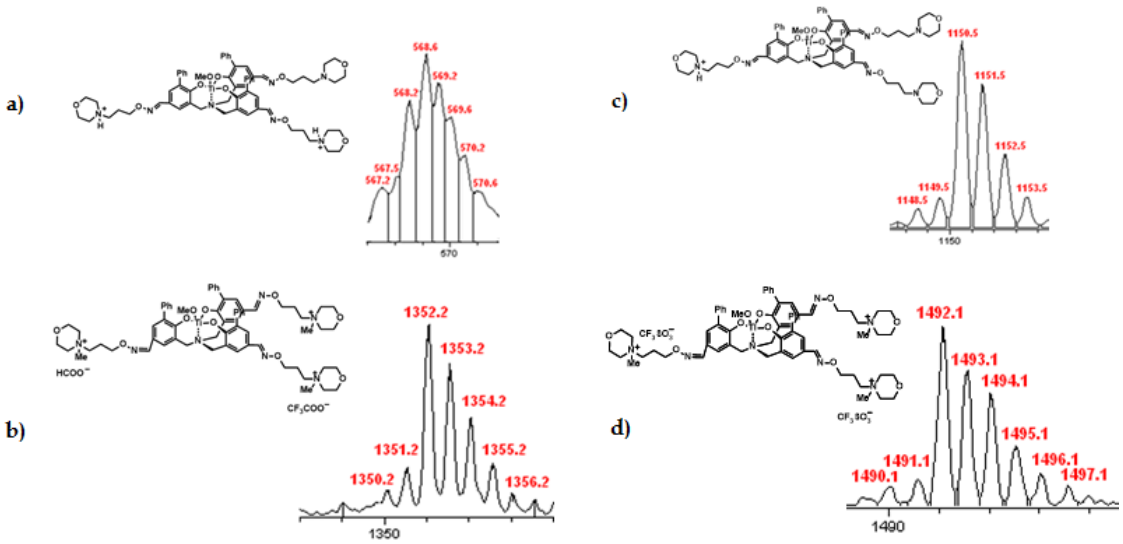

Figure 13. ESI-MS of complexes **14c** (a and b) and **15** (c and d); isotopic distributions for: a) $[M/2(Ti\text{-}OMe) + 2H]^{2+}$; b) $[M/2(Ti\text{-}OMe) + H]^{+}$; c) $[M/2(Ti\text{-}OMe) - 3OTf + HCOO + CF_3COO]^{+}$, d) $[M/2(TiOMe) - OTf]^{+}$.

The same functionalization strategy can be applied to the *meta* positions on Ti(IV) TPA μ-oxo complex **10**, thus leading to the synthesis of complexes **16a,b**, **16d** and **16g** (Figure 14).

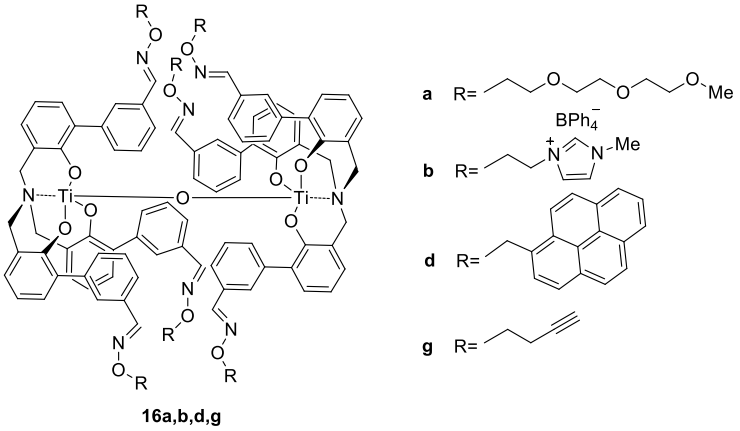

Figure 14. Synthesis of *meta* functionalized of Ti(IV) TPA μ-oxo complexes through oxime bond formation.

In order to have a further proof of the effectiveness of modification reaction, a twelve-fold *para/meta* functionalization of Ti(IV) TPA μ-oxo complexes has been efficiently carried out. Again, a double synthetic pathway can be established: functionalization of TPA **17**, bearing six formyl groups both in *para* and *meta* positions, with alkoxyamine **11a** can be firstly performed, followed by complexation with Ti(O*i*-Pr)$_4$ and reaction with water, to give the twelve-fold

para/meta functionalized Ti(IV) TPA μ-oxo complex **20**. The latter can be also obtained by effecting the complexation reaction on TPA **17**, to give rise to the twelve-fold *para/meta* formylated Ti(IV) TPA μ-oxo complex **19**, which is then functionalized by reaction with alkoxyamine **11a** (Scheme 6).

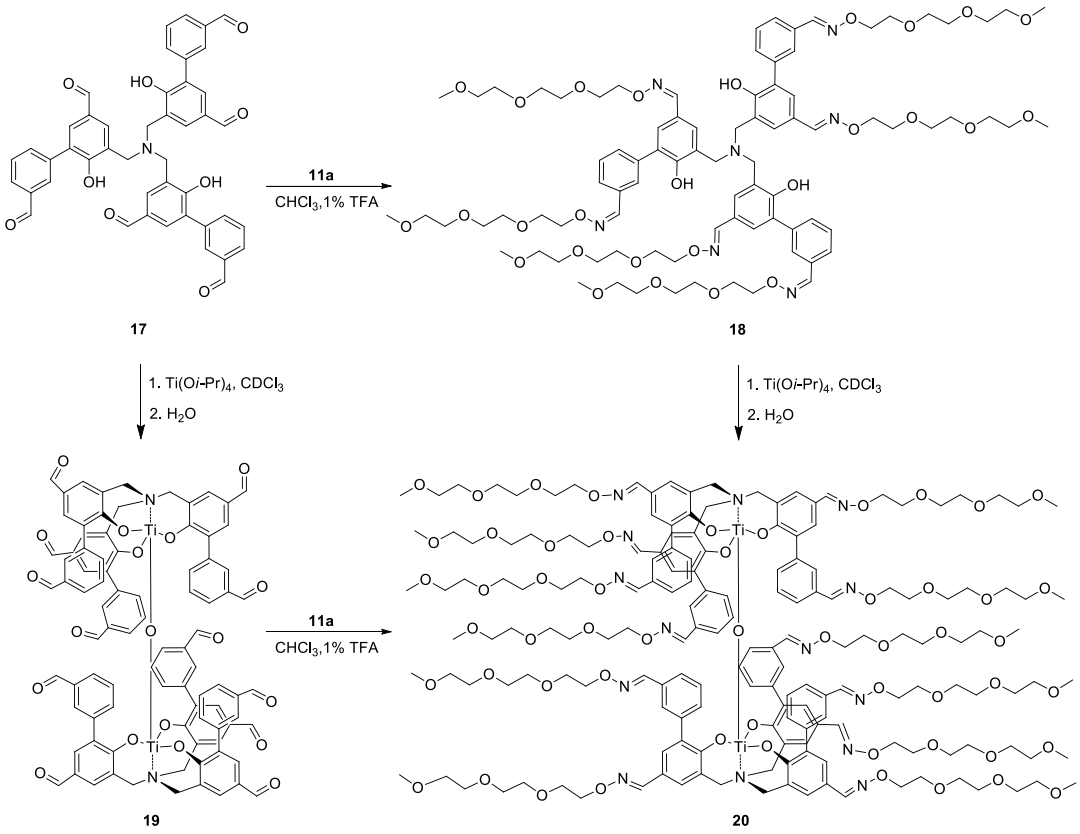

Scheme 6. Synthesis of *para/meta* functionalized of Ti(IV) TPA μ-oxo complex **20**.

In figure 15 ^{1}H-NMR spectra of complexes **17** and **18** are reported.

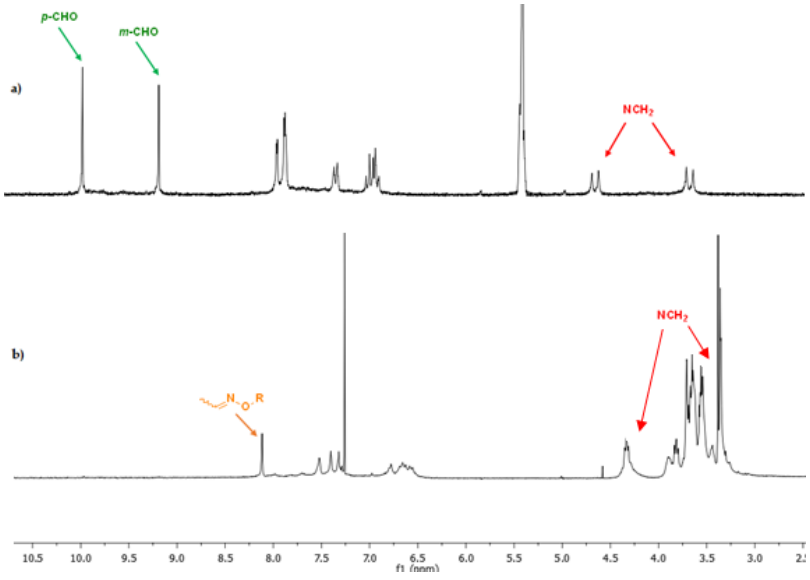

Figure 15. ^{1}H-NMR spectra of: a) complex **19** 200 MHz, CD_2Cl_2); b) complex **20** (300 MHz, $CDCl_3$).

3.3.2 Applications of functionalized Ti(IV) TPA μ-oxo complexes

The modifications introduced on Ti(IV) TPA μ-oxo systems up to now has allowed us to obtain a new class of complexes, whose application in supramolecular chemistry[15] and molecular sciences seems very appealing.

As a first qualitative analysis, we have studied how the introduction of polar residues on Ti(IV) TPA μ-oxo complexes could influence the solubility of the systems in polar organic solvents. Indeed, both complexes **3** and **6** are insoluble in most organic solvents and this characteristic sometimes limits their applicability. Thus, the functionalization of complex **6** with polar chains, such as TEG moieties and positively charged tags, on complexes **14a**, **14b** and **15** let us increase dramatically their solubility in dichloromethane, chloroform and acetonitrile.

However, the most important application concerns the functionalization with pyrene moieties, which can open the possibility to develop novel hybrid molecular scaffolds. Indeed, in last years, organic nanomaterials have received a great interest, due to their thermal and chemical stability and electrical conductivity.[8e,99] Among these materials, surfaces of graphene family, such as fullerenes, carbon nanotubes and carbon-coated metal nanoparticles, are emerging as very interesting scaffolds. Both covalent[100] and non-covalent modifications[8a,c] of the systems can be addressed. However, very often, covalent functionalization is based on harsh chemical reactions, that may damage the nanostructures. Thus, non-covalent π-π interactions between such these nanosized carbon scaffolds and aromatic compounds, such as pyrene molecules, seems more feasible. Moreover, the interaction with matter would be physical rather than chemical and consequently reversible, allowing the release of the interacting molecules by adjusting temperature, solvents or pH.

The use of pyrene as fluorescent probe is widespread, mainly because of its suitable photophysical properties, like the electron donor effect and the strong fluorescence,[6b,9a,101] and its interaction with strong electron acceptor molecules is widely studied. Moreover, its extended π-system makes it suitable for the binding to hydrophobic/aromatic molecules, including fullerene (C_{60}) and carbon nanotubes (CNTs).[7a,102]

Thus, we studied the possibility to generate a supramolecular nanostructure between C_{60} and pyrene functionalized Ti(IV) TPA μ-oxo complexes **14f** and **16d**, bearing pyrene residues in *para* and *meta* positions, respectively.

---

[99] K. Kordatos, T. Da Ros, M. Prato, C. Luo, D. Guldi *Monatshefte für Chemie* **2001**, *132*, 63-69.
[100] (a) R. B. Martin, K. Fu, Y.-P. Sun *Chem. Phys. Lett.* **2003**, *375*, 619-624. (b) V. Georgakilas, K. Kordatos, M. Prato, D. M. Guldi, M. Holzinger, A. Hirsch *J. Am. Chem. Soc.* **2002**, *124*, 760-761.
[101] (a) M. I. Sluch, I. D. W. Samuel, M. C. Petty *Chem. Phys. Lett.* **1997**, *280*, 315-320. (b) D. Tasis, D. T. Mikroyannidis, V. Karoutsos, C. Galiotis, K. Papagelis *Nanotechnology* **2009**, *20*, 135606-135613. (c) I. Ramakanth, A. Patnaik *Carbon* **2008**, *46*, 692-698.
[102] T. Ogoshi, Y. Takashima, H. Yamaguchi, A. Harada *J. Am. Chem. Soc.* **2007**, *129*, 4878-4879.

Firstly, fluorescence studies of the complexes in different solvents were performed. As intensities of pyrene bands in the fluorescence spectrum strongly depend on the polarity of the environment,[103] fluorescence spectra of complex **14f** were recorded using solutions in chloroform, acetonitrile and toluene (Figure 16).

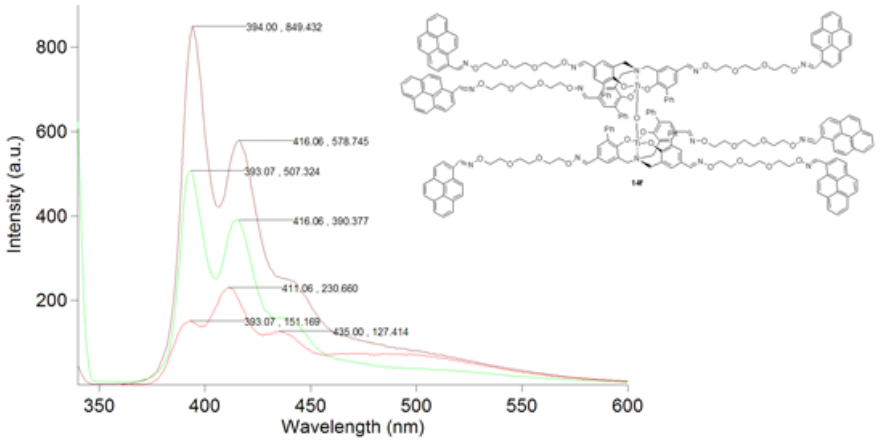

Figure 16. Emission spectra of complex **14f** ($1*10^{-5}$ M) in chloroform (purple), acetonitrile (green), toluene (red). Excitation at 388 nm.

As we can notice, neither shapes nor positions of peaks changed sensitively in chloroform and acetonitrile. We can identify two sharp peaks at 394 and 416 nm (in chloroform), which correspond to pyrene monomer emissions, together with an additional broad band at around 450-550 nm, which corresponds to the pyrene excimer emission. Therefore, we can assume that there are two emitters in the complex. However, as pyrene monomer emission is dominant, we can infer that no strong interaction among the pyrene units in the complex in the excited state is present. When the fluorescence spectrum was recorded in toluene, the emission maxima were different both in shape and position: peaks relative to the monomer were present at 393, 411 and 435 nm, while the broad band of the excimer is stronger and is located at around 450-550 nm. From the analysis of the spectra, it is clear that the intensity of monomers decreases passing from chloroform to acetonitrile and toluene, whereas the intensity of the excimer increases, indicating that the interaction between pyrene molecules is more favoured in nonpolar solvents. So, toluene was chosen as the best solvent in this fluorescence study.

Even the emission spectrum of complex **16d** was recorded in toluene (Figure 17). In this case, we observed a much more intense band of the excimer, thus indicating that the presence of the longer and more flexible TEG chains and/or the relative positions in complex **14f** could facilitate the inter or intramolecular π-π interaction between pyrene groups. This aspect will be explored more in detail in future studies by the synthesis of other TPA μ-oxo complexes with the two pyrene

[103] (a) F. M. Winnik *Chem. Rev.* **1993**, *93*, 587-614. (b) Y. Matsunaga, K. Takechi, T. Akasaka, A. R. Ramesh, P. V. James, K. G. Thomas, P. V. Kamat *Phys. Chem. B* **2008**, *112*, 14539-14547.

linkers in the other positions (TEG-pyrene units in *meta* positions or the shorter linker in para position of the phenol units) and fluorescent studies.

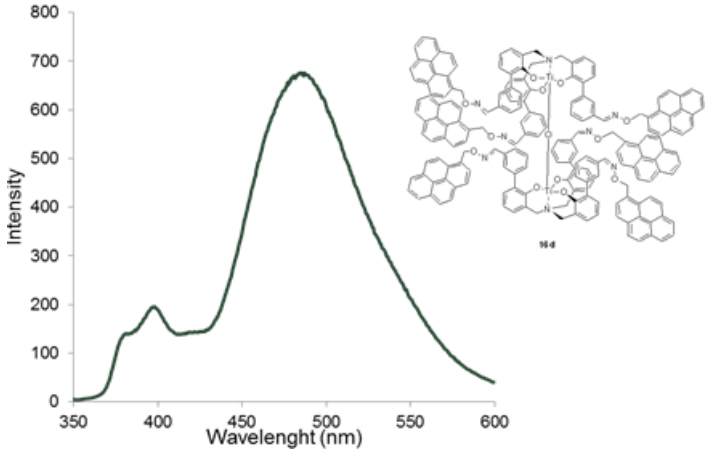

Figure 17. Emission spectrum of complex **16d** (1*10-5 M) in toluene. Emission at 388 nm.

Preliminary studies on the supramolecular host-guest interactions between complexes **14f** and **16d** and fullerene C_{60} were carried out. To toluene solutions ($1*10^{-5}$ M) of both complexes **14f** and **16d** increasing amounts of C_{60} were added and the corresponding fluorescence spectra were recorded. In both cases, the wavelengths of pyrene fluorescence maxima did not change upon addition of C_{60} while pyrene intensities of emission bands gradually decreased, due to pyrene fluorescence quenching after interaction with fullerene (Figure 18).

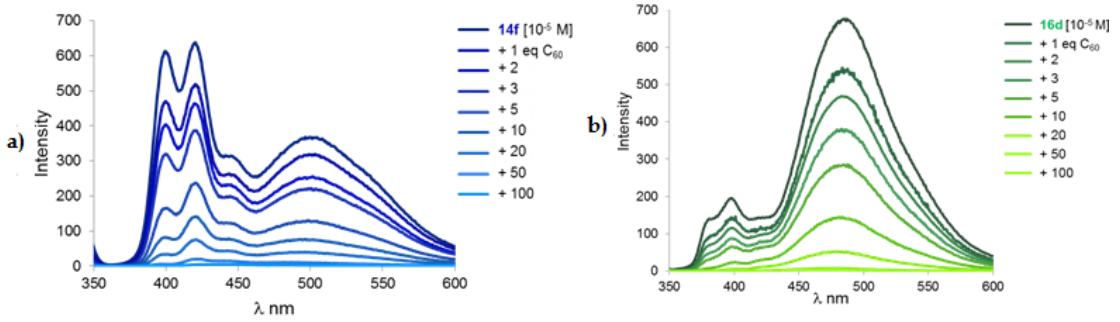

Figure 18. Fluorescence quenching of 10^{-5} M solutions of complexes **14f** (a) and **16d** (b) upon titration with increasing amounts of C_{60}. Excitation at 388 nm.

Monitoring the fluorescence intensity ratios (I_0/I^{-1}) at 420 and 485 nm, respectively, yielded linear Stern-Volmer (SV) plots as a function of C_{60} addition (up to 5 equivalents) (Figure 19).

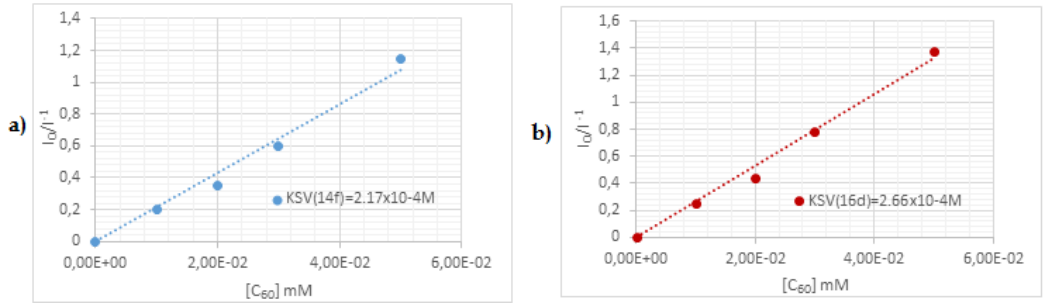

Figure 19. Stern-Volmer plot of fluorescence intensity ratio, I/I_o for a) **14f** 420 nm; and b) **16d** 485 nm as a function of C_{60} concentration.

The resulting binding constants ($K_{SV\mathbf{14f}}$ = 2.2 x 10^4 M^{-1} and $K_{SV\mathbf{16d}}$ = 2.7 x 10^4 M^{-1}) were estimated through linear regression of the points obtained at lower C_{60} concentrations, below [6x10^{-5} M]. At higher [C_{60}] concentrations C_{60} forms aggregates with a consequent decrease in I_0/I ratios due to an "inner filter effect", and curvature of the plot. [104] The comparable values of Ksv for both **14f**/C_{60} and **16d**/C_{60} complexes are consistent with a pyrene-driven host-guest interaction and in line with the data reported in the literature for similar systems.[105] Future studies will explore the system more in detail.

Finally, DOSY-NMR experiments were carried out to obtain further evidence of interaction between pyrene moieties of complexes **14f** and **16d** and C_{60}. Diffusion Ordered NMR SpectroscopY (DOSY) is the two dimensional version of the PGSE (Pulse Gradient Spin-Echo Experiment) NMR experiment, which allows to determine the translational diffusion constants (Dt) of the species present in a solution.[106] Since Dt of a solute is inversely proportional to its hydrodynamic radius, PSGE or DOSY experiments allow to evaluate the relative sizes of species present in a solution, or even determine their hydrodynamic radii provided that the shapes of the diffusing particles are known.[107]

By applying the Stokes-Einstein equation (1) and assuming the molecules as spherical particles:

$$D = k_B T/6\pi\eta r \quad (1)$$

where k_B is Boltzmann constant, T is absolute temperature, η is the viscosity and r the radius of the spherical particle considered. The ratio $1/6\pi\eta r$ is also defined as the particle mobility, μ.

Thus, in our case, DOSY spectra of 1 mM solutions in deuterated benzene of complexes **14f** and **16d** with and without C_{60} (2 eq.) were registered at 298 K. As shown in figure 20, the diffusion constants decreased in the order: **14f** > **14f**/C_{60}

[104] Y. L. Hwang, K. C. Hwang *Fullerene Sci. Techn.* **1999**, *7*, 437-454.
[105] G. Modugno, Z. Syrgiannis, A. Buonasera, M. Carraro, G. Giancane, L. Valle, M. Bonchio, M. Prato *Chem. Commun*. **2014**, *50*, 4881-4883.
[106] T. D. W. Claridge in *High-Resolution NMR Techniques in Organic Chemistry*, 2nd Ed., Elsevier, Amsterdam, **2009**, pp. 303-334.
[107] (a) A. Macchioni, G. Ciancaleoni, C. Zuccaccia, D. Zuccaccia *Chem. Soc. Rev.* **2008**, *37*, 479-489. (b) A. Pastor, E. Martínez-Viviente *Coord. Chem. Rev.* **2008**, *252*, 2314-2345.

and **16d** > **16d**/C_{60}, respectively. From these values, the relative molecular volumes can be approximately determined:

V **14f**/C_{60} > 1.5 V **14f** and V **16d**/C_{60} > 2.7 V **16d**.

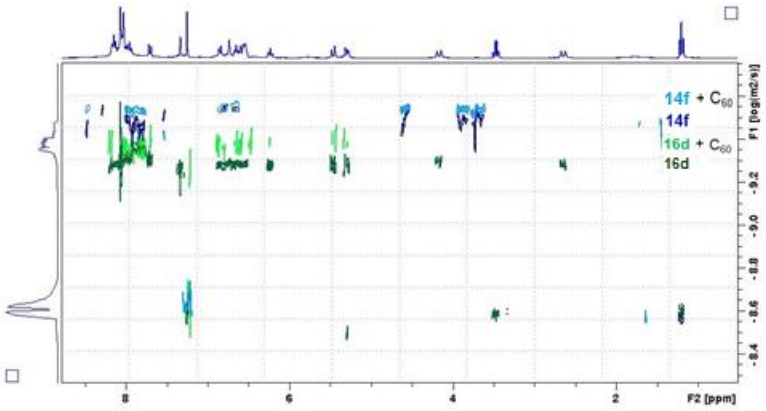

Figure 20. Comparison of DOSY spectra (300 MHz, C_6D_6) of complex **14f** and **16d** in the absence and presence of C_{60} (complexes/C_{60} molar ratio: 1/2).

The interaction of Ti(IV) TPA μ-oxo complex **14f** with SWCNTs has been investigated as well. The binding affinity of **14f** towards low dimensional HiPco and CoMoCAT SWCNTs has been exploited to yield stable dispersions of the tubes upon sonication in DMF/MeOH 1:1 solution (30 min at room temperature), followed by stirring (30 min at room temperature) and centrifugation (1 h at 3000 rpm). The resulting supernatant dispersion was separated from the precipitate, analysed by UV-Vis-NIR absorption and fluorescence spectroscopies, which were compared to those obtained with HiPco and CoMoCAT tubes solubilized using 1% sodium dodecyl sulfate (SDS) in H_2O. From UV-Vis-NIR we can appreciate the interaction between complex **14f** and CNTs (Figure 21).

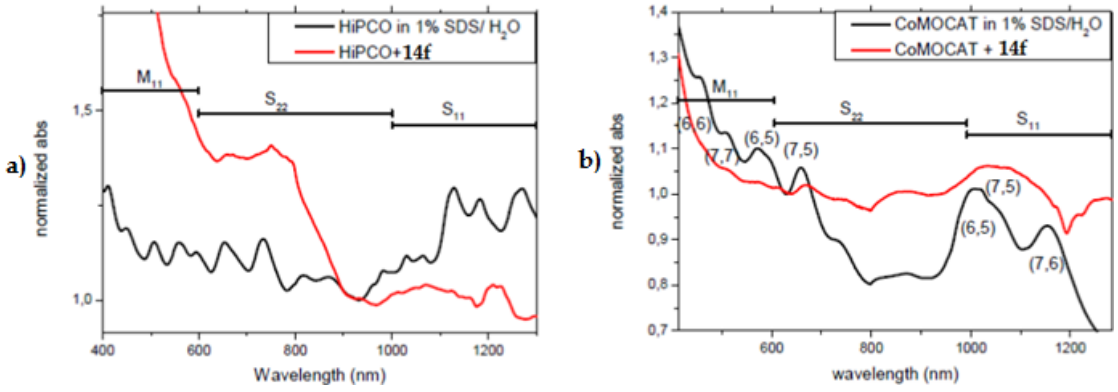

Figure 21. Normalized UV-Vis-NIR spectra of a) **14f**@HiPco in DMF and b) **14h**@CoMoCAT, in comparison with HiPco spectra recorded in 1% SDS in D_2O.

Moreover, from fluorescence experiments a difference in the pattern of pyrene signals from **14f** at the edge of Vis range was observed: pyrene units peaks were red-shifted if referred to **14f** blank peaks, and two new peaks appeared at

around 412 nn and a shoulder at around 444 nm, with no significant variations in intensity of signals (Figure 22).

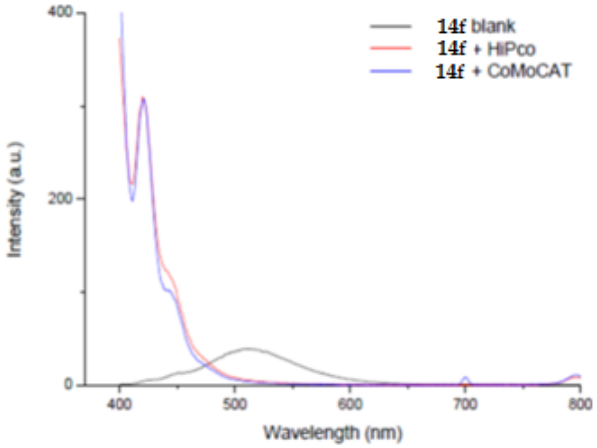

Figure 22. Fluorescence spectra of **14f** (black), **14f**@HiPco and **14f**@CoMoCAT. Excitation at 350 nm.

Concerning Raman spectroscopy, in the case of **14f**@HiPco, a red shift on the RBM region appeared, which may be consistent of the electronic interaction and charge transfer between **14f** and CNTs, whereas no significant shifts were detected in **14f**@CoMoCAT Raman spectrum (Figure 23).

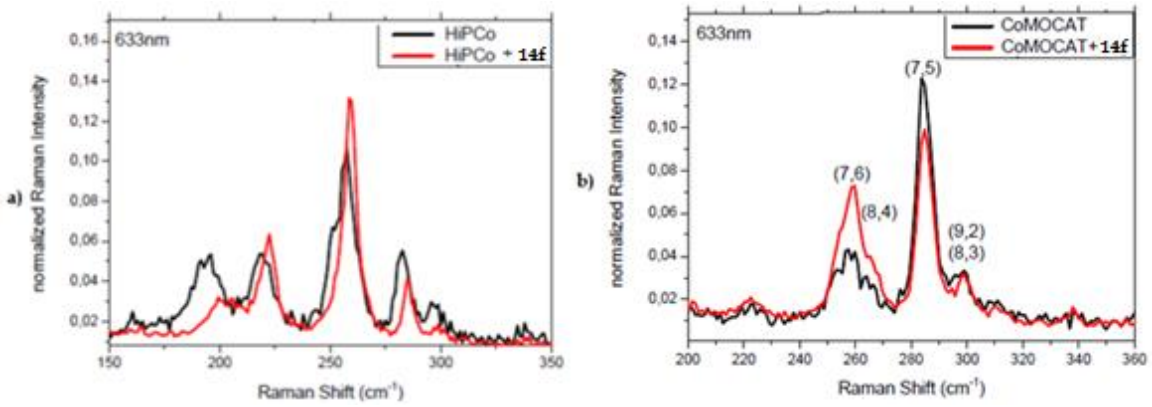

Figure 23. Normalized RBMs of a) HiPco and b) CoMoCAT without and with **14f**. Excitation at 633 nm.

Finally, AFM image confirmed the formation of the hybrid nanostructure between **14f** and CNTs, as the nanotube is covered from **14f** molecules, with an increase from 1.2 to 2 nm in diameter (Figure 24).

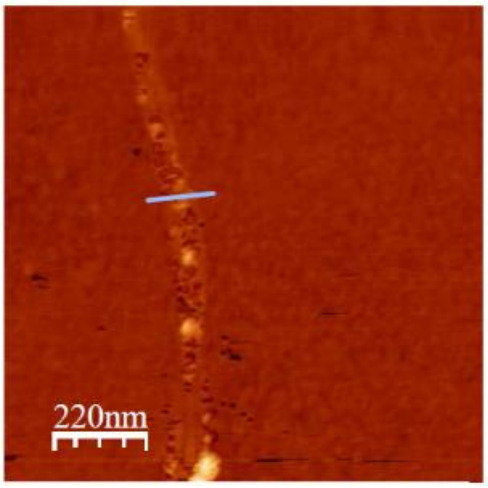

Figure 24. AFM images of **14f**@HiPco.

3.4 Conclusions

The stereoselective self-assembly of Ti(IV) TPA μ-oxo complexes in solution has been investigated in detail as well as their functionalization through oxime bond formation. The synthetic strategy has enabled to introduce a wide variety of functional residues on μ-oxo systems. In particular, functionalization with pyrene moieties has led to the formation of supramolecular structures upon reaction with C_{60} and SWCNTs, through supramolecular π-π interactions. Indeed, pyrene functionalized Ti(IV) TPA μ-oxo complexes have been found to be interesting receptors for fullerene and the development of hybrid nanostructured supramolecular systems with CNTs has been carried out. Additional studies on applications of positively charged Ti(IV) TPA μ-oxo complexes in supramolecular chemistry, upon reaction with polyanions, such as polyoxometalates (POMs), and further modification of alkyne-derived Ti(IV) TPA μ-oxo complexes *via* click chemistry are still under study.

3.5 Experimental

General remarks

Chemicals and dry solvents were purchased from Sigma Aldrich and used without further purification. ^{1}H and $^{13}C\{^{1}H\}$-NMR spectra were recorded at 301K on Bruker AC-200, 250, 300 MHz instruments. DOSY-NMR experiments were recorded at 301K on a Bruker AC-300 MHz instrument. Chemical shifts (δ) have been reported in parts per million (ppm) relative to the residual undeuterated solvent as an internal reference ($CDCl_3$: 7.26 ppm for ^{1}H-NMR and 77.0 ppm for ^{13}C-NMR; CD_3OD: 3.31 ppm for ^{1}H-NMR and 49.05 ppm for ^{13}C NMR; CD_3CN: 1.94 ppm for ^{1}H-NMR and 118.26 ppm for ^{13}C-NMR) or tetramethylsilane. The following abbreviations have been used to explain the multiplicities: *s* = singlet, *d* = doublet, *t* = triplet, *dd* = doublet, doublet, *m* = multiplet, *br* = broad. ^{13}C-NMR spectra have been recorded with complete proton decoupling. ESI-MS spectra have been obtained on a LC/MS Agilent series 1100 spectrometer in both positive and negative modes using acetonitrile/formic acid 0.1% as mobile phase, with ESI-ion trap mass detector. In some cases, an ESI-TOF Mariner™ Biospectrometry™ Workstation of Applied Biosystems by flow injection, using acetonitrile or methanol/formic acid 0.1% as mobile phase, was used. MALDI-TOF analyses were performed using a 4800 MALDI TOF-TOF Analyser from Applied Biosystems. The samples were prepared using the spot overlay method with matrix composed of saturated 2,4,6-trihydroxyacetophenone in 1:1 CH_3CN:H_2O solution containing 0.1% of formic acid. In all cases, isotope patterns were in agreement with values calculated from the molecular formulas. All titanatrane complexes were prepared under nitrogen atmosphere in a MBraun MB 200MD glove-box, equipped with a MB 150 G-I gas recycling system (nitrogen working pressure: 6 bar). Oxygen and water levels inside the box were real-time monitored by MBraun oxygen and moisture analyzers. IR spectra have been recorded on a Nicolet 5700 FT-IR, with range 4000-400 cm^{-1} and resolution 4 cm^{-1}, using KBr pellets or NaCl plates. For experiments with C_{60}, fluorimetric analysis have been performed on a Perkin Elmer LS50B instrument 1 cm quartz cell. For experiments with CNTs, UV-Vis-NIR experiments have been performed at room temperature on a Varian Cary 5000 UV-Vis-NIR double beam spectrophotometer; 10 mm path length Hellma Analytics 100 QS quartz cuvettes have been used. Fluorescence UV-Vis spectra have been recorded on a Varian Cary Eclipse Fluorescence Spectrophotometer; 10 mm path length Hellma Analytics 117.100F QS quartz cuvettes have been used. Raman spectra were acquired with a Renishaw instrument, model Invia reflex equipped with 532, 633, and 785 nm lasers. For the AFM analysis, 100µl of each sample with a concentration of 2 µg/ml were spin coated (4000 rpm, 6 min) over Si wafer, gently rinsed with water and acetone, and blown with dry nitrogen, finally the samples were dry under vacuum in order to remove the excess of

solvents. The samples have been characterized using a Nanoscope V (Digital Instruments Metrology Group, model MMAFMLN) in tapping mode in air at room temperature, using standard µmash® SPM probe (NSC15/AIBS) with tip height 20-25µm, cone angle <40° (Resonant frequency 325 kHz, force constant of ~46N/m).

Syntheses of TPAs **1f**, **4**, **8**, **12a-f**, **17** and **18** are reported in chapter 2.

***In situ* synthesis of mononuclear titanatranes 2f, 5, 13b,c**

Complexes were prepared in glovebox by mixing homogeneous solutions of the corresponding ligands (0.10 M) and Ti(O*i*-Pr)$_4$ (0.18 M) in dry $CDCl_3$ or CD_2Cl_2 in a 1:1 ratio to a final concentration 0.01 M of the complex. Bright yellow/orange solutions were obtained which were used without removing the three equivalents of *i*-PrOH released from the metal precursor. In all cases resonances relative to free *iso*-propanol released in the reaction were present in the NMR spectra: ^{1}H-NMR (200 MHz, $CDCl_3$): 4.04 (1H, *hept*, *J* = 6.1 Hz), 1.22 (6H, *d*, *J* = 6.1 Hz). ^{13}C{^{1}H}-NMR: (50.03 MHz, $CDCl_3$) δ 64.5 (*C*H), 25.1 (*C*H$_3$).

In most cases, for functionalized complexes, the mononuclear species converted rapidly into the dinuclear μ-oxo one and it was difficult to identify them in solution.

Ti(IV)/1f Complex 2f: ^{1}H-NMR: (300 MHz, $CDCl_3$) δ 7.68-7.64 (6H, *m*), 7.41-7.25 (12H, *m*), 7.10-7.08 (3H, *m*), 6.93-6.91 (3H, *m*), 4.64 (1H, *hept*, *J* = 6.0 Hz), 3.62 (6H, *bs*), 1.02 (6H, *d*, *J* = 6.0 Hz).

Ti(IV)/4 Complex 5: ^{1}H-NMR: (250 MHz, $CDCl_3$) δ 9.51 (3H, *bs*), 7.58-7.28 (21H, *bs*), 4.49 (1H, *hept*, *J* = 5 Hz), 3.76 (6H, *bs*), 1.24 (6H, *d*, *J* = 5 Hz).

Ti(IV)/12c Complex 13b: ^{1}H-NMR: (200 MHz, $CDCl_3$) δ 7.93 (3H, *s*), 7.64-760 (6H, *m*), 7.37-7.34 (42H, *m*), 7.01 (24H, *t*, *J* = 8 Hz), 6.91 (3H, *s*), 6.83 (12H, *t*, *J* = 8 Hz), 4.68-4.59 (1H, *m*), 4.04 (6H, *t*, *J* = 6 Hz), 3.93-3.88 (6H, *m*), 3.73 (6H, *s*), 3.37 (9H, *s*), 2.05-2.00 (6H, *m*), 1.24 (6H, d, J = 6 Hz).

Ti(IV)/12e Complex 13c: ^{1}H-NMR: (250 MHz, $CDCl_3$) δ 7.91 (3H, *s*), 7.54-7.45 (6H, *m*), 7.35-7.09 (15H, *m*), 4.53-4.50 (1H, *bs*), 4.14 (6H, *t*, *J* = 7.5 Hz) 3.66-3.61 (12H, *m*), 2.38-2.35 (18H, *m*), 1.80-1.93 (6H, *m*), 0.82 (6H, *d*, *J* = 7.5 Hz).

Synthesis of mononuclear titanatrane complex 7 Ti(OMe)

Ti(IV) TPA μ-oxo complex **6** (0.05 mmol, 0.07 g) was dissolved in $CDCl_3$ (0.5 mL). Then CD_3OD (200 eq.) was added and ^{1}H-NMR and ^{13}C{^{1}H}-NMR spectrum were registered. ^{1}H-NMR: (300 MHz, $CDCl_3$) δ 9.71 (3H, *s*), 7.63 (3H, *s*) 7.43 (3H, *s*), 7.29 (15H, *s*), 3.75 (6H, *s*). ^{13}C{^{1}H}-NMR: (75.5 MHz, $CDCl_3$) δ 161.21, 103.39, 100.49, 99.76, 97.83, 97.09, 47.57.

General synthesis of Ti(IV) TPA μ-oxo complexes 3, 6, 10, 14a-f, 16a,b, 16d, 16g 19 and 20

In the case of titanatrane mononuclear complexes, addition of water allowed the complete formation of μ-oxo complexes. The reaction mixtures were concentrated under pressure and the resulting solids were washed with diethyl ether. Centrifugation of the mixture gave the final products.

Functionalized complexes **14a-f**, **16a,b, 16d, 16g** and **20** could be also obtained by reacting for 12 h at room temperature μ-oxo complexes **6**, **10** and **19** (0.071 mmol), respectively, with alkoxyamines **11a-g** (0.42 mmol) in dichloromethane (1 mL) with 0.1% trifluoroacetic acid. The reaction mixtures were then washed with sat. $NaHCO_{3aq}$ and the organic phases were extracted three times with dichloromethane, dried over anhydrous Na_2SO_4 and evaporated to dryness. The products were purified by precipitation from diethyl ether.

3: IR (KBr) ν (cm^{-1}): 694, 753, 874, 1065, 140, 1269, 1424, 1455, 1585, 2882, 3054, 3433. ^{1}H-NMR: (300 MHz, $CDCl_3$) δ 7.26-7.19 (12H, *m*), 6.96 (6H, *t*, *J* = 7.4 Hz), 6.68 (12H, *d*, *J* = 7.4 Hz), 6.58 (12H, *t*, *J* = 7.4 Hz), 6.23 (6H, *t*, *J* = 7.3 Hz), 4.36 (6H, *d*, *J* = 13.9 Hz), 3.28 (6H, *d*, *J* = 13.9 Hz). ^{13}C{^{1}H}-NMR: (75.5 MHz, DMSO-d_6) δ 160.0 (6xC), 139.4 (6xC), 129.8 (6xCH), 129.4 (6xC), 129.2 (12xCH), 127.8 (12xCH), 127.1 (6xCH), 127.0 (6xCH), 126.5 (6xCH), 118.6 (6xC), 60.8 (6xCH_2). MS (ESI): *m/z* calc. 1232.3; exp. 1233.4 $[M+H]^+$, 1255.5 $[M + Na]^+$. 1271.3 $[M + K]^+$.

6: IR (KBr) ν (cm^{-1}): 750, 867, 973, 1000, 1031, 1110, 1168, 1281, 1384, 1419, 1441, 1464, 1521, 1593, 1635, 1684, 2336, 2361, 2843, 3053, 3420. ^{1}H-NMR: (250 MHz, $CDCl_3$) δ 9.97 (6H, *s*), 7.85 (12H, *d*, *J* = 5 Hz), 6.66-6.57 (24H, *m*), 6.31 (6H, *t*, *J* = 12 Hz), 4.33 (6H, *d*, *J* = 14 Hz), 3.51 (6H, *d*, *J* = 14 Hz). ^{13}C{^{1}H}-NMR: (50.03 MHz, DMSO-d_6) δ 190.38, 165.15, 138.42, 137.56, 132.68, 130.25, 130.01, 128.96, 128.05, 127.50, 126.89, 126.66, 126.18, 63.18. MS (ESI): *m/z* calc. 1401.31; exp. 1423.4 $[M + Na]^+$, 1401.2 $[M]^-$, 1445.2 $[M + HCOO]^-$, 1513.1 $[M + CF_3COO]^-$.

10: IR (KBr) ν (cm^{-1}): 693, 752, 802, 891, 1163, 1193, 1240, 1270, 1366, 1378, 1453, 1588, 1696, 2847, 3059, 3439. ^{1}H-NMR: (300 MHz, $CDCl_3$) δ 9.19 (6H, *s*), 7.34-7.28 (18H, *m*), 7.06 (6H, *t*, *J* = 6 Hz), 6.93 (6H, *d*, *J* = 9 Hz), 6.78 (6H, *d*, *J* = 9 Hz), 6.72 (6H, *t*, *J* = 6 Hz), 4.37 (6H, *d*, *J* = 15 Hz), 3.28 (6H, *d*, *J* = 15 Hz). ^{13}C{^{1}H}-NMR: (75.5 MHz, $CDCl_3$) δ 193.29, 160.62, 140.10, 137.37, 137.31, 132.84, 131.24, 131.11, 129.82, 128.11, 126.66, 123.34, 60.39. MS (ESI): *m/z* calc. 1401.3; exp. 1423.4 $[M + Na]^+$, 1401.2 $[M]^-$, 1445.2 $[M + HCOO]^-$, 1513.1 $[M + CF_3COO]^-$.

14a: IR (KBr) ν (cm^{-1}): 632, 697, 752, 776, 878, 953, 1112, 1246, 1272, 1349, 1408, 1435, 1465, 1599, 1660, 2875, 2922. ^{1}H-NMR: (250 MHz, $CDCl_3$) δ 8.11 (6H, *s*), 7.48 (12H, *d*, *J* = 14 Hz), 6.66-6.54 (24H, *m*), 6.30 (6H, *t*, *J* = 14 Hz), 4.34 (12H, *t*, *J* = 9.5 Hz), 4.28 (6H, *d*, *J* = 12.5 Hz), 3.82 (12H, *t*, *J* = 9.5 Hz), 3.74-3.64 (36H, *m*), 3.57-3.54 (12H, *m*), 3.38 (18H, *s*), 3.35 (6H, *d*, *J* = 12.5 Hz). ^{13}C-NMR: (62.9 MHz, $CDCl_3$) δ 161.2, 155.1,

148.5, 129.8, 129.1, 128.8, 127.6, 127.0, 126.4, 125.3, 124.8, 73.6, 72.0, 71.9, 70.7, 70.6, 69.7, 59.1. MS (ESI): *m/z* calc. 2366.3; exp. 604.4 $[M/2(Ti\text{-}OH) + 2H]^{2+}$, 1207 $[M/2(Ti\text{-}OMe)+H]^{+}$. MS (MALDI): *m/z* 2366 $[M + H]^{+}$, 2389 $[M + Na]^{+}$, 2405 $[M + K]^{+}$.

14b: IR (KBr) ν (cm^{-1}): 705, 778, 865, 917, 953, 1031, 1065, 1110, 1162, 1245, 1268, 1354, 1408, 1426, 1464, 1506, 1538, 1569, 1576, 1597, 1616, 1635, 1652, 1695, 1700, 1734, 2336, 2361, 2982, 3052, 3109, 3447. MS (ESI): *m/z* calc. 4143.92; exp. 374.82 $[M/2(Ti\text{-}OH) - 3BPh_4]^{3+}$, 379.49 $[M/2(Ti\text{-}OMe) - 3BPh_4]^{3+}$, 722.33 $[M/2(Ti\text{-}OH) - 2BPh_4]^{2+}$, 729.83 $[M/2(Ti\text{-}OMe) - 2BPh_4]^{2+}$, 648.83 $[M - 5BPh_4 + HCOO]^{4+}$, 971.77 $[M - 4BPh_4 + HCOO]^{3+}$.

14c: IR (KBr) ν (cm^{-1}): 749, 776, 878, 949, 1066, 1116, 1142, 1244, 1269, 1305, 1354, 1387, 1394, 1408, 1436, 1472, 1496, 1506, 1600, 1684, 1695, 1700, 2336, 2361, 2809, 2851, 2951, 3447. ^{1}H-NMR: (250 MHz, $CDCl_3$) δ 8.00 (6H, *s*), 7.44 (6H, *s*), 7.38 (6H, *s*), 6.60-6.50 (24H, *m*), 6.27-6.20 (6H, *m*), 4.22 (6H, *d*, *J* = 12.5 Hz), 4.15 (12H, *t*, *J* = 7.5 Hz), 3.69-3.64 (24H, *m*), 3.29-3.24 (6H, *d*, *J* = 12.5 Hz), 2.43-2.39 (36H, *m*), 1.94-1.84 (12H, *m*). ^{13}C{^{1}H}-NMR: (50.03 MHz, $CDCl_3$) δ 161.36, 148.13, 136.60, 129.92, 129.25, 129.03, 127.74, 127.00, 126.52, 125.64, 125.03, 72.64, 67.19, 58.72, 55.82, 53.95, 31.11, 26.55. MS (ESI): *m/z* calc. 2252.97; exp. 568.6 $[M/2(Ti\text{-}OH + 2H]^{2+}$, 1150.1 $[M/2(Ti\text{-}OMe) + H]^{+}$.

14d: IR (KBr) ν (cm^{-1}): 697, 746, 845, 914, 993, 1032, 1065, 1113, 1243, 1268, 1387, 1394, 1419, 1436, 1464, 1472, 1554, 1569, 1576, 1635, 1623, 1646, 1669, 1734, 1772, 2336, 2361, 3447. MS (ESI): *m/z* calc. 2690.75; exp. 14284 $[M/2(Ti\text{-}OH) + CH_3O]^{-}$, 1442.4 $[M/2(Ti\text{-}OH + HCOO]^{-}$, 1456.4 $[M/2(Ti\text{-}OMe) + HCOO]^{-}$, 1470.3 $[M/2(Ti\text{-}OCHO) + HCOO]^{-}$.

14e: IR (KBr) ν (cm^{-1}): 774, 842, 947, 1107, 1171, 1244, 1348, 1387, 1419, 1447, 1464, 1472, 1539, 1576, 1646, 1652, 1669, 1675, 1700, 1717, 1734, 2336, 2361, 2863, 3420. MS (ESI): *m/z* calc. 3567.31; exp. $[M/2(Ti\text{-}OMe)]^{+}$, 903.6 $[M/2(Ti\text{-}OMe) + H]^{2+}$.

14f: IR (KBr) ν (cm^{-1}): 696, 848, 878, 920, 1070, 1112, 1245, 1271, 1464,1630, 2849, 2919. ^{1}H-NMR: (250 MHz, $CDCl_3$) δ 9.11 (6H, *s*), 8.54 (6H, *d*, *J* = 8.75 Hz), 8.36 (6H, *d*, *J* = 8.75 Hz), 8.20-7.96 (48H, *m*), 7.40-7.27 (12H, *m*), 6.57-6.47 (24H, *m*), 6.24 (6H, *t*, *J* = 10 Hz), 4.51-4.38 (24H, *m*), 4.06 (6H, *d*, *J* = 14 Hz), 3.94-3.79 (48H, *m*), 2.84 (6H, *d*, *J* = 14 Hz). ^{13}C{1H}-NMR: (62.9 MHz, $CDCl_3$) δ 161, 149.0, 148.1,136.3, 132.3, 131.2, 130.6, 128.9, 128.6, 128.3, 127.4, 126.2, 125.9, 125.6, 125.2, 125.0, 124.9, 122.8, 73.8, 73.6, 73.5, 70.8, 69.9, 69.7.

16a: IR (KBr) ν (cm^{-1}): 616, 630, 658, 752, 781, 802, 841, 885, 966, 1104, 1200, 1239, 1267, 1348, 1407, 1449, 1585, 1660, 2875. ^{1}H-NMR: (250 MHz, $CDCl_3$) δ 7.36 (6H, *s*), 7.20 (12H, *t*, *J* = 15 Hz), 6.96 (6H, *t*, *J* = 15 Hz), 6.84 (6H, *s*), 6.51-6.68 (18H, *m*), 4.37 (6H, *d*, *J* = 14.5 Hz), 3.88-3.99 (12H, *m*), 3.53-3.66 (48H, *m*), 3.47 (12H, *t*, *J* = 10.25 Hz), 3.37 (18H, *s*), 3.17 (6H, *d*, *J* = 14.5 Hz). ^{13}C-NMR: (62.9 MHz, $CDCl_3$) δ 160.2, 149.6,

138.7, 132.4, 131.9, 130.1, 129.6, 129.5, 128.5, 125.6, 124.4, 121.7, 73.5, 72.5, 71.2, 69.9, 59.7. MS (MALDI): *m/z* calc. 2366.94; exp. 2390.9 $[M + Na]^+$, 2406.9 $[M+K]^+$.

16b: IR (KBr) ν (cm^{-1}): 705, 801, 843, 891, 949, 1031, 1161, 1240, 1266, 1339, 1387, 1405, 1419, 1436, 1464, 1476, 1554, 1558, 1576, 1616, 1635, 1652, 1684, 1695, 1717, 1734, 2336, 2361, 2983, 3052, 3447. MS (ESI): *m/z* calc. 4143.92; exp. 374.82 $[M/2(Ti\text{-}OH) - 3BPh_4]^{3+}$, 379.49 $[M/2(Ti\text{-}OMe) - 3BPh_4]^{3+}$, 722.33 $[M/2(Ti\text{-}OH) - 2BPh_4]^{2+}$, 729.83 $[M/2(Ti\text{-}OMe) - 2BPh_4]^{2+}$, 648.83 $[M - 5BPh_4 + HCOO]^{4+}$, 971.77 $[M - 4BPh_4 + HCOO]^{3+}$.

16d: ^{1}H-NMR: (300 MHz, $CDCl_3$) δ 8.15 (9H, *t*, *J* = 6 Hz), 8.08-7.94 (18H, *m*), 7.70 (3H, *d*, *J* = 6 Hz), 6.84 (3H, *d*, *J* = 9 Hz), 6.74 (3H, *s*), 6.68-6.54 (12H, *m*), 6.24 (3H, *t*, *J* = 9 Hz), 5.45 (3H, *d*, *J* = 12 Hz), 5.28 (3H, *d*, *J* = 12 Hz), 4.15 (3H, *d*, *J* = 15 Hz), 2.63 (3H, *d*, *J* = 15 Hz). ^{13}C-NMR: (75.5 MHz, $CDCl_3$) δ 159.48, 149.37, 138.46, 131.89, 131.43, 131.03, 130.68, 129.60, 128.67, 128.10, 127.81, 127.73, 12762, 126.11, 125.42, 125.09, 124.90, 124.60, 123.95, 123.78, 120.90, 74.28, 66.06, 58.68. MS (ESI): *m/z* calc. 2690.75; exp. 14284 $[M/2(Ti\text{-}OH) + CH_3O]^-$, 1442.4 $[M/2(Ti\text{-}OH + HCOO]^-$, 1456.4 $[M/2(Ti\text{-}OMe) + HCOO]^-$, 1470.3 $[M/2(Ti\text{-}OCHO) + HCOO]^-$.

16g: IR (KBr) ν (cm^{-1}): 630, 702, 799, 927, 1008, 1045, 1198, 1262, 1407, 1465, 1600, 1700, 2121, 2240, 2923, 3060, 3287. ^{1}H-NMR: (250 MHz, $CDCl_3$) δ 7.36 (6H, *s*), 7.27-7.18 (12H, *m*), 6.99 (6H, *t*, *J* = 15 Hz), 6.89 (6H, *s*), 6.74-6.54 (18H, *m*), 4.41-4.20 (18H, *m*), 3.17 (6H, *d*, *J* = 14.5 Hz), 2.38 (6H, *t*, *J* = 4.75 Hz). ^{13}C{1H}-NMR: (75.5 MHz, $CDCl_3$) δ 166.80, 153.86, 152.62, 150.09, 134.47, 132.34, 131.27, 130.73, 129.31, 128.42, 126.59, 123.69, 120.42, 79.75, 74.91, 61.94, 56.89, 35.63, 29.90. MS (ESI): *m/z* calc. 1718.46; exp. 901.2 $[M/2(Ti\text{-}OMe) + H_2O]^+$.

19: IR (KBr) ν (cm^{-1}): 694, 804, 891, 1099, 1151, 1197, 1320, 1377, 1472, 1595, 1682, 2730, 2828, 3420. ^{1}H-NMR: (200 MHz, CD_2Cl_2) δ 10.02 (6H, *s*), 9.21 (6H, *s*), 7.96 (6H, *d*, *J* = 4 Hz), 7.88 (12H, *t*, *J* = 2Hz), 7.37-7.32 (6H, *m*), 7.03-6.89 (12H, *m*), 4.57 (6H, *d*, *J* = 14 Hz), 3.58 (6H, *d*, *J* = 14 Hz). ^{13}C{^{1}H}-NMR: (50.03 MHz, CD_2Cl_2) δ 204.74, 162.64, 136.68, 130.92, 119.96, 119.37, 119.13, 118.66, 118.38, 117.94, 26.83. MS (ESI) *m/z* calc. 1568.27; exp. 838.0 $[M/2(Ti\text{-}OH) + HCOO]^-$, 920.0 $[M/2(Ti\text{-}OMe) + CF_3COO]^-$.

20: IR (KBr) ν (cm^{-1}): 542, 633, 639, 722, 799, 848, 947, 1106, 1200, 1248, 1285, 1349, 1463, 1600, 1642, 1692, 2875, 2918. ^{1}H-NMR: (250 MHz, $CDCl_3$) δ 8.12 (6H, *s*), 7.52 (6H, *s*), 7.40 (6H, *s*), 7.32 (6H, *s*), 6.80-6-53 (24H, *m*), 4.33 (24H, *t*, *J* = 9.25 Hz), 3.90-3.44 (132H, *m*), 3.38 (18H, *s*), 3.36 (18H, *s*). MS (MALDI): calc. 3501.54; exp. 3523.6 $[M + Na]^+$, 3539.6 $[M+K]^+$.

Synthesis of *N*-methylated Ti(IV) TPA *μ*-oxo complex 15

To a solution of **complex 14c** (0.04 mmol, 0.09 g) in dichloromethane (8 mL) methyl triflate (0.03 mg/mmol sub., 0.013 g) was added and the mixture was stirred at

room temperature for 72 h. The reaction mixture was evaporated to dryness and the residue was washed with diethyl ether. An orange oil was obtained, which was used without any further modification (60%).

IR (NaCl) ν (cm^{-1}): 667, 751, 878, 953, 1028, 1110, 1171, 1244, 1275, 1419, 1465, 1576, 1618, 1652, 2336, 2361, 3028, 3446. MS (ESI): *m/z* calc. 3236.82; exp. 1352.2 [M/2(Ti-OMe) - $3CF_3SO_3$ + HCOO + CF_3COO]$^+$, 1492.1 [M/2(Ti-OMe) - CF_3SO_3]$^+$.

Fluorimetric titrations of complexes 14f and 16d

C_{60} titration: : 3.67 mg of **complexes 14f** or 2.7 mf of complex **16d** were dispersed in 10 mL of toluene (solution A); at the same time, 7.2 mg of C_{60} were dissolved into 10 mL of toluene (solution B). Both the solutions were stirred for 5 minutes for a complete and homogeneous dispersion of the molecules in solution.
UV-Vis-NIR and fluorimetric titrations were performed with stepwise addition of 20 µl of solution B to 200 µl of solution A and toluene was added to reach a final volume of 2 mL. For the very last add (100 eq. of C_{60}), 1.44 mg of fullerene were added to 1.8 mL of toluene and stirred overnight and then the mixture was added to 200 µl of solution A. About fluorimetric experiments, excitation wavelength was set at 338 nm.

Carbon nanotubes (CNTs) titration: 3 mg of **complex 14f** were dispersed in 3 ml of DMF/MeOH 1:1 solution; after stirring the mixture for 5 minutes for increasing solubilisation, 3 mg of CNTs were added. The solution was sonicated for 30 minutes, and then was stirred for further 30 minutes. The mixture was centrifugated for 1 h at 3000 rpm, and after this, the supernatant solution was collected. UV-Vis-NIR and fluorimetric experiments were performed directly on the supernatant solutions without any dilutions; excitation wavelength was set at 350 nm.

Chapter 4

Catalytic activity of functionalized V(V) TPA complexes in non-conventional media

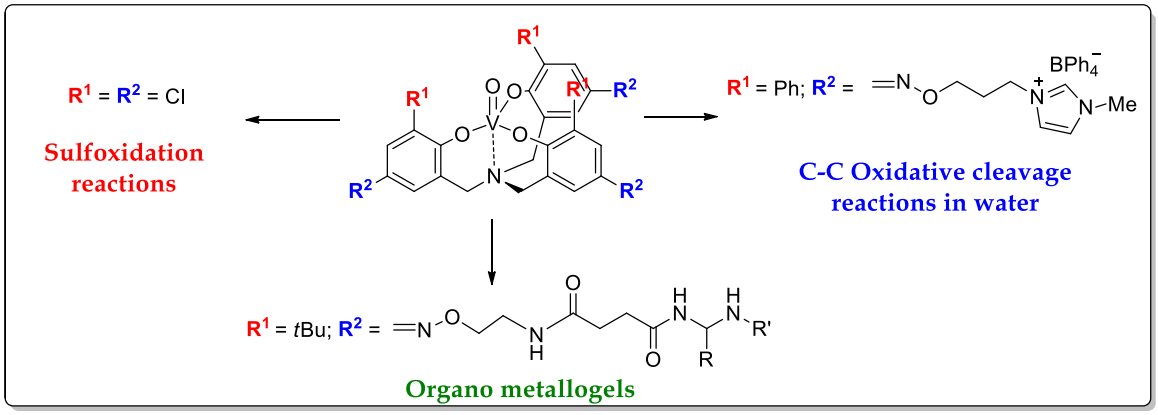

V(V) TPA complexes bearing electron withdrawing groups both in *ortho* and *para* positions to the phenolate show excellent catalytic activity towards sulfoxidation reactions, with high TONs and TOFs. Moreover, a new positively charged vanadium complex has been found to be very active in C-C oxidative cleavage reactions in water, upon solubilisation in micelles. Finally, functionalization of V(V) TPA complexes with gelator moieties leads to the synthesis of a new class of systems that are able to give rise to organo metallogels, with potential application in metallogel catalysis.

4.1 Introduction

The development of water-soluble catalytic systems represents a great interest nowadays, as it can offer the possibility to perform organic transformations in a selective and reactive way using a cheap and harmless solvent. Water is the green solvent *par excellence*, as it is economic, non-toxic and non-flammable. Its role as solvent in catalytic processes is fundamental, as it offers the possibility to recycle the catalyst, with products recovered by extraction with water immiscible organic solvents. Moreover, its hydrophobic effect and donor-acceptor hydrogen bonding affinity translate in both enhanced activity and selectivity in several catalytic reactions.[108]

However, such these features represent a limit in the use of water as solvent in organic reactions and catalysis, as the hydrophobic effect makes it segregate non-polar species and impede their solvation. Thus, alternative routes to overcome the problem of heterogeneity of organic reactions in aqueous media have been developed, such as the use of micelles[109] and supramolecular gels, either in the form of organo- or hydrogels.[110] In addition, the possibility to incorporate metal centres within these nanoreactors makes it possible to generate new active heterogeneous catalytic systems.

Thus, the involvement of supramolecular catalysis, as a contact between supramolecular chemistry and homogeneous catalysis, is necessary.[111] In this context, the development of enzyme mimics has experienced a wide spread. The principle underlying the use of host-guest chemistry in catalysis, as a tool to develop artificial enzymes, takes inspiration from enzyme's lock-and-key theory: a substrate fits nicely in a host molecule that also carries a catalytic function, thus enhancing the rate of reaction. Furthermore, in host-guest catalysis, non-covalent interactions involved in the construction of the host also favour the confinement of the guest within it and help stabilise the transition state. One of the most common ways of mimicking enzymes behaviour is to exploit self-assembling materials that give rise to highly ordered structures that surround the catalytic centre, in order to generate a nanometric environment, as the enzyme pockets, which is able to accommodate the substrate, accelerate the reaction and control selectivity of reactions.[112]

---

[108] (a) U. M. Lindström, F. Andersson *Angew. Chem. Int. Ed.* **2006**, *45*, 548-551. (b) M.C. Pirrung *Chem.-Eur. J.* **2006**, *12*, 1312-1317. (c) S. Narayan, J. Muldoon, M. G. Finn, V. V. Fokin, H. C. Kolb, K. B. Sharpless *Angew. Chem. Int. Ed.* **2005**, *44*, 3275-3279.

[109] G. La Sorella, G. Strukul, A. Scarso *Green Chem*. **2015**, DOI: 10.1039/C4GC01368A and references therein.

[110] B. Escuder, F. Rodrìguez-Llansola, J. F. Miravet *New. J. Chem.* **2010**, *34*, 1044-1054.

[111] (a) M. Raynal, P. Ballester, A. Vidal-Ferran, P. W. N. M. van Leeuwen *Chem. Soc. Rev.* **2014**, *43*, 1660-1733. (b) M. Raynal, P. Ballester, A. Vidal-Ferran, P. W. N. M. van Leeuwen *Chem. Soc. Rev.* **2014**, *43*, 1734-1787.

[112] D. M. Vriezema, M. Comellas Aragonès, J. A. A. W. Elemans, J. J. L. M. Cornelissen, A. E. Rowan, R. J. M. Nolte *Chem. Rev.* **2005**, *105*, 1445-1490.

4.1.1 Micelles and gels in supramolecular catalysis

Micelles may be considered enzyme-like nanoreactors.[113] Actually, like enzymes, micelles display a hydrophobic core and a hydrophilic surface that ensures their solubility in water. The hydrophobic core captures apolar molecules and catalytic species from the bulk solvent, thus improving solubilisation of organic molecules in water, enhancing reagents local concentration upon compartmentalization and stabilizing the transition state by electrostatic effects.[114] Moreover, charged micelles can concentrate and dissolve oppositely charged metal complexes, thanks to electrostatic interactions among them. In particular, the use of water as solvent makes it possible to recover the products of metal catalysis by extraction and to recycle the catalyst. Indeed, when the metal catalyst and the surfactant are oppositely charged and the organic reagents and reaction products are apolar, it is very easy to remove the products from the micellar medium, leaving the catalyst confined in the micelle. Metal catalysts can be divided into four classes, with respect to their solubility in water: intrinsically soluble catalysts (Figure 1A); organic soluble catalysts modified with water-soluble tags, in particular pony tails (Figure 1B);[115] supramolecular aggregates that dissolve the catalyst (Figure 1C); metallo-surfactant molecules that self-assemble into micelles in solution (Figure 1D). While the second strategy can alter the electronic and steric properties of the catalyst, the third one guarantees the integrity of the original organic soluble catalytic system. Moreover, it favours the interaction between the reaction partners in the Stern layer of the micelles, especially in the case of water-soluble charged catalysts and surfactants that have complementary charge with respect to the catalyst.

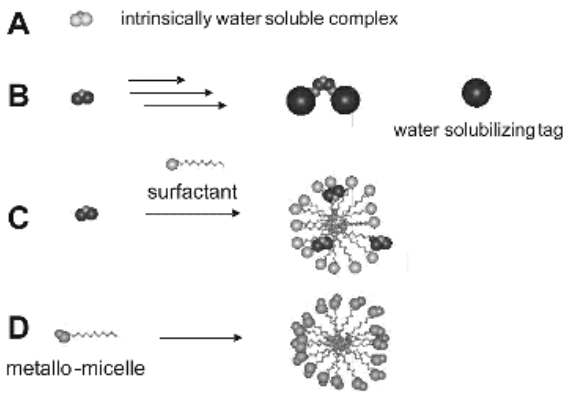

Figure 1. A) Intrinsically water-soluble catalysts; B) covalent modification of ligands with water solubilizing residues; C) solubilisation of catalyst in micelles as a consequence of the hydrophobic effect; D) covalent metal-surfactant adducts that forms metallo-micelles.[2]

[113] A. Sorrenti, O. Illa, R. M. Ortuño *Chem. Soc. Rev.* **2013**, *42*, 8200-8219.
[114] C. A. Bunton *Adv. Colloid Interface Sci.* **2006**, *123-126*, 333-343.
[115] N. Pinault, D. W. Bruce *Coord. Chem. Rev.* **2003**, *241*, 1-25.

Thus, in the field of micellar catalysis, a lot of organometallic catalytic reactions have been performed,[2] such as hydrogenations,[116] C-C coupling reactions,[117] Diels-Alder reactions,[118] ring-closing metathesis,[119] hydrolytic DNA cleavage[120] and oxidations.[121]

On the other hand, in catalytic supramolecular gels, non-covalent interactions are involved in the construction of a catalytic centre. From a general viewpoint, gels are classified in different ways, depending on their source (natural or artificial), the medium they encompass (organo-, hydro- aero/xerogels), their constitution (supramolecular or molecular) and the kind of cross-linking that is involved in the construction of the 3D network (Figure 2).[122]

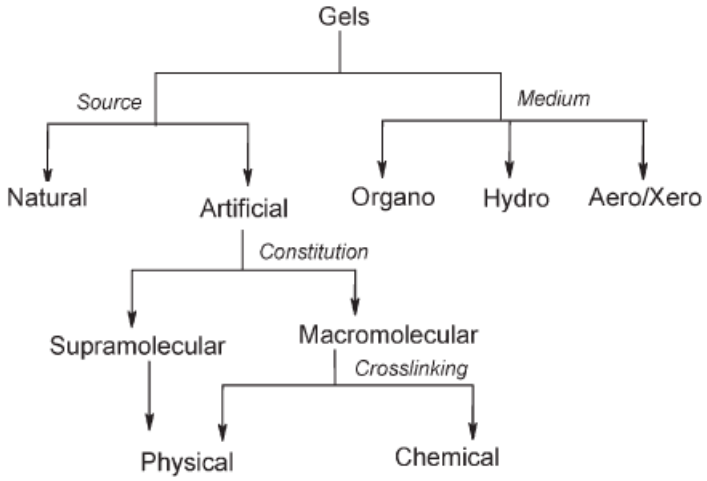

Figure 2. Classification of gels.[15]

More in detail, supramolecular gels are soft materials that are formed by low-molecular-weight organic molecules that self-assemble in nanostructured aggregates, by means of non-covalent intermolecular interactions, such as ionic, H-bonding, π-π stacking, van der Waals, solvophobic and metal coordination interactions.[3,123] Supramolecular gels are hierarchically built-up from molecular to supramolecular level. All the information that is required for their function and

[116] M. Schwarze, J. S. Milano-Brusco, V. Strempel, T. Hamerla, S. Ille, C. Fischer, W. Baumann, W. Artl, R. Schomäcker *RSC Adv.* **2011**, *1*, 474-483.
[117] G. La Sorella, M. Bazan, A. Scarso, G. Strukul *J. Mol. Catal. A-Chem.* **2013**, *379*, 192-196.
[118] F. Trentin, A. Scarso, G. Strukul *Tetrahedron Lett.* **2011**, *52*, 6978-6981.
[119] L. Laville, C. Charnay, F. Lamaty, J. Martinez, E. Colacino *Chem.-Eur. J.* **2012**, *18*, 760-764.
[120] B. Gruber, E. Kataev, J. Aschenbrenner, S. Stadlbauer, B. König *J. Am. Chem. Soc.* **2011**, *133*, 20704-20707.
[121] (a) S. Handa, J. C. Fennewald, B. H. Lipshutz *Angew. Chem. Int. Ed.* **2014**, *53*, 3432-3435. (b) D. Banerjee, F. M. Apollo, A. D. Ryabov, T. J. Collins *Chem.-Eur. J.* **2009**, *15*, 10199-10209. (c) A. Cavarzan, A. Scarso, G. Strukul *Green Chem.* **2010**, *12*, 790-794.
[122] N. M. Sabgeetha, U. Maitra *Chem. Soc. Rev.* **2005**, *34*, 821-836.
[123] (a) P. Terech, R. G. Weiss *Chem. Rev.* **1997**, *97*, 3133-3160. (b) J. H. van Esch, B. L. Feringa *Angew. Chem. Int. Ed.* **2000**, *39*, 2263-2266. (c) J. H. van Esch *Langmuir*, **2009**, *25*, 8392-8394. (d) B. Escuder, J. F. Miravet *Functional Molecular Gels* RSC, Cambridge, **2014**.

self-assembly is contained in the low-molecular-weight compounds, which constitute the final 3D network (Figure 3).

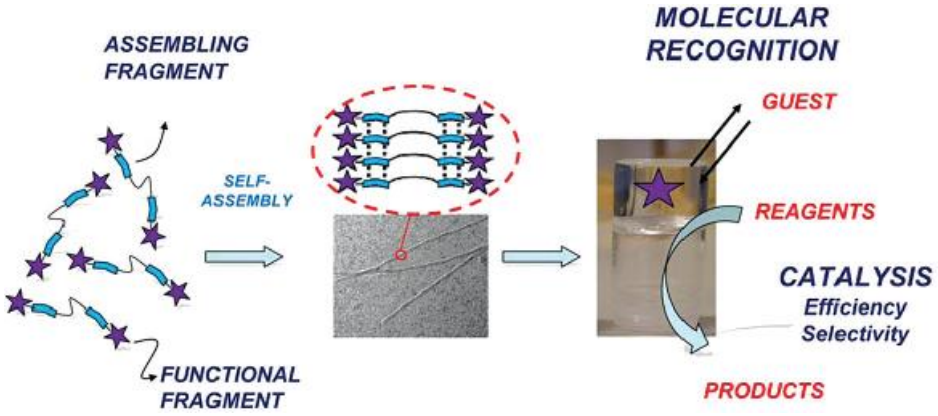

Figure 3. Bottom-up construction of functional gels.[3]

Gelation can be affected and modulated by physical and chemical stimuli, like temperature, pH and light.[124] The gels sensitivity for stimuli makes them very appealing for functional applications, as upon changing the stimuli, their activity can be finely tuned. Furthermore, as the network of the gel has a large surface area in contact with solution, if the fibres are provided with active groups, the final gel can ideally and effectively perform any task, from molecular recognition to catalysis. In the case of supramolecular catalysis, these solid-like properties can allow an easy recovery of the catalytic gelator by simple filtration. The reactions can take place within the gel phase, on the gel surface or in solution, depending on the affinity between gelator, solvent and reagents. The catalytic functional site can be inserted into the assembling fragment, so that, upon aggregation and self-assembly, the catalytic supramolecular gel can form. The possibility to immobilise a metal catalyst in a gel matrix entails the increase of the contact superficial area, the accessibility of active sites, thanks to the porosity of the material, and the diffusion of the reagents. Moreover, the thermo-reversibility of the materials makes it possible to recover the catalyst at the end of reaction.[125] However, the use of coordination chemistry for the construction of gel-supported catalysts is still poorly investigated.

So far, three different kinds of catalytic gels have been proposed, such as self-supported metallogels (Figure 4A), in which metal coordination creates a cross-linked coordinated polymer that entraps the solvent and forms a gel with potential catalytic activity. The other category consists in the formation of gels as supramolecular multitopic ligands (Figure 4B). In this case, the network will be formed by free ligand sites, which will coordinate the metal *a posteriori*, after gel

[124] (a) G. O. Lloyd, J. W. Steed *Nature Chem.* **2009**, *1*, 437-442. (b) Z. Ge, J. Hu, F. Huang, S. Liu *Angew. Chem. Int. Ed.* **2009**, *48*, 1798-1802. (c) H. Maeda *Chem.-Eur. J.* **2008**, *14*, 11274-11282. (d) T. Muraoka, H. Cui, S. I. Stupp *J. Am. Chem. Soc.* **2008**, *130*, 2946-2947.
[125] J. Zhang, C.-Y. Su *Coord. Chem. Rev.* **2013**, *257*, 1373-1408.

formation. Finally, metallogels can be formed by aggregation and self-assembly of gelators that already contain a metal in the structure (Figure 4C).[3]

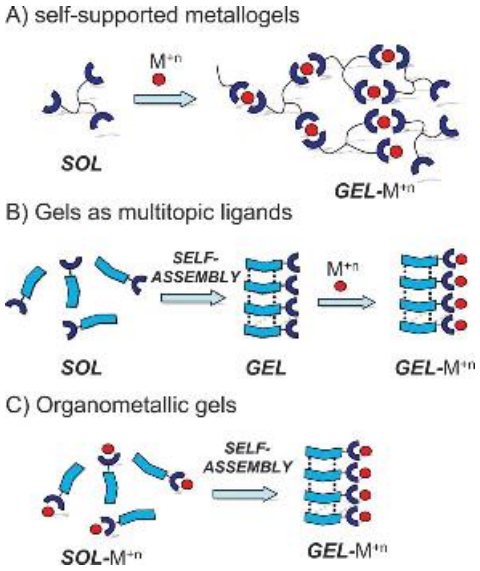

Figure 4. Classification of catalytic metallogels.[3]

In this context, the design of pH responsive hydrogels is very attractive. Miravet and Escuder developed pyridine-functionalized ambidextrous gelators, which are able to form gels in both water and organic solvents (Figure 5).[126]

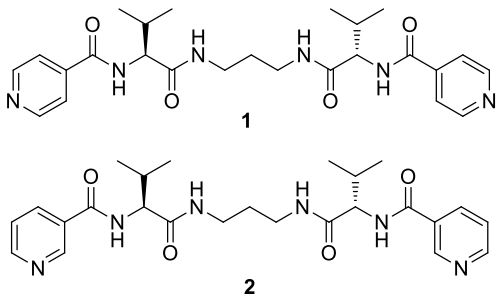

Figure 5. Pyridine-functionalized ambidextrous gelators **1** and **2**.

The organogel of compound **2** in toluene has been loaded with Pd(II) ions and a metallogel catalyst has been developed and its catalytic activity in the aerobic oxidation of benzyl alcohol has been tested. Furthermore, the possibility of obtaining hydrogels of both **1** and **2** is very interesting, as intriguing pH responsive gels can be developed: indeed, **1** and **2** hydrogels have been found to be soluble in acidic water (HCl 0.1 M), while form transparent gels after exposure to concentrated ammonia vapours in a few minutes.

Thus, the choice of the right catalytic system to be incorporated into these supramolecular systems can then give rise to efficient catalytic systems that can be active in non-conventional media.

[126] J. F. Miravet, B. Escuder *Chem. Commun.* **2005**, 5796–5798.

4.2 Vanadium (V) TPA complexes

The interest in vanadium chemistry comes from the discovery of its involvement in biological processes. For example, vanadium haloperoxidases (VHPOs) are vanadium-dependent enzymes, which are able to activate hydrogen peroxide for the oxidation of halides to the corresponding 'X$^+$' species.[127] It has been found that they are also able to catalyse the oxidation of sulfides to sulfoxides and phosphine to phosphinoxides.[128] Such these enzymes feature vanadium in its highest oxidation state: a trigonal bipyramidal geometry is observed for the five-coordinated V(V) centre, which is surrounded by three equatorial oxygen donors, an axial oxygen and nitrogen (histidine residue) donors.[129] Taking inspiration from these structural motifs, different model compounds have been developed, in which V(V) complexes emulate the coordination sphere of the metal in the active site of vanadium-dependent enzymes and are proposed as functional and structural models of vanadium haloperoxidases.[130] These systems mimic the oxygen-rich coordination environment of the metal and the binding to histidine, the alkoxides moieties and the nitrogen donor. Among them, Kol and co-workers, synthesized for the first time V(V) amine triphenolate complexes **3a-c** *via* reaction of the TPA ligand with VO(O*i*-Pr)$_3$, respectively (Scheme 1).[131] The nature of TPA ligands that strongly bind to the metal makes it possible to tune finely the complex structures, providing a "natural environment" for vanadium.

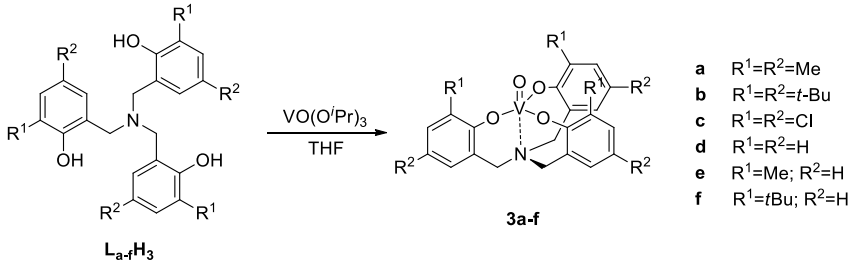

Scheme 1. General synthesis of V(V) amine triphenolate complexes.

---

[127] A. Butler *Coord. Chem. Rev.* **1999**, *187*, 17-35.

[128] (a) M. A. Andersson, A. Willetts, S. G. Allenmark *J. Org. Chem.* **1997**, *62*, 8455-8458. (b) V. m. Dembitsky *Tetrahedron* **2003**, *59*, 4701-4720.

[129] A. Messerschmidt, R. Wever *Proc. Natl. Acad. Sci. U.S.A.* 1996, 93, 392-396. (b) A. Messerschmidt, R. Wever *Biol. Chem.* **1997**, *378*, 309-315. (c) S. Macedo-Ribeiro, W. Hemrika, R. Renirie, R. Wever, A. Messerschmidt *J. Biol. Inorg. Chem*. **1999**, *4*, 209-219.

[130] (a) R. I. de La Rosa, M. J. Clague, A. Butler *J. Am. Chem. Soc.* **1992**, *114*, 760-761. (b) M. J. Clague, N. L. Keder, A. Butler *Inorg. Chem.* **1993**, *32*, 4754-4761. (c) G. J. Colpas, B. J. Hamstra, J. W. Kampf, V. L. Pecoraro *J. Am. Chem. Soc.* **1996**, *118*, 3469-3478. (d) V. Conte, O. Bortolini, M. Carraro, S. Moro *J. Inorg. Biochem.* **2000**, *80*, 41-49. (e) T. S. Smith, II, V. L. Pecoraro *Inorg. Chem.* **2002**, *41*, 6754-6760. (f) D. Rehder, G. Santoni, G. Licini, C. Schulzke, B. Meier *Coord. Chem. Rev.* **2003**, *237*, 53-63. (g) G. Santoni, G. Licini, D. Rehder *Chem.-Eur. J.* **2003**, *9*, 4700-4708. (h) S. Nica, A. Pohlmann, W. Plass *Eur. J. Inorg. Chem.* **2005**, 2032-2036. (i) C. Wikete, P. Wu, G. Zampella, L. De Gioia, G. Licini, D. Rehder *Inorg. Chem.* **2007**, *46*, 196-207. (j) C. J. Schneider, J. E. Penner-Hahn, V. L. Pecoraro *J. Am. Chem. Soc.* **2008**, *130*, 2712-2713.

[131] S. Groysman, I. Goldberg, Z. Goldschimdt, M. Kol *Inorg. Chem.* **2005**, *44*, 5073-5080.

X-ray structures of complexes 3**a** and 3**b** showed that both of them assume a trigonal bypyramidal (TBP) geometry, with the oxo group occupying an axial position, *trans* to the nitrogen.
However, in the case of electron-deficient ligand $\mathbf{L_cH_3}$, the mode of reactivity is completely different. Indeed, complex **3c**, which bears chloro groups in both *ortho* and *para* position to the phenolate, is present in solution as a mixture of compounds, **3c** and **3c'**, that have different ligand coordination environments (Scheme 2).

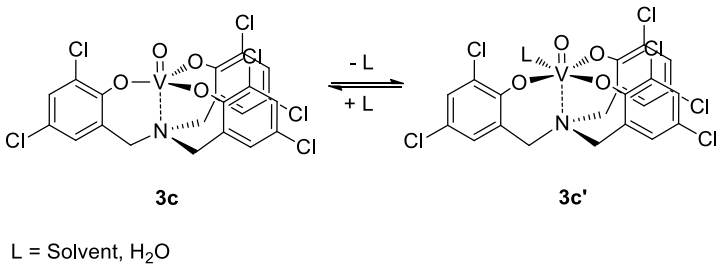

Scheme 2. Equilibrium between **3c** and **3c'** complexes in solution.

^{1}H-NMR spectrum shows the presence of a minor compound, **3c**, which features two aromatic signals and a broad signal for the methylene protons in α to the nitrogen. Its structure is then consistent with the formation of a C_3 trigonal bipyramidal geometry. The major product, **3c'**, has two sets of aromatic protons (2:1), an AB system for the four methylene protons and a sharp singlet for the remaining benzylic protons, characteristic of an octahedral geometry (Figure 6).

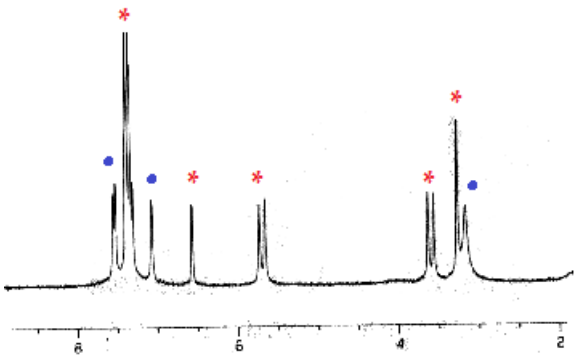

Figure 6. ^{1}H-NMR (chlorobenzene-*d5*, 55 °C) of complex **3c** (•) and **3c'** (*).[24]

X-ray structure confirms the formation of the hexa-coordinate octahedral geometry for **3c'**, with the oxo moiety in *trans* position to the nitrogen and a molecule of water in the apical position (Figure 7).

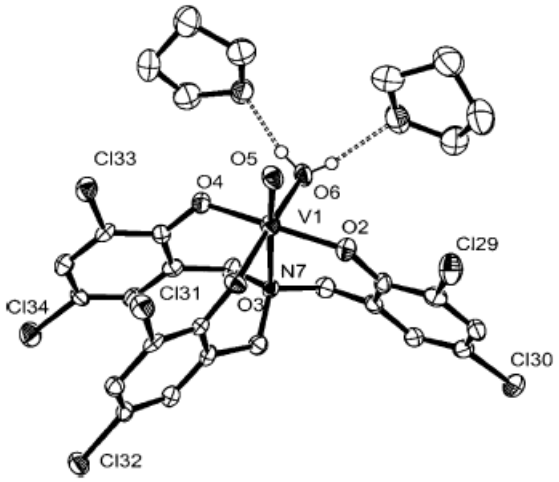

Figure 7. X-ray structure of complex **3c′**.[24]

Considering the ability of vanadium in VHPOs in activating a peroxide molecule, as the first step of the catalytic oxidation (halogenation) of organic substrates,[132] complexes **3a-c** were tested to see if they were able to promote peroxide-driven oxidations of olefins. It was found that they were able to oxidise styrene and *t*-stilbene to their corresponding epoxides in presence of *t*BuOOH (Scheme 3), even if the reactions are very slow (0.5-5 turnover per day). However, these results were indicative that they can be effectively regarded as models of vanadium-dependent haoloperoxidases.

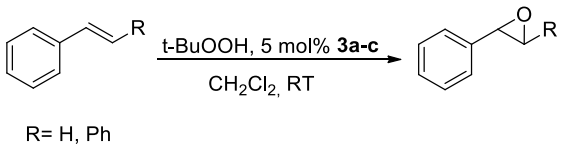

Scheme 3. Epoxidation reactions catalysed by V(V) TPA complexes **3a-c**.

Lately, our group reported a similar synthesis for complexes **3d-f**.[133] In the case of complex **3a**, ^{1}H-NMR spectrum is quite complicated, maybe because of the formation of some aggregates. On the contrary, C_3-symmetric mononuclear species were obtained in the case of complexes **3e** and **3f**. X-ray structure showed that complex **3f** adopts a trigonal bipyramidal geometry, with the oxo function that occupies the axial position, *trans* to the central nitrogen, similarly to the reported X-ray structure of complexes **3a,b**.[24] The vanadium centre is slightly above the plane defined by the phenolate oxygens (Figure 8).

[132] D. C. Crans, J. J. Smee, E. Gaidamauskas, L. Yang *Chem. Rev.* **2004**, *104*, 849-902.
[133] M. Mba, M. Pontini, S. Lovat, C. Zonta, G. Bernardinelli, P. E. Kündig, G. Licini *Inorg. Chem.* **2008**, *47*, 8616-8618.

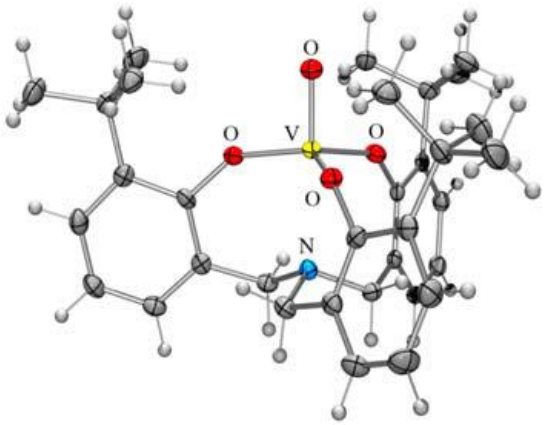

Figure 8. X-ray structure of V(V) TPA complex **3f**.[25]

Even in this case, the coordination environment of vanadium in these complexes mimics that of vanadium centre in vanadate-dependent haloperoxidases, so the possibility to use these complexes as model compounds of VHPOs has been tested, both in halide and sulfide oxidations. Complex **3f** was used as catalyst in bromination of 1,3,5-trimethoxybenzene using tetrabutyl ammonium bromide (TBAB) as halogen source, in the presence of one equivalent hydrogen peroxide as oxidant and in acidic conditions ($HClO_4$, 1 eq.), according to the stoichiometry of the reaction. The brominated product 2,4,6-trimethoxybromobenzene was afforded in high yield, up to 92%, with TONs up to 1260 (Scheme 3, left).

In the case of sulfoxidation reactions, complex **3f** was found to efficiently catalyse the reaction in fast and highly selective way, using hydrogen peroxide as terminal oxidant. It was possible to decrease the catalyst loading to 0.01 mol%, obtaining a high TON (9900). The procedure was extended to different sulfides and even in this case short reaction times, quantitative yields and high selectivity towards sulfoxides formation were observed (Scheme 4, right).

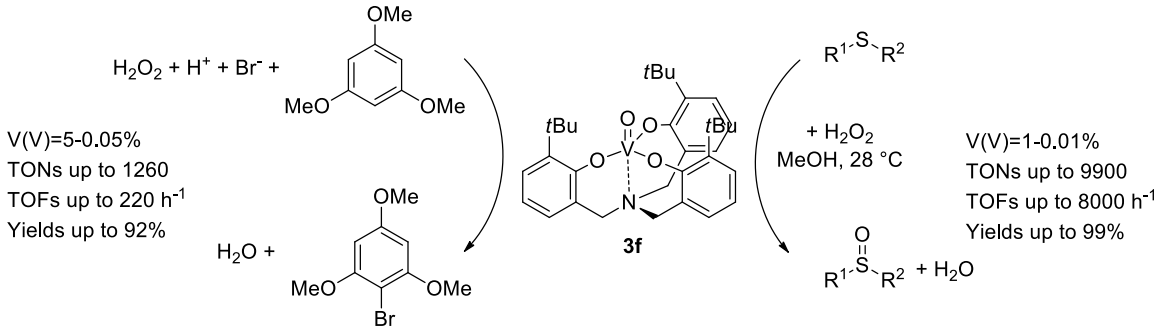

Scheme 4. Bromination (left) and sulfoxidation (right) reactions catalysed by V(V) TPA complex **3f**.

Thus, C_3-symmetric complex **3f** can be considered as a functional and structural model of vanadium-dependent haloperoxidases.

4.3 New functionalized V(V) TPA complexes: synthesis and catalytic activity

The study of the catalytic activity of new complexes, that may find application in both heterogeneous and homogeneous catalysis, supposes the identification of the most active and stable catalyst in solution. For this reason, we first concentrated our attention on the study of the catalytic activity of complex **3c** in sulfoxidation reactions. The presence of electron withdrawing chloro groups in both *ortho* and *para* positions, indeed, makes complex **3c** more electron-deficient, increasing its Lewis acid character. Similar to complex **3f**, the catalytic activity of complex **3c** towards oxidation of sulfides to sulfoxides, in presence of hydrogen peroxide as terminal oxidant, was tested. The reaction course was followed by ^{1}H-NMR in methanol-d_4 using 1-0.001% catalyst loading and a 1:1 ratio of thioanisole **4** and H_2O_2 (35% or 70% in water). In Table 1, the effect of increasing the substrate/catalyst ratio on the oxidation of thioanisole **4** is reported. In particular, 10:1, 10^3:1, 10^4:1 and 10^5:1 ratios were used. Substrate concentrations were varied from 0.1 to 1 M. In all cases, high yields and rates were observed.

Table 1. Oxidation of **4** by aqueous H_2O_2 (35% or 70%) catalysed by complex **3c**.[a]

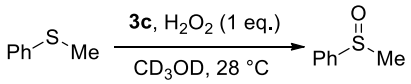

4 **5**

Entry	$[4]_o$ (M)	3c (%)	$t_{1/2}$ (min)[b]	yields (%)[c]	4:5[c]	time (min)[d]	TON	TOF (h^{-1})[e]
1	0.1	1	3.8	99	99:1	15	99	nd
2	1.0	0.1	21	>99	95:5	71	1000	1330
3	1.0[f]	0.1	<1	95	98:2	2.5	950	20000
4	1.0	0.01	160	91	97:3	980	9100	3160
5	1.0[f]	0.01	28	96	98:2	60	9600	7143
6	1.0[f]	0.001	222	89	97:3	740	89000	18461

[a]Reaction conditions: **4**:H_2O_2 =1:1, 28 °C, CD_3OD. [b]Time for 50% decrease of $[\mathbf{4}]_o$. [c]Determined on the oxidant by ^{1}H NMR (CD_3OD, 300 MHz), in the presence of DCE as internal standard. [d]Time required for the oxidant total consumption. [e]Determined at 20% conv. [f]Reaction performed with H_2O_2 (70%).

As we can notice, using 0.1% catalyst and 70% aqueous H_2O_2 (Table 1, entry 3), reaction time was drastically reduced to less than 3 minutes with respect to the reaction performed with 1% catalyst and a remarkable TOFs (20000) were obtained. The catalyst loading was then decreased to 0.01%, without affecting the efficiency of the system, but simply slowing down the reactions (Table 1, entry 4).

Even in this case, the reaction carried out with more concentrated H_2O_2 (Table 1, entry 5), increased the reaction performances. Additionally, we were able to further decrease the catalyst to 0.001% and the reaction gave the sulfoxide **5** in quite high yields in less than 13 hours (Table 1, entry 6), with an extremely high TON (90000).

The results obtained show that system **3c** is more performing than the previously reported complex **3f**.[26] At the same reaction conditions (0.1% catalyst, 70% aqueous H_2O_2), complex **3c** was 2.5 times faster than complex **3f**. The possibility to further decrease the catalyst loading makes complex **3c** very active in sulfoxidation reactions, with high yields and chemoselectivities. Thus, to the best of our knowledge, system **3c**/H_2O_2 is the most active VHPOs model, so far reported, as far as TONs (89000) and TOFs (20000 h^{-1}) are concerned.[23e]

4.3.1 Synthesis of organogelator-derived V(V) TPA complexes

Metal–organic gels (MOGs) are a class of supramolecular metallogels, in which metal–ligand coordination is associated with the formation of 3D structures *via* supramolecular interactions, such as hydrogen-bonding, *π-π* stacking, van der Waals and hydrophobic interactions.[134] MOG-based materials have had particular interest for catalytic applications as their short-range ordered structures provide highly regulated metal centres or microenvironments for catalyst immobilization.[135] More importantly, the reversibility of coordination bond formation makes MOGs have some promising properties that traditional supports with rigid bonds (e.g. organic polymers and inorganic oxides) do not have. However, application of metal-organic gels in catalysis is still in its infancy and only a few transition metal catalysts have been immobilised by MOGs *via* direct incorporation[28,136] or post-modification[137] with catalytically active metal ions. In most cases, catalyst immobilization in gel systems exhibited an improved catalytic activity with respect to the same catalyst in homogeneous conditions, with the possibility to easily recycle the catalyst and reuse it for several times.

---

[134] (a) L. Applegarth, N. Clark, A. C. Richardson, A. D. M. Parker, I. Radosavljevic-Evans, A. E. Goeta, J. A. K. Howard, J. W. Steed *Chem. Commun.* **2005**, 5423-5425. (b) Q. Wei, S. L. James *Chem. Commun.* **2005**, 1555-1556. (c) J. Zhang, X. Xu, S. L. James *Chem. Commun.* **2006**, 4218-4220. (d) F. Fages *Angew. Chem. Int. Ed.* **2006**, *45*, 1680-1682. (e) G. De Paoli, Z. Džolic, F. Rizzo, L. De Cola, F. Vögtle, W. M. Müller, G. Richardt, M. Žinic *Adv. Funct. Mater.* **2007**, *17*, 821-828. (f) Q. Liu, Y. Wang, W. Li, L. Wu *Langmuir* **2007**, *23*, 8217-8223. (g) W. L. Leong, A. Y.-Y. Tam, S. K. Batabyal, L. W. Koh, S. Kasapis, V. W.-W. Yam, J. J. Vittal *Chem. Commun.* **2008**, 3628-3630.

[135] Y.-R. Liu, L. He, J. Zhang, X. Wang, C.-Y. Su *Chem. Mater.* **2009**, *21*, 557-563.

[136] (a) B. Xing, M.-F. Choi, B. Xu *Chem.-Eur. J.* **2002**, *8*, 5028-5032. (b) Y. M. A. Yamada, Y. Maeda, Y. Uozumi *Org. Lett.* **2006**, *8*, 4259-4262. (c) T. Tu, W. Assenmacher, H. Peterlik, R. Weisbarth, M. Nieger, K. H. Dötz *Angew. Chem. Int. Ed.* **2007**, *46*, 6368-6371. (d) T. Tu, W. Assenmacher, H. Peterlik, G. Schnakenburg, K. H. Dötz *Angew. Chem. Int. Ed.* **2008**, *47*, 7127-7131.

[137] (a) J. Zhang, X. Wang, L. He, L. Chen, C.-Y. Su, S. L. James *New J. Chem.* **2009**, *33*, 1070-1075. (b) J. Huang, L. He, J. Zhang, L. Chen, C.-Y. Su *J. Mol. Catal. A-Chem.* **2010**, *317*, 97–103.

Different molecules are able to self-assemble in water and in organic solvents with different polarity, giving rise to molecular gels. Escuder and Miravet reported that compound **7** can form molecular gels either through *in situ* synthesis-gelation, by reacting precursor **6** with succinic anhydride (Scheme 5), or by heating-cooling procedure.[138]

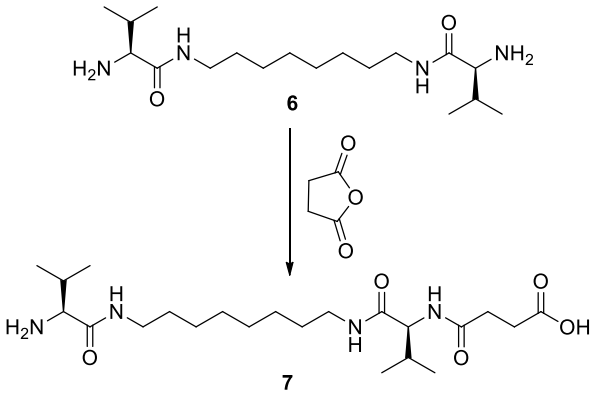

Scheme 5. Synthesis of gelator **7**.

Compound **7** is found to form gels in different solvents, whose microscopic structure depends on the gelation methods adopted. However, the authors proposed that gel formation might come from the formation of 12 hydrogen bonds with vicinal molecules as shown in figure 9.

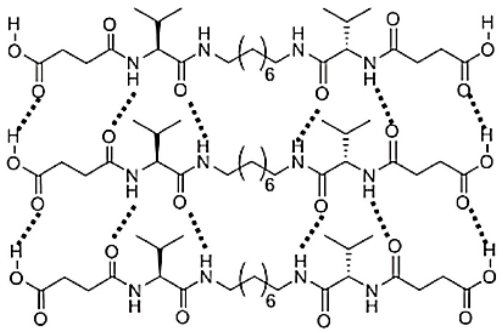

Figure 9. Schematic drawing of the proposed model of aggregation of **7**.[31]

In this view, we were interested in functionalizing V(V) TPA complexes with some functional organogelators, like the ones reported in figure 10. The project has been carried out in collaboration with Escuder and Miravet group in the frame of COST Action CM1005 "Supramolecular Chemistry in Water".

[138] M. Fontanillo, C. A. Angulo-Pachón, B. Escuder, J. F. Miravet *J. Coll. Interf. Sci.* **2013**, *412*, 65-71.

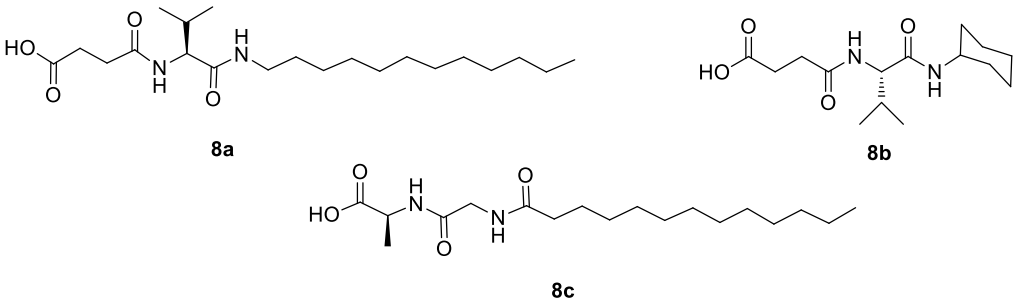

Figure 10. Functional organogelators **8a-c**.

For the functionalization strategy, we wanted to exploit the well-established oxime bond formation, reported in chapter 2.[139] As the procedure involves the reaction between an aldehyde and an alkoxyamine, complex **10** was synthesized by reaction of ligand **9** with VO(O*i*-Pr)$_3$ (Scheme 6).

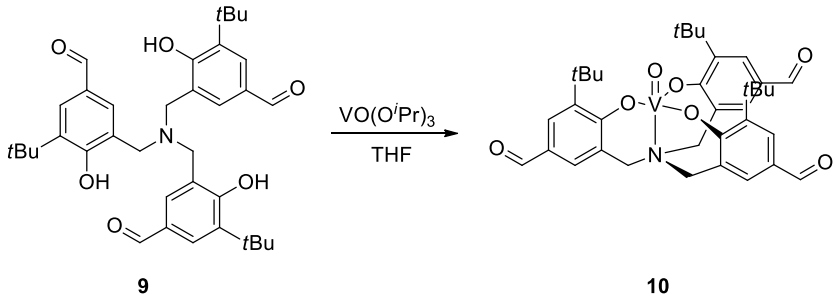

Scheme 6. Synthesis of V(V) TPA complex **10**.

The new V(V) complex **10** was fully characterized. ^{1}H-NMR (300 MHz, CD_3OD) spectrum shows the presence of two species in solution, making it suppose the formation of an equilibrium between a trigonal bipyramidal and an octahedral geometries, as in the case of complex **3c** (Scheme 7).

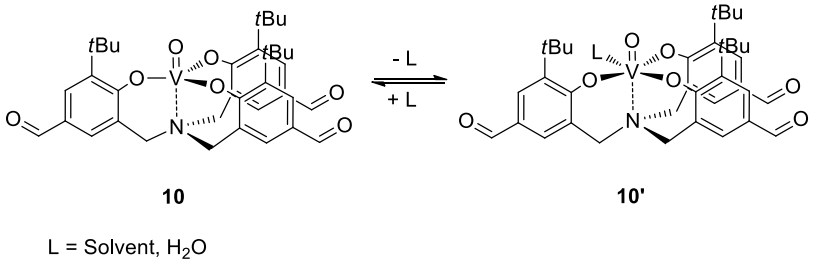

Scheme 7. Equilibrium between complexes **10** and **10′** in solution.

^{1}H-NMR (300 MHz, CD_3OD) for complex **10** is reported in figure 11.

[139] (a) O. Mitsunobu, M. Yamada *Bull. Chem. Soc. Jpn.* **1967**, *40*, 2380-2382. (b) O. Mitsunobu, M. Yamada, M. Teruaki *Bull. Chem. Soc. Jpn.* **1967**, *40*, 935-939. (c) O. Mitsunobu *Synthesis* **1981**, 1-28. (d) M. Karskela, M. Helkearo, P. Virta, H. Lönnberg *Bioconjugate Chem.* **2010**, *21*, 748-755.

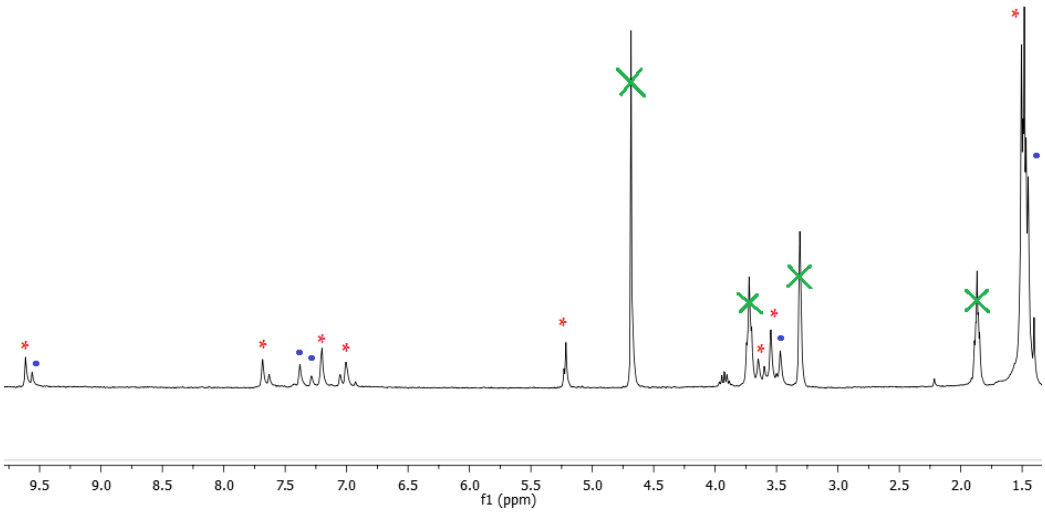

Figure 11. ^{1}H-NMR (300MHz, CD_3OD) of complexes **10** (•) and **10′** (*).

Even the gelator molecules **8a-c** had to be modified in order to introduce an alkyloxyamine residue (Scheme 8). The amine group on 2-aminoethanol **11** was firstly protected with di-*tert*-butyl dicarbonate (Boc).[140] Compound **12** then suffered Mitsunobu reaction, obtaining compound **13**, which was then deprotected at the amino end, by reaction with trifluoroacetic acid (TFA).[141] An amide coupling reaction was carried out, by reacting compound **14** with *O*-(1*H*-benzotriazol-1yl)-*N*,*N*,*N*′,*N*′-tetramethyluronium tetrafluoroborate (HATU) and *N*,*N*-di-*iso*propyl ethylamine (DIPEA).[142] Compounds **15a,c** were underwent hydrazinolysis to give organogelator-derived alkoxyamines **16a,c**.

[140] A. Sarkar, S. Raha Roy, N. Parikh, A. K. Chakraborti *J. Org. Chem.* **2001**, *76*, 7132-7140.
[141] D. M. Shendage, R. Fröhlich, G. Haufe *Org. Lett.* **2004**, *6*, 3675–3678.
[142] V. Dourtoglou, J.-C. Ziegler, B. Gross *Tetrahedron Lett.* **1978**, 1269-1972.

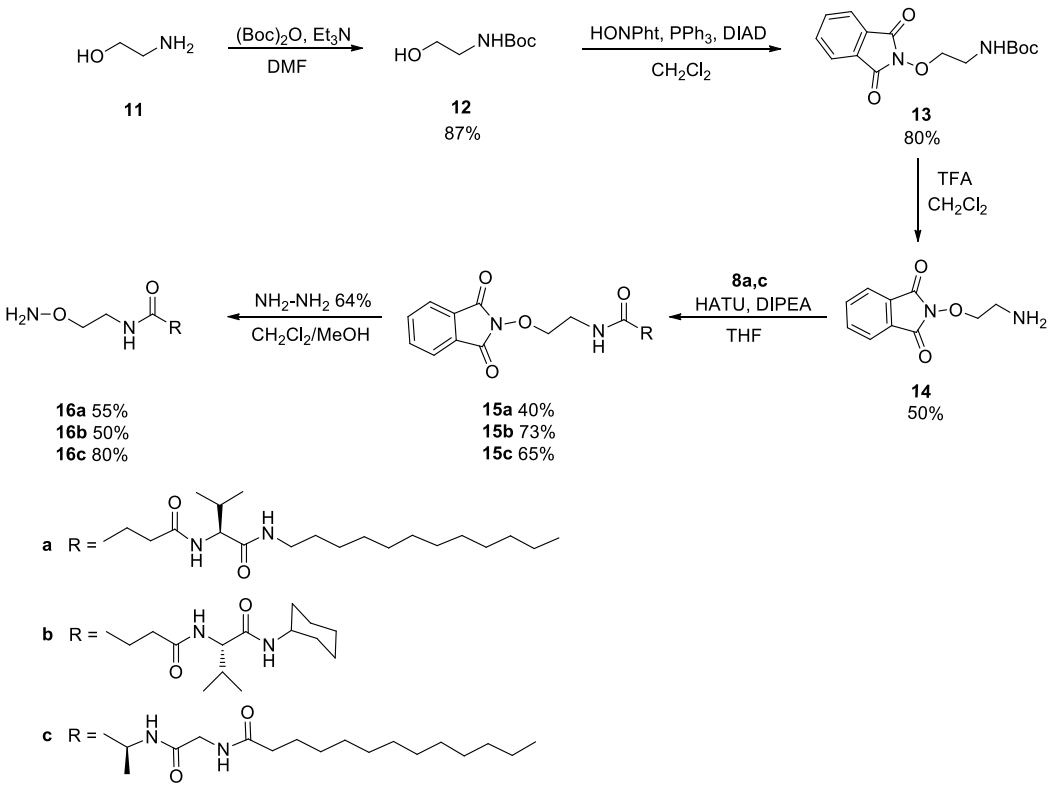

Scheme 8. Synthesis of gelator-derived alkoxyamines **16a-c**.

Functionalization of ligand **9** was then performed, by using alkoxyamines **16b,c** (Scheme 9).

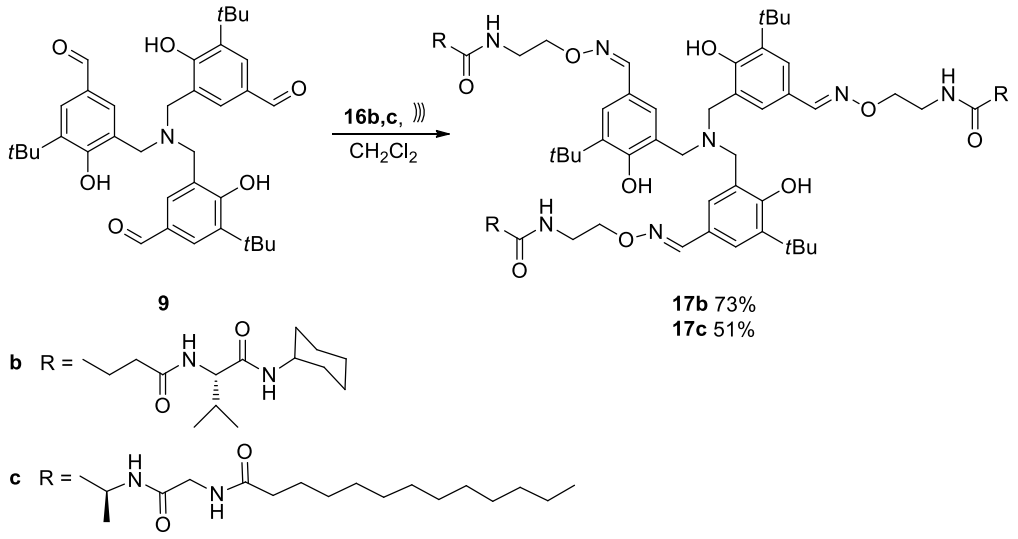

Scheme 9. Functionalization of ligands **9** with organogelator moieties.

The possibility to obtain hydro- or organogels of ligands **17b,c** was investigated and interestingly, an organogel of **17b** was obtained ($1.24*10^{-2}$ M in acetonitrile), through heating-cooling procedure (Figure 12).

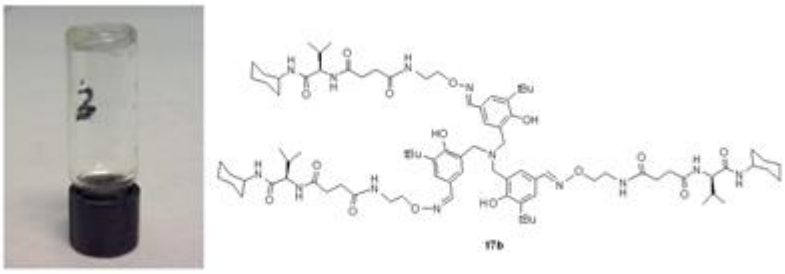

Figure 12. Gel of ligand **17b** (1.24*10^{-2} M in ACN).

Finally, complex **10** was directly functionalized with alkoxyamines **16a** and **16c** (Scheme 10).

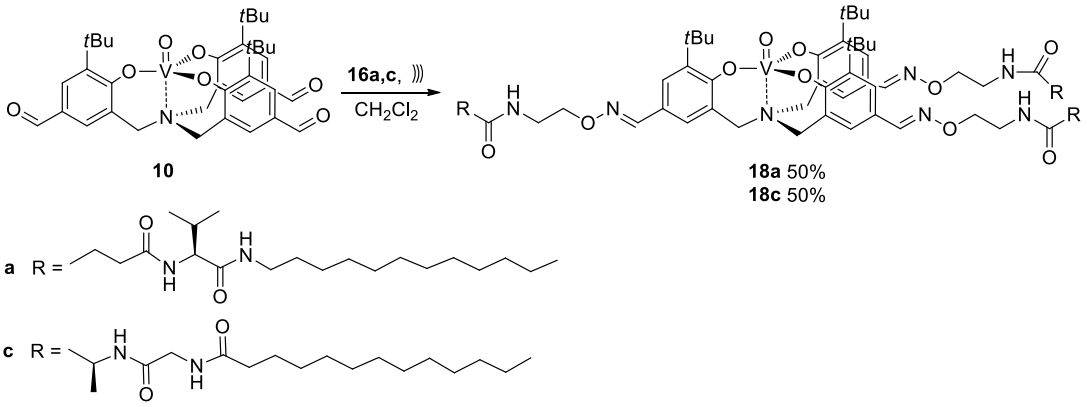

Scheme 10. Synthesis of organogelator-derived V(V) TPA complexes **18a** and **18c**.

Complexes **18a** and **18c** gave organogels in dioxane (Figure 13).

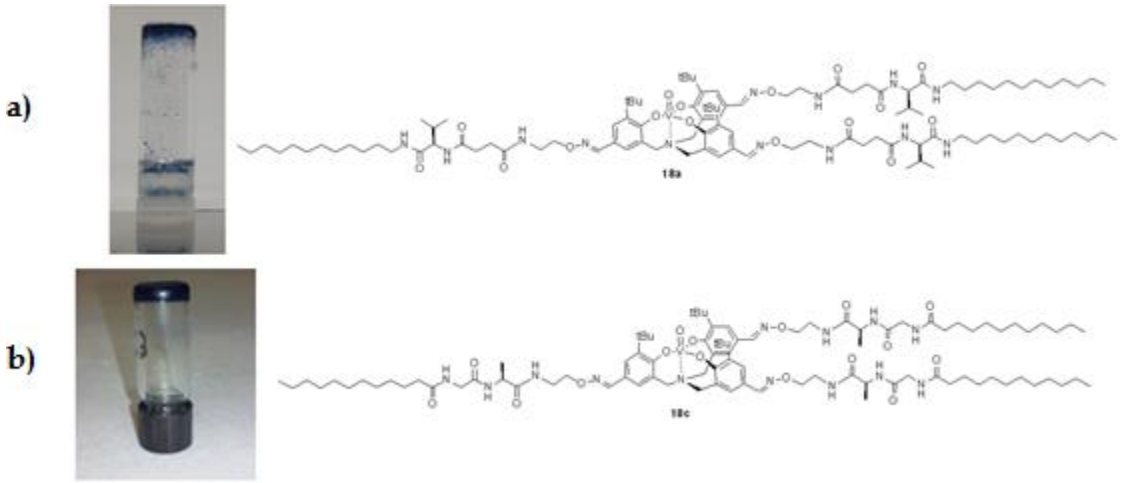

Figure 13. a) Gel of complex **18a** in dioxane (5*10^{-3} M); (b) gel of complex **18c** in dioxane (1*10^{-2} M).

The catalytic activity of complex **18a** in gel-phase was tested towards sulfoxidation reactions. Unfortunately, the system was not stable in the reaction conditions and the gel was disrupted.

TEM analyses on the gels are still under study, as well as the possibility to anchor other hydro- or organogelators functionalities on vanadium systems in order to obtain metallogels in different solvents and make their use as catalysts in sulfoxidation reaction more feasible.

4.3.2 Positively charged V(V) TPA complexes as micellar catalysts

The possibility of charged micelles to incorporate and dissolve oppositely charged metal species, through electrostatic interactions,[2] is important for the introduction of metal catalysts in micelle media and the realization of micellar catalysis.

In this view, we were interested in the development of new sustainable and recyclable micellar-V(V) TPA systems that can be used as micellar catalysts in water. In order to do so, we exploited the possibility to introduce positively charged moieties on TPA skeleton, as shown in chapter 2, to obtain a new positively charged V(V) TPA complex **20** by reacting ligand **19** with $VO(O\textit{i}\text{-}Pr)_3$ (Scheme 11).

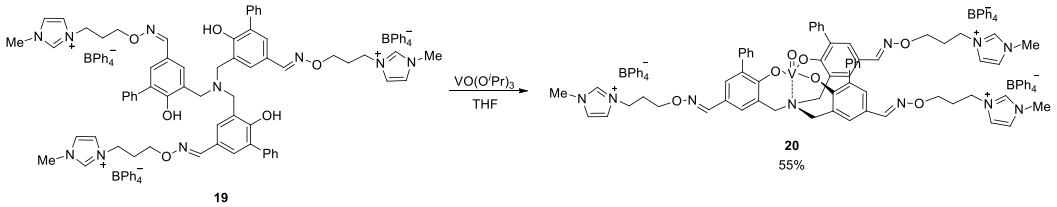

Scheme 11. Synthesis of positively charged V(V) TPA complex **20**.

Complex **20** was fully characterized. ESI-TOF spectrum presents different clusters, as double- and triple-charged species could be detected (Figure 14). All the spectra showed the characteristic isotopic distribution of vanadium complexes and are in complete agreement with the calculated ones.

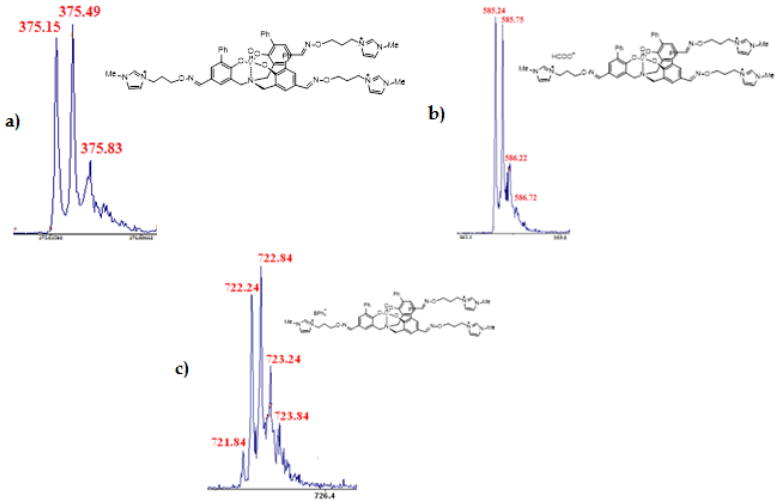

Figure 14. ESI-TOF spectrum of complex **20**, with isotopic distributions for: a) $[M - 3BPh_4]^{3+}$; b) $[M - 3BPh_4 + HCOO]^{2+}$; c) $[M - 2BPh_4]^{2+}$.

Once we obtained V(V) TPA complex **20**, we tried to solubilize it in water upon reaction with the oppositely charged sodium dodecyl sulfate (SDS) surfactant (CMC_{SDS} = 8.2 mM). The complex, firstly insoluble in water, was then easily dissolved by incorporation in a micellar-like system (Figure 15). Studies on the localization of the complex into the micelle are still under investigation.

Figure 15. Schematic representation of the micellar system of V(V) complex **20** and SDS.

In order to test the catalytic activity of the new system, a different reaction, which is being studied very recently in our group for V(V) TPA complexes, was explored, i.e. aerobic oxidative C-C cleavage.[143] In such these catalytic studies, V(V) TPA complexes **3b,c** and **3f** were tested in the oxidative cleavage of vicinal diols to aldehydes (Scheme 12).

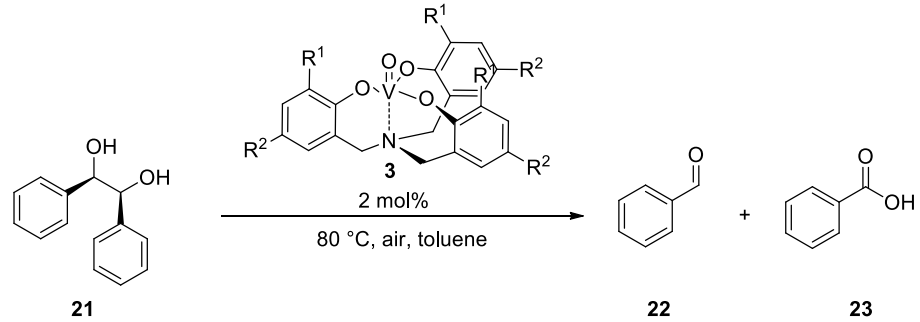

		22 : 23
3b	R^1=R^2= *t*Bu	91 : 9 (3h)
3c	R^1=R^2= Cl	99 : 1 (0.5h)
3f	R^1= *t*Bu; R^2 = H	93 : 7 (2h)

Scheme 12. Oxidative C-C cleavage of *meso*-hydrobenzoin **21** catalysed by V(V) TPA complexes **3b,c** and **3f**.

In all cases, reaction yields were almost quantitative (96-99%). The major product of C-C cleavage of *meso*-hydrobenzoin **21** is benzaldehyde **22**. The carboxylic acid **23** comes from further oxidation of **22**. From selectivities and conversion times of the three V(V) complexes, we can notice the same trend we had for the sulfoxidation reactions: the electron-poorest V(V) TPA complex **3c**, which bears six chloro atoms, is the most active, with best selectivities and less reaction times.

[143] E. Amadio, G. Licini *unpublished results*.

Thus, micellar system V(V) TPA complex **20**/SDS was tested in the same reaction. In particular, in an agate mortar, complex 20 and SDS were milled and then water was added and the suspension was milled again untill complete dissolution. The solution was transferred into a 5-mL screw-cap vial and *meso*-hydrobenzoin **21** was added and the mixture was heated at 80 °C. The reaction course was monitored by HPLC analysis (Scheme 13).

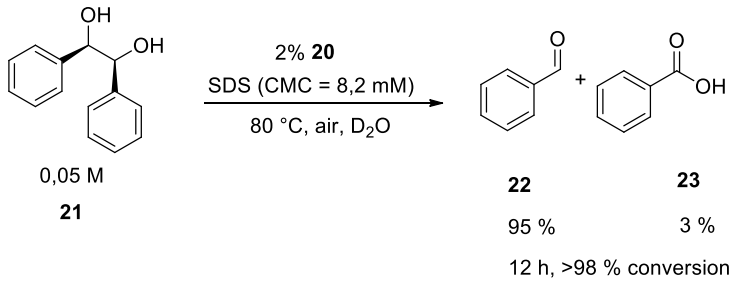

Scheme 13. Aerobic oxidative C-C cleavage reaction catalysed by micellar system complex **20**/SDS.

The reaction gave product **22** with high yield and selectivity in 12 h. Figure 16 shows reaction profile.

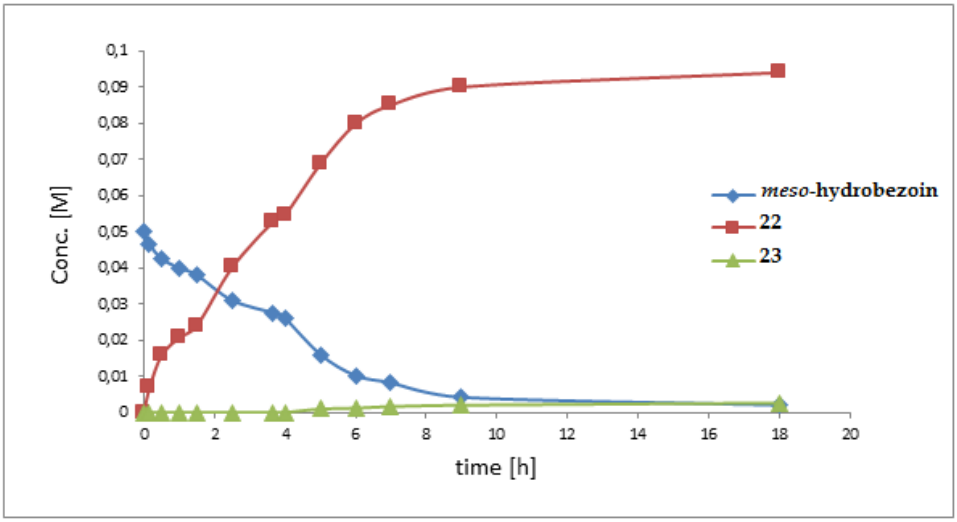

Figure 16. Reaction profile for oxidative C-C cleavage of *meso*-hydrobenzoin in micellar conditions.

Moreover, the organic compounds could be extracted with CH_2Cl_2 and the aqueous phase containing the catalytic system could be reused up to three times, ensuring anyway good yields.

4.4 Conclusions

The catalytic activity of V(V) TPA complexes has been investigated towards sulfoxidation and aerobic oxidative C-C cleavage reactions. The modification of electronic properties of the ligand, by the introduction of electron-withdrawing

chloro groups, has enabled to obtain excellent and highly reactive V(V) TPA catalysts in sulfoxidation reactions, with performances higher than the ones reported in literature.[26] Moreover, decoration with organo-gelators has led to the realization of new functionalized V(V) TPA complexes in gel-phase, which seem to be very promising as hetereogeneous systems in catalysis. Finally, functionalization of V(V) complexes with positively charged moieties let us obtain micelles upon reaction with sodium dodecyl sulfate, which have been found to be very reactive in oxidative cleavage reaction of C-C bonds in water.

4.5 Experimental

General remarks

All chemicals and dry solvents have been purchased from Aldrich and used as provided, without further purification. ^{1}H and $^{13}C\{^{1}H\}$-NMR spectra were recorded at 301K on Bruker AC-200, 250, 300 MHz or Varian 300 and 500 MHz instruments. ^{51}V-NMR spectra were recorded at 301K on a Bruker AC-300 instrument.. Chemical shifts (δ) have been reported in parts per million (ppm) relative to the residual undeuterated solvent as an internal reference ($CDCl_3$: 7.26 ppm for ^{1}H-NMR and 77.0 ppm for ^{13}C-NMR; CD_3OD: 3.31 ppm for ^{1}H-NMR and 49.05 ppm for ^{13}C-NMR) or tetramethylsilane. The following abbreviations have been used to explain the multiplicities: *s* = singlet, *d* = doublet, *t* = triplet, *dd* = doublet, doublet, *m* = multiplet, *br* = broad. ^{13}C-NMR spectra have been recorded with complete proton decoupling. ESI-MS spectra have been obtained on a LC/MS Agilent series 1100 spectrometer in both positive and negative modes using acetonitrile/formic acid 0.1% as mobile phase, with ESI-ion trap mass detector. In some cases, an ESI-TOF Mariner™ Biospectrometry™ Workstation of Applied Biosystems by flow injection, using acetonitrile or methanol/formic acid 0.1% as mobile phase, was used. All vanadatrane complexes were prepared under nitrogen atmosphere in a MBraun MB 200MD glove-box, equipped with a MB 150 G-I gas recycling system (nitrogen working pressure: 6 bar). Oxygen and water levels inside the box were real-time monitored by MBraun oxygen and moisture analyzers. IR spectra have been recorded on a Nicolet 5700 FT-IR, with range 4000-400 cm^{-1} and resolution 4 cm^{-1}, using KBr pellets or NaCl plates. For HPLC analyses, an HPLC equipped with Hyper sil BDS inverse phase C18 on silica (5 μl of active phase, 250x4.6 mm column), operating at room temperature was used. The UV detector was set at 210 nm wavelength. The eluent phase was water (A) and acetonitrile (B) (both with 0.01% of CF_3COOH). The concentration of both reagents and products were estimated from the calibration curves using naphthalene as internal standard. For experiments performed with *meso*-hydrobenzoin **21** the following gradient was used: 0- 12 min 50 % B, 14 min 95% B, 18 min 50 % B; 0.8 mL/min.

Syntheses of TPAs **9** and **19** are reported in chapter 2. Syntheses of ligand $\mathbf{L_cH_3}$[144] and complex **3c**[24] were performed by following previously reported procedures. All characterizations were in agreement with those reported in literature.

[144] (a) S. Groysman, S. Segal, I. Goldberg, M. Kol, Z. Goldschmidt *Inorg. Chem. Commun*. **2004**, *7*, 938-941. (b) C. J. Whiteoak, B. Gjoka, E. Martin, M. Martínez Belmonte, E. C. Escudero-Adán, C. Zonta, G. Licini, A. W. Kleij *Inorg Chem*. **2012**, *51*, 10639-10649.

Organogelators 8a-c

Organogelators **8a-c** were provided by prof. Beatriu Escuder from Universitat Jaume I in Castellón, Spain.

8a: IR (KBr) ν (cm^{-1}): 704, 712, 720, 733, 1184, 1246, 1348, 1397, 1433, 1548, 1638, 1721, 2851, 2920, 2958, 3099, 3288. ^{1}H-NMR: (500 MHz, DMSO-d_6) δ 11.98 (1H, *bs*), 7.86 (2H, *bs*), 4.08-4.06 (1H, *m*), 3.05-3.03 (1H, *m*), 2.99-2.97 (1H, *m*), 2.40 (4H, *s*), 1.93-1.91 (1H, *m*), 1.37 (2H, *s*), 1.23 (20H, *s*), 0.85-0.81 (9H, *m*). ^{13}C{^{1}H}-NMR: (125 MHz, $CDCl_3$) δ 173.81, 170.70, 57.86, 38.52, 31.26, 28.66, 26.29, 22.04, 19.15, 13.89. MS (ESI): *m/z* calc. 384.30; exp. 383.029 $[M - H]^-$.

8b: IR (KBr) ν (cm^{-1}): 695, 712, 719, 750, 929, 1153, 1179, 1229, 1245, 1348, 1403, 1440, 1552, 1632, 1737, 2666, 2854, 2928, 2961, 3085, 3285. ^{1}H-NMR: (200 MHz, DMSO-d_6) δ 12.02 (1H, *s*), 7.81-7.69 (2H, *m*), 4.06 (1H, *t*, *J* = 6 Hz), 3.54-3.44 (1H, *m*), 2.37 (4H, *s*), 1.91-1.81 (1H, *m*), 1.69-1.60 (4H, *m*), 1.54-1.48 (1H, *m*), 1.26-1.05 (5H, *m*), 0.81-0.77 (6H, *m*). ^{13}C{^{1}H}-NMR: (50.03 MHz, DMSO-d_6) δ 174.32, 171.36, 170.29, 58.00, 47.79, 33.01, 32.86, 32.62, 31.17, 30.34, 29.70, 25.62, 24.96, 24.89, 19.56, 18.64. MS (ESI): *m/z* calc. 298.19; exp. 299.2 $M + H]^+$, 321 $[M + Na]^+$.

8c: IR (KBr) ν (cm^{-1}): 719, 728, 742, 845, 984, 1144, 1225, 1237, 1348, 1378, 1045, 1472, 1535, 1626, 1651, 1726, 2564, 2611, 2849, 2915, 2955, 3060, 3289, 3379. ^{1}H-NMR: (500 MHz, DMSO-d_6) δ 8.12-8.10 (1H, *bs*), 7.99-7.97 (1H, *bs*), 4.22-4.20 (1H, *m*), 3.75-3.68 (2H, *m*), 2.11 (2H, *t*, *J* = 5 Hz), 1.48-1.45 (2H, *m*), 1.32 (19H, *s*), 0.85 (3H, *t*, *J* = 5 Hz). ^{13}C{^{1}H}-NMR: (125 MHz, $CDCl_3$) δ 173.89, 168.68, 47.38, 41.59, 35.15, 25.14, 22.05, 17.29, 13.90. MS (ESI): *m/z* calc. 328.24; exp. 328.2 $[M]^+$, 350.1 $[M + Na]^+$.

General procedure for prepration of oxovanadatrane complexes 10 and 20

Complexes **10** and **20** were prepared in glovebox by slowly addition of VO(O*i*-Pr)$_3$ (0.615 mmol) in dry THF (1 mL) to a solution of the corresponding ligand (0.160 mmol) in dry THF (5 mL). An immediate change in colour of VO(O*i*-Pr)$_3$ solutions was observed (from colourless to dark blue). The solutions were stirred for 1 h at room temperature and then the solvents were evaporated under vacuum leading to dark-blue solids, which were repeatedly washed with small volumes of hexane and dried in vacuum.

VO(V) complex 10: yield: 70%. IR (KBr) ν (cm^{-1}): 693, 729, 801, 954, 1094, 1135, 1261, 1381, 1419, 1576, 1616, 1684, 2338, 2360, 2720, 2866, 2907, 2962, 3447. ^{1}H-NMR: (300 MHz, CD_3OD) δ 9.64 (3H, *s*), 9.60 (3H, *s*), 7.70-7.68 (6H, *m*), 7.45-7.43 (1H, *m*), 7.37-7.35 (1H, *m*), 7.17 (1H, *s*), 7.04 (1H, *s*), 5.23-5.20 (2H, *m*), 3.64 (6H, *s*), 3.57-3.59 (4H, *m*), 3.53 (2H, *s*), 1.49 (18H, *s*), 1.43 (27H, *s*), 1.38 (9H, *s*). ^{13}C{1H}-NMR: (50.03 MHz, CD_3OD) δ 194.08, 169.65, 139.79, 137.75, 137.49, 133.84, 133.31, 133.08, 130.96, 130.29, 129.98, 128.74, 126.70, 106.26, 37.44, 32.48, 32.28, 32.08. ^{51}V-NMR (78.28 MHz, CD_3OD): δ -410.00. MS (ESI): *m/z* calc. 651.24; exp. 652.24 $[M + H]^+$.

VO(V) complex 20: yield: 55%. IR (KBr) ν (cm^{-1}): 704, 733, 777, 1063, 1161, 1265, 1438, 1456, 1576, 1594, 1669. 1675, 2336, 2361, 2924, 3052, 3447. ^{1}H-NMR: (300 MHz, CD_3CN) δ 8.10 (3H, *s*), 7.94-7.87 (3H, *s*), 7.74 (3H, *s*), 7.68-7.66 (6H, *m*), 7.54-7.48 (3H, *m*), 7.34 (6H, *s*), 7.34 (6H, *s*), 7.26-7.23 (24H, *m*), 7.14 (3H, *s*), 6.80 (24H, *t*, *J* = 6 Hz), 6.64 (12H, *t*, *J* = 6 Hz), 4.16-4.14 (6H, *m*), 4.06-4.04 (6H, *m*), 3.64 (9H, *s*), 3.55 (6H, *s*), 2.15-2.13 (6H, *m*). ^{13}C{1H}-NMR: (75.5 MHz, CD_3CN) δ 150.52, 150.20, 137.21, 131.11, 130.85, 130.78, 130.37, 129.47, 129.30, 129.07, 128.41, 128.32, 127.78, 127.14, 125.01, 123.90, 123.29, 71.52, 48.42, 37.28, 32.80, 30.77, 23.86, 14.86. ^{51}V-NMR (78.28 MHz, CD_3CN): δ -356.30. MS (ESI): *m/z* calc. 2082.95; exp. 375.15 $[M - 3BPh_4]^{3+}$, 585.24 $[M – 3BPh_4 + HCOO]^{2+}$, 722.84 $[M – 2BPh_4]^{2+}$.

Synthesis of *tert*-butyl (2-hydroxyethyl)carbamate 12

To a solution of 2-aminoethanol **11** (32.74 mmol, 2 g) in dry THF (76.3 mL) Et_3N (32.74 mmol, 3.34 g) and $(Boc)_2O$ (32.02 mmol, 7.86 g) were added and the mixture is stirred for 2 h at room temperature. The reaction mixture was then washed with brine (3 x 50 mL) and the organic phase was extracted three times with dichloromethane, dried over anhydrous Na_2SO_4 and evaporated to dryness. A pale yellow oil formed, which was used without any further purification (87%).

IR (KBr) ν (cm^{-1}): 663, 1100, 1172, 1254, 1390, 1437, 1689, 2933, 3423. ^{1}H-NMR: (200 MHz, $CDCl_3$) δ 3.69 (2H, *t*, *J* = 6 Hz), 3.27 (2H, *t*, *J* = 6 Hz), 1.44 (9H, *s*). ^{13}C{^{1}H}-NMR: (50.3 MHz, $CDCl_3$) δ 156.46, 78.16, 60.99, 42.45, 27.48. MS (ESI): *m/z* calc. 161.11; exp. 184 $[M + Na]^+$.

Synthesis of *tert*-butyl (2-((1,3-dioxoisoindolin-2-yl)oxy)ethyl)carbamate 13

To a solution of *tert*-butyl (2-hydroxyethyl)carbamate **12** (28.10 mmol, 4.55 g) in dry dichloromethane (280 mL), *N*-hydroxyphtalimide (33.72 mmol, 5.53 g) and triphenylphospine (33.72 mmol, 8.84 g) were added. The mixture was cooled to 0 °C and diisopropyl azodicarboxylate (DIAD, 33.72 mmol 6.82 g) was added dropwise. The mixture was stirred for 20 h at room temperature and evaporated to dryness. The product was purified by recrystallization from diethyl ether and a white solid was obtained (80%).

Mp: 85-95 °C. IR (KBr) ν (cm^{-1}): 876, 1273, 1436, 1509, 1740, 2936, 2981, 3054, 3224, 3439. ^{1}H-NMR: (200 MHz, $CDCl_3$) δ 7.88-7.75 (4H, *m*), 4.26 (2H, *t*, *J* = 6 Hz), 3.44 (2H, *t*, *J* = 6 Hz), 1.47 (9H, *s*). ^{13}C{^{1}H}-NMR: (50.03 MHz, $CDCl_3$) δ 132.74, 132.53, 129.14, 128.89, 70.17, 21.73. MS (ESI): *m/z* calc. 306.12; exp. 329 $[M + Na]^+$, 345 $[M + K]^+$.

Synthesis of 2-(2-aminoethoxy)isoindoline-1,3-dione 14

To a solution of *tert*-butyl (2-((1,3-dioxoisoindolin-2-yl)oxy)ethyl)carbamate **13** (10.29 mmol, 3.15 g) in dry dichloromethane (15.4 mL), TFA (1.5 mL/mmol sub., 15.4 mL) is added and the mixture is stirred for 1 h at room temperature. Then the mixture was evaporated to dryness and sat. $NaHCO_{3aq}$ was added and the organic

phase was extracted with CH_2Cl_2 (3 x 50 mL), dried over anhydrous Na_2SO_4 and concentrated under reduced pressure to give a white solid (50%).

Mp: 50-65 °C. IR (KBr) ν (cm^{-1}): 1011, 1399, 1709, 2939, 3294. ^{1}H-NMR: (200 MHz, $CDCl_3$) δ 7.84-7.77 (4H, *m*), 3.94 (2H, *t*, *J* = 6 Hz), 3.80 (2H, *t*, *J* = 6 Hz). ^{13}C{^{1}H}-NMR: (50.03 MHz, $CDCl_3$) δ 135.05, 134.76, 134.57, 134.37, 124.06, 123.96, 123.87, 36.21. MS (ESI): *m/z* calc. 206.07; exp. 207 $[M]^+$, 229 $[M + Na]^+$.

General synthesis of *N*-phtalimido-derived organogelators 15a-c

To a solution of 2-(2-aminoethoxy)isoindoline-1,3-dione **14** (0.078 mmol) and organogelators **8a-c** (0.052 mmol) in dry THF (3 mL/mmol), DIPEA (0.812 mmol) and *O*-(1*H*-benzotriazol-1yl)-*N*,*N*,*N*′,*N*′-tetramethyluronium tetrafluoroborate (HATU, 0.182 mmol) were added and the mixtures were stirred at room temperature for 12 h. The residues were washed with water and the organic phases were extracted three times with dichloromethane, dried over anhydrous Na_2SO_4 and evaporated to dryness. The products were purified by precipitation from diethyl ether.

15a: white solid. Yield: 40%. Mp: 140-145 °C. IR (KBr) ν (cm^{-1}): 843, 1437, 1635, 1652, 1675, 1717, 2337, 2361, 2852, 2922, 2958, 3111, 3286. ^{1}H-NMR: (200 MHz, $CDCl_3$) δ 7.86-7.75 (4H, *m*), 4.19 (1H, *s*), 4.04-4.00 (4H, *dd*, *J* = 5 Hz, *J* = 15 Hz), 3.24-3.21 (2H, *m*), 2.75 (1H, *s*), 2.59-2.56 (4H, *m*), 1.40 (1H, *s*), 1.24 (18H, *s*), 0.95-0.87 (9H, *m*). ^{13}C{^{1}H}-NMR: (125 MHz, DMSO-d_6) δ 171.03, 170.67, 167.67, 134.70, 131.62, 123.03, 71.86, 64.88, 40.11, 39.61, 38.34, 36.11, 31.26, 30.66, 30.41, 30.23, 29.00, 28.93, 28.66, 26.29, 22.06, 19.15, 18.01, 13.92. MS (ESI): calc. 572.36; exp. 573.2 $[M + H]^+$.

15b: white solid. Yield: 73%. IR (KBr) ν (cm^{-1}): 697, 720, 976, 1085, 1246, 1314, 1394, 1496, 1517, 1554, 1558, 1635, 1669, 1675, 1714, 1734, 1761, 1772, 2336, 2361, 2854, 2935, 3279, 3366. ^{1}H-NMR: (300 MHz, DMSO-d_6) δ 7.90-7.86 (2H, *m*), 7.85-7.80 (2H, *m*), 7.78 (1H, *bs*), 7.76 (1H, *bs*), 7.72-7.70 (1H, *m*), 4.10-4.05 (1H, *m*), 3.98-.394 (2H, *m*), 3.80-3.78 (2H, *m*), 3.53-3.49 (1H, *m*), 2.38-2.34 (2H, *m*), 2.162.13 (2H, *m*), 1.90-1.87 (1H, *m*), 1.96-1.62 (3H, *m*), 1.54-1.50 (1H, *m*), 1.26-1.18 (4H, *m*), 1.15-1.07 (2H, *m*), 0.84-0.78 (6H, *m*). ^{13}C{^{1}H}-NMR: (75.5 MHz, DMSO-d_6) δ 171.88, 171.70, 160.93, 136.66, 136.37, 125.03, 81.36, 80.48, 59.55, 49.32, 34.37, 34.13, 32.51, 30.86, 27.16, 26.50, 26.42, 21.06, 20.09. MS (ESI): calc. 486.25; exp. 487.23 $[M + H]^+$, 509.23 $[M + Na]^+$.

15c: white solid. Yield: 65%. IR (KBr) ν (cm^{-1}): 722, 878, 976, 1044, 1154, 1192, 1293, 1326, 1357, 1419, 1467, 1506, 1539, 1576, 1652, 1695, 1700, 1775, 2336, 2361, 2850, 2920, 3071, 3277. ^{1}H-NMR: (300 MHz, DMSO-d_6) δ 7.54-7.48 (2H, *m*), 7.44-7.39 (2H, *m*), 4.22-4.20 (1H, *m*), 3.76-.72 (2H, *m*), 3.67-3.64 (2H, *m*), 3.46-3.40 (2H, *m*), 1.97 (2H, *t*, *J* = 6 Hz), 1.32-1.28 (1H, *m*), 1.00-0.93 (20H, *m*), 0.58 (3H, *t*, *J* = 6 Hz). ^{13}C{^{1}H}-NMR: (50.03 MHz, $CDCl_3$) δ 174.24, 169.35, 169.02, 141.51, 134.58, 132.09, 123.79, 72.72,

54.88, 47.70, 43.47, 42.99, 36.62, 35.63, 32.09, 29.79, 29.67, 29.51, 25.78, 22.87, 18.87, 17.92, 17.55, 14.29, 12.48.MS (ESI): calc. 516.29; exp. 517 $[M + H]^+$, 539 $[M + Na]^+$, 555 $[M + K]^+$.

General synthesis of organogelator-derived alkoxyamines 16a-c

16a: To a solution of *N*-phtalimido-derived organogelators **15a-c** (0.49 mmol) in MeOH (5mL), hydrazine monohydrate 80% (1.176 mmol) was added and the reaction mixtures were stirred overnight at room temperature. The precipitated were then filtered under vacuum and the filtrates were concentrated under reduced pressure.

16a: white solid. Yield: 55%. IR (KBr) ν (cm^{-1}): 722, 840, 1138, 1207, 1378, 1419, 1441, 1472, 1496, 1539, 1576, 1616, 1669, 1684, 1717, 1739, 2336, 2361, 2851, 2921, 3287. ^{1}H-NMR: (500 MHz, DMSO-d_6) δ 8.08-8.05 (1H, *m*), 7.88-7.82 (3H, *bs*), 4.08-4.02 (4H, *m*), 3.91-3.86 (1H, *m*), 3.01-2.97 (2H, *m*), 2.38-2.33 (2H, *m*), 2.26-2.21 (2H, *m*), 1.40-1.36 (1H, *m*), 1.22 (20H, *s*), 0.87-0.79 (9H, *m*). ^{13}C{^{1}H}-NMR: (125 MHz, DMSO-d_6) δ 159.56, 65.36, 58.26, 38.85, 31.75, 31.15, 30.90, 24.49, 29.47, 29.44, 29.42, 29.15, 26.81, 25.18, 19.68, 18.06, 15.63, 14.41. MS (ESI): calc. 442.35; exp. 443 $[M + H]^+$.

16b: white solid. Yield: 50%. ^{1}H-NMR: (500 MHz, $CDCl_3$) δ 4.17-4.15 (1H, *m*), 3.86-6.368 (4H, *m*), 3.49-3.46 (1H, *m*), 2.55-2.51 (2H, *m*), 1.87-1.85 (1H, *m*), 1.70-1.68 (2H, *m*), 1.61-1.59 (2H, *m*), 1.33-1.25 (5H, *m*), 1.23-1.15 (3H, *m*), 0.94-0.91 (6H, *m*). ^{13}C{^{1}H}-NMR: (75.5 MHz, $CDCl_3$) δ 173.5, 173.2, 170.9, 75.5, 62.5, 49.8, 36.7, 32.5, 32.4, 32.2, 25.7, 24.6, 18.8. MS (ESI): calc. 356.24; exp. 357.25 $[M + H]^+$, 379.23 $[M + Na]^+$.

16c: white solid. Yield: 80%. ^{1}H-NMR: (300 MHz, DMSO-d_6) δ 8.06-8.03 (2H, *m*), 7.97-7.94 (1H, *m*), 7.81-7.78 (2H, *m*), 4.22 (1H, *t*, *J* = 6Hz), 3.67-3.65 (2H, *m*), 3.49 (2H, *t*, *J* = 6 Hz), 3.22 (2H, *q*, *J* = 6 Hz), 2.10 (2H, *t*, *J* = 6 Hz), 1.49-1.43 (1H, *m*), 1.22-1.16 (18H, *m*), 0.84 (3H, *t*, *J* = 6 Hz). ^{13}C{^{1}H}-NMR: (50.03 MHz, DMSO-d_6) δ 173.48, 172.81, 169.29, 73.70, 48.71, 38.12, 35.81, 31.95, 29.67, 29.60, 29.48, 29.36, 25.84, 22.75, 19.07, 14.61. MS (ESI): calc. 386.29; exp. 387. 29 $[M + H]^+$.

General synthesis of organogelator functionalized ligands 17b,c

To a solution of ligand **9** (0.052 mmol) in chloroform (10 mL/mmol) organogelator-derived alkoxyamines **16b,c** (0.156 mmol) were added and the mixture was stirred for 15 min. Then trifluoroacetic acid (TFA, 1%) was added and the mixtures were firstly sonicated for 30 min and then stirred for 12 h at room temperature. The reaction mixtures were washed with sat. $NaHCO_{3aq}$ and the organic phases were extracted three times with dichloromethane, dried over anhydrous Na_2SO_4 and evaporated to dryness. The products were purified by precipitation from diethyl ether.

17b: yellow solid. Yield: 73%. IR (KBr) ν (cm^{-1}): 1176, 1260, 1387, 1394, 1419, 1436, 1464, 1472, 1506, 1554, 1635, 1645, 1669, 1684, 1695, 1734, 2336, 2361, 2853, 2928,

3280. ^{1}H-NMR: (500 MHz, DMSO-d_6) δ 8.05 (3H, *s*), 7.85-7.75 (6H, *m*), 7.55 (3H, *s*), 7.35 (3H, *s*), 7.25 (3H, *s*), 4.11-4.09 (3H, *m*), 3.91 (6H, *s*), 3.37-3.35 (3H, *m*), 2.40-2.35 (12H, *m*), 1.98-1.91 (3H, *m*), 1.71-1.64 (4H, *m*), 1.31 (27H, *s*), 1.26-1.21 (18H, *m*), 0.85-0.81 (18H, *m*). ^{13}C{^{1}H}-NMR: (50.03 MHz, $CDCl_3$) δ 172.38, 171.64, 170.06, 151.75, 151.46, 131.54, 127.17, 126.50, 124.90, 70.14, 60.92, 58.37, 48.06, 35.11, 34.90, 33.08, 32.84, 31.47, 31.30, 31.08, 30.08, 29.94, 29.58, 25.87, 25.16, 19.80. MS (ESI): *m/z* calc. 1602.2; exp. 1603.03 $[M + H]^+$.

17c: yellow solid. Yield: 51%. IR (KBr) ν (cm^{-1}): 1419, 1436, 1447, 1456, 1464, 1472, 1490, 1525, 1533, 1545, 1554, 1569, 1616, 1623, 1646, 1669, 1695, 1717, 1734, 2336, 2361, 2923, 3420. ^{1}H-NMR: (500 MHz, DMSO-d_6) δ 8.31 (3H, *s*), 8.07-7.90 (9H, *m*), 7.36 (3H, *s*), 7.23 (3H, *s*), 4.27-4.23 (3H, *m*), 4.03 (6H, *s*), 3.74-3.66 (12H, *m*), 3.37-3.35 (6H, *m*), 2.13-2.11 (6H, *m*), 1.51-1.46 (6H, *m*), 1.33 (27H, *s*), 1.24-1.19 (57H, *m*), 0.86 (9H, *t*, *J* = 5Hz). ^{13}C{^{1}H}-NMR: (50.03 MHz, $CDCl_3$) δ 176.9, 172.14, 153.4, 152.9, 133.29, 125.98, 125.46, 123.82, 123.25. 71.48, 55.52, 48.96, 36.05, 35.79, 35.23, 31.93, 31.33, 30.16, 29.65, 29.57, 29.47, 29.33, 25.80, 22.73, 18.94, 14.59. MS (ESI): *m/z* calc. 1693.29; exp. 1694.17 $[M + H]^+$.

General synthesis of organogelator-derived V(V) TPA complexes 18 a and 18c
To a solution of complex **10** (0.014 mmol) in CH_2Cl_2 (2 mL), organogelator-derived alkoxyamines **16a** and **16c** (0.051 mmol) were added and the reaction mixtures were firstly sonicated for 30 min and then stirred for 48 h at room temperature. The mixtures were then concentrated under reduced pressure. The products were purified by precipitation from diethyl ether.

18a: yellow solid. Yield: 50%. IR (KBr) ν (cm^{-1}): 848, 1147, 1292, 1456, 1472, 1525, 1539, 1558, 1576, 1646, 1669, 1675, 1695, 2336, 2361, 2854, 2925, 3420. MS (ESI): *m/z* calc. 1924.26; exp. 1926.27 $[M]^+$.

18c: yellow solid. Yield: 50%. IR (KBr) ν (cm^{-1}): 1082, 1262, 1378, 1436, 1458, 1472, 1521, 1539, 1558, 1576, 1662, 1675, 1695, 1717, 2336, 2361, 2850, 2920, 2957, 3291. MS (ESI): *m/z* calc. 1756.08; exp. 1779.06 $[M + Na]^+$.

General procedure for monitoring thioanisole 4 oxidation catalysed by 3c using aqueous H_2O_2 as oxidant (Table 1).
A screw-cap NMR tube was charged with a solution of complex **3c** in CD_3OD and then the internal standard (1,2-dichloroethane, DCE), H_2O_2 (35% or 70% in water, as indicated in Table 1) and thioanisole **4** were added to a final volume of 1 mL, with the final concentrations reported in Table 1. Monitoring of sulfide, sulfoxide and sulfone concentrations was made by integration of methyl group signals: Ph-S-*Me* (2.4 ppm), Ph-SO-*Me* (2.8 ppm) and Ph-SO_2-*Me* (3.1 ppm). Final yields were determined by 1H-NMR (300 MHz) with respect to the internal standard DCE (3.78 ppm).

General procedure for preparation of micellar system complex 20/SDS

In an agate mortar, positively charged V(V) TPA complex **20** (0.001 mmol, 2.1 mg) was finely milled in presence of SDS surfactant (0.082 mmol, 2.36 mg). After some minutes, D_2O (1 mL) was added (CMC_{SDS} = 8.2 mM) and the suspension was milled again till complete dissolution of the solid.

General procedure for catalytic oxidative cleavage reaction in micellar system complex 20/SDS

In an agate mortar, positively charged V(V) TPA complex **20** (0.002 mmol, 4.3 mg) and SDS (0.0164 mmol, 4.72 mg) were milled and dissolved into water (2 mL). The solution was transferred into a 5-mL screw-cap vial and *meso*-hydrobenzoin 21.4 (0.1 mmol, 21.4 mg) was added. The mixture was then heated up at 80 °C under stirring. The vial was periodically opened to air and monitored by HPLC by transferring 10 µL of the solution to a 1 mL of acetonitrile/water (50% v/v) and adding 10 µL of a solution of naphthalene (6.4 mg in 10 mL of CH_3CN) as internal standard. After 9 h at 80°C, the analysis revealed that 96% of the starting material had been consumed. The main products consisted of benzaldehyde **22** (90% yield) with traces of benzoic acid **23** (2%). The organic compounds could be extracted by addition of CH_2Cl_2 (2 x 2 mL) and the catalytic water phase could be reused again.

Abbreviations

ACN	Acetonitrile
AFM	Atomic Force Microscopy
ATP	Adenosine Triphosphate
Bn	Benzyl
Boc	*tert*-Butyloxy carbonyl
CMC	Critical Micelle Concentration
CNT	Carbon Nanotube
CuAAC	Copper^{I}-Catalysed Azide-Alkyne 1,3-dipolar Cycloaddition
DCE	1,2-Dichloroethane
DIAD	Di-*iso*propyl azodicarboxylate
DIPEA	*N*,*N*-di-*iso*propyl ethylamine
DMF	Dimethylformamide
DMSO	Dimethyl sulfoxide
DNA	Deoxyribonucleic Adic
DOSY-NMR	Diffusion Ordered Nuclear Magnetic Resonance Spectroscopy
ESI-MS	Electron Spray Mass Spectrometry
ESI-TOF	Electron Spray Mass Spectrometry – Time of Flight
Et_3N	Triethylamine
EtOAc	Ethyl acetate
FC	Flash Chromatography
FT-IR	Fourier Transform Infrared Spectroscopy
GC-MS	Gas Chromatography Mass Spectrometry
HATU	*O*-(1*H*-benzotriazol-1yl)-*N*,*N*,*N*′,*N*′-tetramethyluronium tetrafluoroborate
HPLC	High Performance Liquid Chromatography

***i*-Pr**	Isopropyl
***i*-PrO**	Isopropoxide
LC-MS	Liquid Chromatography Mass Spectrometry
MALDI-TOF	Matrix Assisted Laser Desorption Ionization – Time of Flight
Me	Methyl
MeOH	Methanol
MOG	Metal-Organic Gels
MOM	Methoxy Methyl
mp	Melting point
MS	Mass Spectrometry
MW	Microwave
NMR	Nuclear Magnetic Resonance
OCT	Octahedral geometry
PEG	Polyethylene glycol
PGSE	Pulse Gradient Spin-Echo Experiment
Ph	Phenyl
PMA	Phosphomolibdic Acid
POM	Polyoxometalate
r.t.	Room temperature
RNA	Ribonucleic Acid
ROP	Ring Opening Polymerization
SDS	Sodium Dodecyl Sulfate
Sub	Substrate
SWCNT	Single Walled Carbon Nanotube
TBP	Trigonal-bipyramidal geometry
***t*-Bu**	*tert*-Butyl
***t*-BuOOH**	*tert*-Butyl hydroperoxide
TEG	Triethylene glycol

TFA	Trifluoroacetic acid
THF	Tetrahydrofuran
TLC	Thin Layer Chromatography
TMP	Trigonal-monopyramidal geometry
TMV	Tobacco Mosaic Virus
TOF	Turn Over Frequency
TON	Turn Over Number
TPA	Triphenolamine
UV-Vis	Ultraviolet-Visible
UV-Vis-NIR	Ultraviolet-Visible-Near Infrared
VHPO	Vanadium Haloperoxidase

Summary

This Ph.D. thesis describes the versatility of amine triphenolate complexes to be used either as self-assembling molecular scaffolds with applications in material sciences and molecular recognition, like titanium (IV) μ-oxo TPA complexes, or as active catalysts in homogeneous and heterogeneous catalysis, mainly vanadium (V) TPA complexes.

In *Chapter 1*, the principles of self-assembly are listed, i.e. control on the electronic properties and size discrimination for the realization of supramolecular structures, error-checking, and efficiency, in the way of building up ordered and highly-structured entities under mild conditions. Different examples are proposed, but the analysis is mainly focused on the possibility of applying self-assembly in metal coordination chemistry in order to design highly ordered and functional systems, that may find applications in catalysis or material sciences. In this view, the coordination chemistry and the behaviour in solution of Ti(IV) TPA complexes are presented and in particular the possibility to switch between mononuclear and dinuclear μ-oxo species, depending on the steric nature of peripheral substituents, as well as the feasibility to build up highly functional Ti(IV) molecular scaffolds. A brief introduction on V(V) TPA complexes is reported as well, especially on their Lewis acid nature and structural characteristics that make them be considered as functional models of natural vanadium-dependent haloperoxidases and be used as active catalysts in oxygen transfer reactions.

As the realization of new efficient and functional supramolecular systems supposes the design of the right building blocks, in *Chapter 2*, the modification of amine triphenolate skeleton is proposed. The functionalization strategy that has been adopted is based on a click-type oxime bond formation upon reaction of an aldehyde group, which can be effectively and selectively inserted on TPA ligands through the so-called Duff reaction, and a wide variety of alkoxyamines. In this way, the ligand skeleton has been efficiently decorated with polar and positively charged moieties, such as TEG arms and imidazolinium residues, and with pyrene groups. The functionalization has interested diverse positions of the ligand and even a double functionalization of two different positions on the same *tri*-phenolamine can be achieved.

Chapter 3 deals with titanium (IV) amine triphenolate complexes and with the thermodynamic stability in solution of a Ti(IV) complex obtained by complexation with tris-(2-hydroxy-3-phenylbenzyl)amine. In more details, the reaction gives rise to a mononuclear complex, which upon reaction with water stereoselectively self-assembles into a highly stable, inert, dinuclear, heterochiral S_6-symmetric μ-oxo TPA complex. Highly decorated Ti(IV) μ-oxo TPA complexes can be efficiently obtained by effecting the complexation reaction on functionalized ligands reported in Chapter 2, or by directly functionalizing Ti(IV) μ-oxo TPA complexes, which bear six aldehyde groups in *para* and/or *meta* positions,

with the appropriate alkoxyamine. The functionalization strategy enables to construct stable and spatially ordered materials. In particular, two different Ti(IV) μ-oxo TPA complexes, bearing pyrene groups in *para* and *meta* positions, respectively, have been used as molecular receptors for fullerene. Fluorescence spectroscopies and DOSY-NMR analyses clearly indicate that pyrene groups on titanium complexes interact with fullerene through π-π interactions. Additionally, interactions between pyrene groups in *para* position on Ti(IV) μ-oxo TPA complex and SWCNTs (single walled carbon nanotubes) has been studied as well. Even in this case, fluorescence studies have been carried out and AFM images clearly show that CNTs are covered from Ti(IV) μ-oxo TPA complexes, highlighting the possibility to use such these systems for the design of ordered and functional supramolecular structures.

Finally, in *Chapter 4*, the catalytic activity of V(V) TPA complexes is studied, both in sulfoxidation and aerobic oxidative C-C cleavage reactions. Firstly, the activity of an electron-poor V(V) TPA complex, bearing six chloro groups in *ortho* and *para* positions, is investigated in sulfoxidation reactions in presence of hydrogen peroxide as terminal oxidant. The reactions are performed with high yields and selectivities (catalyst loading down to 0.001% and TONs up to 89000). Both reaction rates and selectivities confirm the higher activity of the new catalyst with respect to the ones reported in literature. Moreover, modification of V(V) complexes through oxime bond formation has also led to the realization of organogelator-derived complexes, which have been found to form organogels in dioxane. Lastly, functionalization of V(V) complexes with positively charged moieties makes it possible to obtain water-soluble micelles, upon solubilisation with SDS (sodium dodecyl sulphate). The micellar like system has been tested in aerobic oxidative C-C cleavage of vicinal diols, with high selectivity and quite short reaction times. The compartmentalization of the catalytic system allowed its recycling and reuse for three times by extraction of products with organic solvents.

Riassunto

Questa tesi di dottorato descrive la sintesi e la funzionalizzazione di complessi amminotrifenolati di titanio (IV) e vanadio (V) per applicazioni in reazioni di riconoscimento molecolare e in catalisi.

Nel *Capitolo 1*, sono illustrati i principi che regolano il *self-assembly*, quali controllo, correzione degli errori ed efficienza. E' mostrato come questi possano essere applicati per la realizzazione di entità ordinate e strutturate in chimica di coordinazione, per la costruzione di sistemi metallo-supramolecolari, con applicazione in catalisi o scienze dei materiali. In quest'ottica, sono studiati la chimica di coordinazione e il comportamento in soluzione di complessi TPA di titanio (IV) e in particolare la capacità di fornire specie mono- o dinucleari a seconda dell'ingombro sterico dei sostituenti periferici e la possibilità di costruire *scaffolds* molecolari di titanio (IV) altamente funzionalizzati. Inoltre, è riportata una breve introduzione sui complessi TPA di vanadio (V). Le loro proprietà di acidi di Lewis e le caratteristiche strutturali fanno sì che essi vengano considerati dei modelli funzionali delle aloperossidasi naturali vanadio-dipendenti e quindi vengano utilizzati come catalizzatori in reazioni di trasferimento di ossigeno.

Nel *Capitolo 2*, viene proposta una strategia sintetica per modificare lo scheletro trifenolamminico. La funzionalizzazione prevede la formazione di un legame ossimico, mediante una reazione *click*-simile tra un'aldeide, che può essere selettivamente introdotta sul legante mediante reazione di Duff, e una varietà di alcossiammine. In questo modo, lo scheletro del legante può essere efficientemente decorato con residui polari e carichi positivamente, come residui TEG o imidazolinio, e con gruppi pirene. La funzionalizzazione può coinvolgere diverse posizioni del legante, così come una doppia derivatizzazione di posizioni differenti sulla stessa trifenolammina.

Nel *Capitolo 3*, sono riportate la sintesi e la funzionalizzazione di complessi dinucleari μ-oxo amminotrifenolati di titanio (IV) per reazione di complessazione della tri-(2-idrossi-3-fenilbenzil)ammina con Ti(O*i*-Pr)$_4$. Più in dettaglio, il complesso mononucleare, che si forma dalla reazione, in presenze di tracce d'acqua è in grado di auto-assemblarsi in maniera stereoselettiva, dando origine a un complesso dinucleare, altamente stabile, inerte, eterochirale, con simmetria S_6. La funzionalizzazione del complesso può essere ottenuta efficacemente mediante una duplice via: effettuando la reazione di complessazione sui leganti funzionalizzati riportati in Capitolo 2, oppure funzionalizzando direttamente complessi TPA μ-oxo di titanio (IV), che portano sei gruppi aldeidici in *para* e/o *meta*, con un'appropriata alcossiammina. La strategia di funzionalizzazione permette di costruire dei materiali stabili e spazialmente ordinati. In particolare, due complessi μ-oxo di titanio che portano gruppi pirene rispettivamente in *para* e *meta* sono stati utilizzati come recettori molecolari per il fullerene. Spettroscopie di fluorescenza ed esperimenti DOSY-NMR indicano chiaramente che i gruppi pirene sui complessi di titanio interagiscono con il fullerene mediante interazioni π-π. Come ulteriore applicazione, sono state studiate le interazioni tra gruppi pirene dei complessi TPA μ-oxo di titanio e nanotubi di carbonio

(SWCNTs). Anche in questo caso, sono stati condotti studi di fluorescenza e analisi AFM mostrano chiaramente che i nanotubi sono rivestiti dai complessi di titanio, evidenziando la possibilità di usare questi sistemi per generare strutture supramolecolari ordinate e funzionali.

Infine, nel *Capitolo 4*, è studiata l'attività catalitica di complessi TPA d vanadio (V), sia in reazioni di solfossidazione che in reazioni di *cleavage* aerobico ossidativo di legami C-C. Prima di tutto, viene analizzata l'attività catalitica di un complesso di vanadio (V) elettron-povero, portante sei atomi di cloro in posizioni *orto* e *para*, in reazioni di solfossidazione in presenza di perossido d'idrogeno come ossidante terminale. Le reazioni sono condotte con alte rese e selettività, anche in presenza dello 0.001% di catalizzatore, con TON fino a 89000. Le velocità di reazione e le selettività confermano una attività maggiore del catalizzatore rispetto ai catalizzatori riportati in letteratura. In più, la modificazione di complessi TPA di vanadio (V) mediante formazione di un'ossima ha portato anche alla realizzazione di complessi funzionalizzati con catene *organogelator* e alla formazione di *organogel* in diossano. In conclusione, la funzionalizzazione di complessi TPA di vanadio (V) con residui carichi positivamente permette di ottenere micelle solubili in acqua, in seguito a solubilizzazione con SDS (sodio dodecil solfato). Il sistema micellare è stato poi testato in reazioni di *cleavage* aerobico ossidativo di legami C-C di dioli vicinali, con elevate selettività e tempi di reazione relativamente bassi. Il sistema catalitico può essere inoltre riciclato e riutilizzato fino a tre volte in seguito a estrazione dei prodotti con solventi organici.

Ringraziamenti

Vorrei innanzitutto ringraziare la Prof.ssa Giulia Licini per avermi dato la possibilità di svolgere il dottorato nel suo gruppo. Grazie per avermi insegnato ad avere uno sguardo critico sul lavoro, a lavorare in maniera indipendente, ad avermi stimolato a conoscere e a cercare di superare i miei limiti. Grazie anche a Cristiano Zonta per i suoi consigli da "collega" maggiore.

I would like to thank Prof. Beatriu Escuder for giving me the opportunity to work in her group during my stay in Castellón for the STSM within COST Action CM1005. Thanks also to César for his collaboration and help.

Ringrazio tutti i ragazzi che ho conosciuto in questi tre anni, Elena, Jack, Nadia, Carlo, Valeria, Alejandro, Sara, Francesca Di Sarra e Alessandro Cazzolaro. Grazie ai piccolini, Rosa, Matteo, Federico e Giulia, perché anche loro aiutano a crescere e a maturare. Vorrei esprimere dei grazie particolari a Blerina, per essermi stata vicina sempre, anche ora che siamo distanti, per i consigli, le chiacchere e le giornate passate insieme. E' come se avessi avuto una seconda sorella qui. Grazie a Gloria e Agusia per le risate, serate e i momenti da ricordare. Grazie a Claudia, perché è stata sempre pronta ad ascoltare le mie paranoie nell'ultimo anno, quando le persone che conoscevo di più erano andate via e avevo bisogno di un'amica qua dentro. Grazie a Emanuele per i suoi consigli, i preziosi aiuti, il tempo che mi ha dedicato, nonostante le mille cose da fare, e per avermi insegnato ad avere passione per il proprio lavoro.

Ringrazio la mia famiglia, mio papà Nicola, mia mamma Maria e i miei fratelli Cosimo e Piera. Mi hanno sempre fatto sentire la loro vicinanza, hanno sempre creduto in me e mi hanno sempre appoggiata in qualsiasi mia scelta con entusiasmo.

Ringrazio infine Piero per essermi stato accanto in tutto questo tempo e aver sopportato il mio caratterino soprattutto nell'ultimo periodo, per avermi sostenuto e consigliato sinceramente e solo per il mio bene.

Rosalia